The University of Strathclyde

THE INFLUENCE OF TOOL EXCITATION ON MATERIAL DEFORMATION
(Part I)

Malgorzata Rosochowska

For Degree of Doctor of Philosophy

Department of Design, Manufacture and
Engineering Management

DECLARATION OF AUTHOR'S RIGHTS

ABSTRACT

"Forming with ultrasonic excitation" refers to the plastic deformation of engineering materials while the forming tool is excited at ultrasonic frequency. The original research in this subject was initiated about five decades ago but this subject continues to remain popular. Reports on the use of ultrasonics for material deformation tend to focus on parametric conditions that are beneficial to the process; little is stated of the need to develop tool design methodologies and acceptable tool geometries, and the limitations to the application of excitation to material-deformation processes.

The objective of this thesis is to assess the applicability of ultrasonic vibrations to industrial metal-forming processes; this is an essential prerequisite to decision-making by industrial process designers. To achieve this, it was necessary to perform experimental and analytical assessments of equipment design and manufacturing requirements. Two sets of equipment were designed and constructed. In both, the forming tool vibrated in the longitudinal mode; in the first, the tool vibrated in the direction perpendicular to the forming force while in the second vibrations were parallel to this force. The potential for applying ultrasonic excitation to industrial processes was evaluated with reference to currently known processes. Those selected were indentation, heading, wire-flattening and back-extrusion. Experiments were conducted to determine the influence of vibration on the reduction of forming forces.

Finite element (FE) analysis was used to support tool design, particularly for the design of tool geometry to minimise vibration-induced stresses and for tuning the tools, the latter was essential for attaining resonance without the need for proving trials. This relied on the use of Finite Element techniques for determining the modal behaviour of tool-configurations. FE techniques were also used to identify the zones of high stress-concentration with a view to refining tool geometry.

FE simulations were also used to simulate material flow in back extrusion under various excitation conditions. Two Finite Element models were developed for these;

the first modelled the tools as rigid bodies while, in the second the punch of dimensions complying with the resonant conditions was modelled as an elastic body. Simulations showed that the decrease in forming force could be partially attributable to changes in the direction of friction forces. It was also revealed that the amplitude of vibration at the working surface of the punch was smaller than that measured at remote points on the tooling.

A kinetic model of ultrasonically-assisted forging operations, based on the interaction between the rigid tool and the elasto-plastic work material was proposed. The model has been used successfully to describe experimental result, qualitatively.

Experiments revealed that the forging force is inversely proportional to excitation amplitude and directly proportional to process velocity. The influence of excitation diminishes at a rapid rate with process velocity; thus, ultrasonic excitation is particularly suitable for application to relatively slow deformation-rate processes. The dominant consideration in such applications is the extent to which the process is sustained in a steady-state over the duration of the process; processes in which the work-material is subjected to continuously changing deformation fields would show, neither economic nor tool-performance related gains. Further, high-strength work-materials and/or large components would require a level of excitation, which would demand the use of large generators. Conventional tool-steels would not be able to withstand the induced stresses and thermal changes. The power required for the excitation of tools and the poor efficiency of the ultrasonic systems will remain a constraint to the applicability of ultrasonics to material-deformation processes. The cost of power expended may outweighs the tool-force related advantages

Acknowledgements

The research presented in this thesis was conducted at the Department of Design, Manufacture and Engineering Management (DEMEM), University of Strathclyde throughout a part-time study. The work was supervised by Professor Raj Balendra, whose support, encouragement, advice and discussion throughout is appreciated.

The author would also like to thank Dr K.Chodnikiewicz for his constant support in solving theoretical and technical problems, assistance in experiments and numerous technical discussions. I also wish to thank Dr. Qin Yi for usful suggestions in conducting Finite Element simulations. Thanks are also due to Mr J.Gorczynski from Instytut Tele-Radiotechniczny and Dr P.Fabianski from Technical University in Warsaw, Poland, for providing advice on ultrasonic tool design and permitting the use of their facilities.

Support provided by colleagues in DMEM is gratefully acknowledged.

List of Publication

1. M. Rosochowska, R. Balendra, K. Chodnikiewicz
   "Measurement of thermal contact conductance", Accepted for publication in Journal of Material Processing Technology.
2. A. Rosochowski, M. Rosochowska
   "Dimensional effects in warm calibration of a stainless steel cylinder", Accepted for publication in Journal of Material Processing Technology
3. K. Chodnikiewicz, M. Rosochowska, R. Balendra
   "Thermal contact conductance – new approach", Submitted to Journal of Materials Processing Technology
4. T. Wisniewski, M. Rosochowska, K. Chodnikiewicz
   "A new method of measurement of thermal contact conductance in metal forming operations", 3rd Baltic Heat Transfer Conference, Gdansk, 1999
5. R. Diduszko, H. Marciniak, M.Rosochowska
   "RDF investigation of amorphous $Fe_{80}B_{20}$, $Fe_{60}B_{20}Mn_{20}$ alloys", XI European Crystallographic Meeting, Moscow, 1989
6. E. Czerwosz, A. Pajaczkowska, M. Rosochowska
   "The Raman and X-ray study of the crystal BI-Sr-Ca-CU-O systems", Proceedings of European Conference on High-T_C Superconducting Thin Films and Single Crystals, Uston,1989
7. M. Rosochowska, A. Pajaczkowska
   "Durability of High-T_C superconductor $YBa_2Cu_3O_7$ at elevated temperature and humidity", Symposium on X-Ray Diffraction Methods. Varna, 1987
8. J. Wojcik, M. Rosochowska, A Pajaczkowska
   "Crystal growth and thermal analysis of $YBa_2Cu_3O_7$", Journal of Crystal Growth, Vol. 91, 1988, pp 255-260
9. M. Rosochowska
   "X-ray investigation of high-T_C superconductors Y-Ba-Cu-o type", Prace OBREP, No 2, 1988, pp 17-29,

CONTENTS

DECLARATION I
ABSTRACT II
ACKNOWLEDGEMENT IV
LIST OF PUBLICATIONS V
CONTENTS VI
NOMENCLATURE XI

PART I

1. INTRODUCTION 1

2. LITERATURE REVIEW 8

2.1. EFFECTS OF ULTRASONIC VIBRATIONS ON MATERIAL FLOW 9
2.1.1. Volume effect 9
2.1.2. Surface effect 12
2.2. APPLICATION OF ULTRASONIC VIBRATION TO METAL FORMING PROCESSES. 15
2.2.1. Wire drawing 16
2.2.2. Tube drawing 19
2.2.3. Tube bending and expansion 21
2.2.4. Deep drawing 21
2.2.5. Ironing 23
2.2.6. Extrusion, indentation and compression 23
2.2.7. Patents 24

3. OBJECTIVE 26

4. EQUIPMENT 29

4.1. THEORETICAL CONSIDERATION OF RESONANT CONDITIONS. 29
4.1.1. Length of the vibrating components 29

4.1.2. Resonant conditions.. 30
4.2. MATERIALS FOR THE ULTRASONIC TOOLS. 34
4.3. OPERATING FREQUENCY, GENERATOR, TRANSDUCERS AND BOOSTERS. 36
4.4. WT/P TOOL. 38
4.4.1. Concept 38
4.4.2. WT/P tool design. 39
4.4.3. Design of the beams and the supporting blocks. 40
4.5. WT/I TOOL. 44
4.5.1. Concept 44
4.5.2. Design of WT/I Tool. 46
4.5.3. Design of punch holder. 47
4.5.4. Design of anvil.. 50
4.5.5. Design of punches. 51
4.6. INSTRUMENTATION 54
4.6.1. WT/P Tool 54
4.6.2. WT/I Tool 55
4.6.3. Data retrieving system and signal processing 56
5. EXPERIMENTAL PROCEDURE. 59
5.1. WT/P TOOL 59
5.2. WT/I TOOL 61
5.2.1. Indentation 61
5.2.2. Heading 63
5.2.3. Back extrusion 63
5.2.4. Wire flattening 66
6. FINITE ELEMENT ANALYSIS 69
7. RESULTS 75
7.1. WT/P TOOL 75
7.2. WT/I TOOL 77
7.2.1. Indentation 77
7.2.2. Heading 78

7.2.3. Back extrusion 79
7.2.4. Wire flattening 83
7.3. FINITE ELEMENT ANALYSIS 85
7.3.1. Wire Flattening 85
7.3.2. Back Extrusion 87
8. DISCUSSION 96
8.1. THE WP/T TOOL 96
8.2. THE WT/I TOOL 98
8.2.1. Deformation mechanism 98
8.2.2. Kinetic model 102
8.2.3. Energy consideration 116
9. CONCLUSION AND SUGGESTIONS FOR FURTHER RESEARCH 122
9.1. CONCLUSIONS 122
9.2. SUGGESTIONS FOR FURTHER RESEARCH 126
10. REFERENCES 128
APPENDICES
Appendix 1.1. Elastic-plastic wave propagation theory 136
Appendix 4.2.1. Energy dissipated in the vibrating element 140
Appendix 7.1. Variables and results of experiment using the WT/P tool 142
Appendix 7.2. Amplitude measurements 149
Appendix 8.2.3.1. Energy stored in a vibrating element 157

PART II

Diagrams

1. INTRODUCTION 160
2. LITERATURE REVIEW 165
2.1. EFFECTS OF ULTRASONIC VIBRATIONS ON MATERIAL FLOW 166
2.1.1. Volume effect 166

2.1.2. Surface effect....168
2.2. APPLICATION OF ULTRASONIC VIBRATION TO METAL FORMING PROCESSES....170
2.2.1. Wire drawing....171
3. OBJECTIVE....172
4. EQUIPMENT....172
4.1. THEORETICAL CONSIDERATION OF RESONANT CONDITIONS....172
4.1.1. Length of the vibrating components....172
4.1.2. Resonant conditions....173
4.2. MATERIALS FOR THE ULTRASONIC TOOLS....176
4.3. OPERATING FREQUENCY, GENERATOR, TRANSDUCERS AND BOOSTERS....177
4.4. WT/P TOOL....181
4.4.1. Concept....181
4.4.2. WT/P tool design....182
4.4.3. Design of the beams and the supporting blocks....183
4.5. WT/I TOOL....186
4.5.1. Concept....186
4.5.2. Design of WT/I Tool....190
4.5.3. Design of punch holder....194
4.5.4. Design of anvil....198
4.5.5. Design of punches....201
4.6. INSTRUMENTATION....204
4.6.1. WT/P Tool....204
4.6.2. WT/I Tool....206
5. EXPERIMENTAL PROCEDURE....208
5.1. WT/P TOOL....208
5.2. WT/I TOOL....209
6. FINITE ELEMENT ANALYSIS....210
7. RESULTS....216
7.1. WT/P TOOL....216

7.2. WT/I TOOL 226
7.2.1. Indentation 226
7.2.2. Heading 228
7.2.3. Back extrusion 229
7.2.4. Wire flattening 244
7.3. FINITE ELEMENT SIMULATIONS 247
7.3.1. Wire Flattening 247
7.3.2. Back Extrusion 252
8. DISCUSSION 270
8.1. WP/T TOOL 270
8.2. THE WT/I TOOL 271
8.2.1. Deformation mechanism 271
8.2.2. Kinetic model 272
8.2.3. Energy consideration 285

NOMENCLATURE

K		stiffness metrix
M		mass metrix
A	m	amplitude
A_i, B_i		constants
a_i,a_{i+1}	m	amplitude of successive oscillation
b	m	length of the supporting beam
c	m/s^2	sound velocity
c	Ns/m	coefficient of visous damping
C	pF	capacitance
C_O	pF	capacitance of the piezoelectric disks
C_T	pF	capacitance in the equivalent circuit of transducer
C_S	pF	capacitance in the equivalent circuit of ultrasonic system
D	m	diameter
D_i	m	inner diameter
D_o	m	outer diameter
DI	mm	indentation depth
E	N/m^2	Young's modulus
E_K	J	kinetic energy
E_P	J	potential enrage
e	mm	partial springback
e_{sb}, e_{sbav}	mm	decreas and average decrease in work-material delcection during unloading
e_{Total}	mm	total springback
f	$1/s$	frequency
f_s	$1/s$	series resonant frequency
f_p	$1/s$	parallel resonant frequency
F	N	force
F'	N	force at partial springback
F_S	N	forming force under static conditions
F_D	N	dynamic force
F_M	N	force applied by the forming machine
$\widehat{F}$	N	average force
f_p	$1/s$	parallel resonant frequency
f_S	$1/s$	series resonant frequency

G	N/m^2	torsion modulus or distance between forming tools
H_D, H_S	mm	height of a specimen obtained under dynamic , static condition
H_o	mm	initial height
h	m	height
i	A	current or i-th component (1, 2 3 ....)
k	N/m	stiffness or magnification
l	m	length
L	H	inductance
L_S	m	specimen length
L_R	H	inductance in the equivalent circuit of transducer
L_S	H	inductance in the equivalent circuit of ultrasonic system
m	kg/m	mass
P	W	power
P_{abs}	W	absorbed power
P_{sup}	W	supplied power
$\overline{p}$	MPa	mean pressure
R	$m,\ \Omega$	radius, resistance
R_R	Ω	resistance in the equivalent circuit of transducer
R_T	Ω	resistance in the equivalent circuit of ultrasonic system
r	mm	radius
s	mm	total deformation during one cycle
s_A	mm	deformation attributed to the anvil movement
s_P	mm	deformation attributed to the punch movement
S	m^2	area
S_1	m^2	reduced area
S_o	m^2	initial area
t	s	time
T	s	period of vibration
T_o	^oC	temperature
u	m	displacement
U	V	voltage
v	m/s	velocity
v_A	m/s	anvil velocity
v_L	m/s	vibrational velocity of the lower beam

1. INTRODUCTION

Forming with ultrasonic vibration refers to forming processes in which the tool vibrate at ultrasonic frequency. Ultrasonic vibrations are defined as mechanical vibrations and waves in gases, liquids and solid elastic media of frequencies above the upper limit of the audible range for human beings: the threshold above which vibrations and waves are recognised as ultrasonic is about 16kHz. Ultrasonic vibrations have been successfully applied in processes such as cleaning and plastic welding. The use of ultrasonic vibrations in metal forming processes has not been implemented yet in spite the benefits claimed by researchers. Frequencies at the lower end of the scale i.e. in the range 20 to 40 kHz are commonly used in these applications. The use of higher frequencies is restricted by the maximum tolerable mechanical stress in the vibrating components as well as by the difficulty and cost of producing high-powered, high-frequency generators.

An ultrasonically assisted, metal forming system (UMFORM)

The system consists of two parts (Fig.1-1). The first is a conventional metal forming machine (press, drawing), while the second is an ultrasonic device, consisting of a generator, transducer (occasionally refereed to as excitor) and a booster. Metal forming tools belong to both parts of the UMFORM since their behaviour is affected by both components of the system.

The source of energy for the ultrasonic system is the generator. To ensure optimum energy efficiency, the system should be operated at the resonant frequency. To comply with this requirement, the generator should be equipped with a feedback control loop, which monitors any changes in the resonant conditions and re-sets the generator to sustain the system at resonant conditions.

An electrical signal produced by the generator is converted into mechanical vibrations by a magnetostrictive (Fig.1-2a) or, more commonly, piezoelectric transducer (Fig.1-2b). The former is based on magnetostriction principles: a magnetic field causes elongation or contraction of some metals. A coil of wire wrapped around

a metal core creates a magnetic field proportional to the electric current, which results in the elastic deflection of the core as the field fluctuates. Typical magnetostrictive materials are nickel, its alloys with iron and alloys iron-aluminium. Contemporary produced magnetostractive materials are characterised not only by exelent magnetostrictive properties, but also by high mechanical strength and minimal losses due to eddy currents. Materials belonging to this group are alloys of aluminium and ferromagnetic alloys e.g. Al-Fe (alfery) or Al-Co-F3 (alcofery). Magnetostrictive transducer are extremely robust, tolerant of the frequency mismatching and can operate over a wide frequency range; however, its efficiency is relatively low (60%) due to non-linearity of the magnetostrictive effect, the induction of eddy currents in the core and energy losses in the windings. These limit the vibration amplitude that can be generated. A piezoelectric transducer comprises a number of piezoelectric discs, which are retained in compression by a metal clamp. The applied alternating voltage results in the elastic deflection of the discs in proportion to the current voltage. The length of the excitor is half wavelength of the propagating longitudinal wave; thus, during resonance the small longitudinal deflection of the disks (usually <0.1μm) is amplified to create an amplitude of the order of 5μm at the ends of this excitor. Quartz and barium titanate are among the materials which display the piezoelectric effect. Stronger piezoelectric properties are exhibited by materials marketed under product names such as PZT and PLZT; the former is a solid solution composed of $PZrO_3$-$PbTiO_3$ while the latter has as the main components $(Pb,La)(Zr,Ti)O_3$. Piezoceramics are brittle; consequently the discs are liable to fracture if subjected to tensile stress, therefore have to be compressively preloaded by the clamp. The resonant frequency of a piezoelectric transducer depends on the properties of the piezoelectric material, namely its density, elasticity, piezoelectric and dielectric properties and its geometry. It is common for these parameters to change with temperature. Transducers used in practical applications are designed for operation at a specified temperature T_o. The resonant frequency remains constant within a narrow range of temperature. The efficiency of a piezoelectric transducer is approximately 95%. However, the disadvantage is the narrow frequency bandwidth.

Generally, the amplitude of vibrations produced by a transducer is not sufficient for practical applications. Amplification may be achieved by transmitting the generated vibrations to the tool through a half-wavelength element, of decreasing cross section to the end, which is in contact with the forming tool. This element, often referred to as a booster or horn, acts as an amplifier due to a fact that energy transmitted through the cross section remaining constant. To fulfil energy balance, the smaller end would vibrate at higher amplitude. Boosters are of different forms; common forms are stepped, conical exponential, catenoidal and Fourier, and are characterised by a magnification factor [1], defined by:

$$k = \frac{A_1}{A_o} \tag{1-1}$$

The exponential booster has a magnification factor equal to $\sqrt{\frac{S_o}{S_1}}$ but has relatively low flexural stiffens. The stepped booster is characterised by a high magnification factor of $\frac{D_o^2}{D_1^2}$ but suffers from high stress concentrations in the region of the step-change of section. The catenoidal booster also has a high magnification factor but as in the case of the exponential booster has a low flexural stiffness. The Fourier booster has a combined high-magnification and high-stiffness characteristic. The forms of booster and corresponding amplitude distributions along their length are shown in Fig.1-3 [2].

Wave propagation theory.

The propagation of mechanical waves in solid media is based on two properties – elasticity and inertia. Application of a load to an elastic medium results in a mechanical disturbance of the medium. Due to inertia, the transmission of the disturbance from particle to particle in the medium occurs with a delay. The disturbance propagates to the position at the distance from its source in the form of wave [3]. The propagating disturbance results in the propagation of a stress wave. The propagation of stress waves plays a significant role in metal forming processes

which are characterised by high-rate plastic deformation such forging, peening and processes in which the work material is subjected to a dynamic loads. The propagating stress waves generate disequilibrium stress distribution, which may be different form the static stress state. The stress wave theory is the basis of estimating the maximum stress in the process.

Mechanical waves are characterised by the transport of energy by motion of the particles about their equilibrium position. Depending on the trajectory of the particle, the propagated wave may be classified in one of two groups: a pulse or single wave and a series of waves. An imaginary surface joining particles undergoing identical disturbance in a propagated wave is called a wavefront. The propagation of the wave may be considered in terms of the advancing wavefront. If the wave propagation is in a single direction, the wavefront has the shape of a plane. In a solid of infinite dimensions, the plane waves may propagate in either longitudinal (Fig.1-4a) or transverse modes (Fig.1-4b). In the longitudinal mode, particles of the body oscillate along the direction of the propagated waves. In the latter mode, the oscillations are perpendicular to the wave. Longitudinal waves are commonly used in high-powered ultrasonic applications.

The equation describing the motion of the longitudinal wave in one-dimensional medium (lateral displacement during longitudinal motion can be neglected) is [*4*]:

$$\frac{\partial^2 u}{\partial^2 t} = c_o^2 \frac{\partial^2 u}{\partial^2 x} \tag{1-2}$$

where

$$c_o = \left(E/\rho_o\right)^{1/2} \tag{1-3}$$

is a velocity of the elastic wave propagated in the bar (see Appendix 1.1).

In media of finite dimensions, the other aspects of wave motion such as transmission, reflection and interaction between the original and reflected waves influence the propagated wave. When a stress wave of intensity σ_o encounters a boundary

separating two media with different properties part of the wave is reflected and part transmitted to the second medium. In a bar with discontinuous cross-sections, made form two different materials (Fig.1-5), the intensities σ_T and σ_R of the transmitted and reflected waves respectively, are [4]:

$$\sigma_T = \frac{2 \cdot S_1 \cdot \rho_2 \cdot c_2}{S_1 \cdot \rho_1 \cdot c_1 + S_2 \cdot \rho_2 \cdot c_2} \cdot \sigma_o \qquad (1\text{-}4)$$

$$\sigma_R = \frac{S_2 \cdot \rho_2 \cdot c_2 - S_1 \cdot \rho_1 \cdot c_1}{S_1 \cdot \rho_1 \cdot c_1 + S_2 \cdot \rho_2 \cdot c_2} \cdot \sigma_o \qquad (1\text{-}5)$$

The transmitted wave is always of the same type as the original wave; a tensile wave is transmitted as tensile and compressive as compressive. The reflected wave may be of similar or opposite sign to the original (Eq.1-5). At the fee surface ($S_2 = 0$), the tensile wave is reflected as a compressive, and vice versa ($\sigma_R = -\sigma_o$). When a series of sinusoidal waves of a wavelength $\lambda = i \cdot c/(2l)$ is produced at one end of a free bar of a length l, the original and reflected waves interact to produce a standing wave (Appendix 1.1). Standing waves form modes of free vibration of an elastic body. Frequencies of these modes are called natural frequencies.

Operational principles.

Applications of ultrasonic vibrations utilise two physical phenomena: natural frequency and resonance. When a bounded element is force vibrated by a periodic driving force at a frequency close to the natural frequency of the element, vibrations of maximum amplitude are produced. This is the resonant condition. The propagating wave is a standing wave. The nodal points are characterised by maximum induced stresses while antinodes experience the maximum amplitude of vibration. This type of wave provides the optimal working condition for ultrasonic tools; this enables the concentration of energy in the deformation zone and the isolation of the vibrating elements from the remainder of the system. Operation in the resonant regime ensures a high operating efficiency. Variation of the amplitude along the length of the vibrating system, when the tool vibrates longitudinally, is shown in Fig.1-6. Different configurations of the tool-transducer-booster system would yield torsional or radial tool vibrations.

The deformation zone may be located either at the node or antinode of the standing wave. Examples illustrating both arrangements are shown in Fig.1-7.

All components of the vibrating system i.e. the transducer, booster and the tool, would have to be designed to have the same natural frequency to obtain resonant conditions. The efficiency of the system depends on the extent to which the components are tuned to resonate. Typically, the transducer and the booster are half wavelength elements. The metal forming tool may be of either a half wave or a full wavelength. Since velocity of a wave propagated in a solid elastic medium depends on its density and elasticity (Eq.1-3) a wave of a particular frequency, propagated in different solid elastic media, will have different wavelengths. Since the transducer, booster and the tool are made from different materials, their lengths, equal to a half wavelength of the propagated wave, would also be different.

The choice of tool vibration (longitudinal or radial) and location of the deformation zone depends on the application and should be consider with a view to maximising the effect of ultrasonic vibrations on parameters such reduction of deformation force, reduction of friction, surface finish and quality of the product. For a given application, the desired physical effect has to be defined prior to the design of the ultrasonic equipment. The mechanics of deformation would define the particular ultrasonic effect that has to be operable. This, in turn, determines the means by which energy is supplied to the deformation zone.

This thesis.

Chapter 2 contains the review of published research. The first part of this review describes phenomena by which vibration assists metal forming processes. In the second part, applications of vibration to industrial processes are discussed. Chapter 3 presents objectives of the research and a short description of the activities, which were carried out to fulfil these objectives. Chapter 4 provides details of the designed equipment. Experiments using these equipment, experimental procedures and instrumentation are described in Chapter 5. Chapter 6 provides the description of the

developed numerical models, which were used in Finite Element simulations. Results of the experiments and FE simulations are presented in Chapter 7. Discussions and theoretical considerations are considered in Chapter 8. These are follows by the conclusions and recommendations for the further work.

2. LITERATURE REVIEW

Research on the influence of ultrasonic vibrations on metal forming processes dates back to the late 1950's when Blaha and Langenecker [5] observed the apparent reduction in the magnitude of force when ultrasonic vibrations were superimposed on a tensile force for deforming metal crystals at a constant elongation rate. Upon termination of the vibrations the tensile force increased to its original magnitude. The observed phenomenon is illustrated in Fig.2-1. The upper graph shows the reduction in force after superimposing vibrations; the value returned to its original magnitude when vibrations were terminated. The lower curve shows that continuous application of vibration lowered the tensile force throughout the entire test. Later experiments showed that the force reduction caused by the superimposed ultrasonic vibration is directly proportional to the amplitude of the ultrasonic vibrations and is independent of frequency [6].

Subsequent results, obtained from tensile tests on zinc crystals with superimposed ultrasonic vibrations of a range of amplitudes [7], demonstrated that return of the magnitude of the stress, after removal of ultrasonic vibrations, to the value that it would have attained in the absence of vibration occurred only at low amplitudes. Work hardening was observed to occur after high-powered ultrasonic vibration. The higher the intensity of the applied ultrasonic vibrations, the more pronounced the hardening effect (Fig.2-2).

Since Blaha and Langenecker's discovery, several studies have attempted to establish the fundamental influence of ultrasonic vibrations on the plasticity of metals [6, 8, 9, 10, 11], its influence on interfacial friction [12, 13, 14, 15, 16] and its application to industrial metal forming processes. A number of industrial applications have been developed, including wire drawing [1, 17, 18, 19, 20, 21], tube drawing [20, 21, 22, 23], deep drawing [20, 24, 25, 26,], ironing [26, 27] and other applications of marginal interest [28, 29, 30].

2.1. Effects of ultrasonic vibrations on material flow

In general, the gains from the application of ultrasonic vibration to the tool in metal forming processes refer to the reduction of the static force required to deform material and/or the increase in deformation for the same force. As a result, as in the case of tube and wire drawing, higher reductions can be achieved in single stage and consequently, the number of passes, which are required to obtain the final product, can be reduced. The reduction in the forming force is attributed to two basic phenomena: the "volume effect" and "surface effect". The first, also referred to as "softening effect", relates to the reduction in the flow strength of the work material while the second, to the changes in friction at the interface between the vibrating tool and the work material. It was also observed that superimposed vibrations improve the surface texture of the finished component [21, 22, 26,].

2.1.1. Volume effect

Several theories have been developed to explain the softening effect of ultrasonic vibrations on materials. Blaha and Langenecker [8] attributed the phenomenon to the activation of anchored dislocations when the additional energy from vibrations was supplied. This hypothesis was discounted by Nevill and Brotzen [6] who discussed three mechanisms - resonance, relaxation and simple hysteresis - by which the dislocation may absorb energy and concluded that none of these could be responsible for the observed phenomenon. The resonance mechanism was discarded because of the fact that the decrease in Yield Strength was observed in experiments in which the frequency of superimposed vibrations was much lower than the natural frequency of dislocation loops which is of the order of 10^8 sec^{-1}. Experimental results showed that the decrease in Yield Strength was not dependent on frequency and temperature; this excluded the relaxation mechanism as a possible explanation. The absorption of energy by simple hysteresis was found not to be a suitable explanation for the decrease in Yield Strength. Instead, they proposed, a mechanism based on the superposition of steady and alternating stresses (Fig.2.1.1-1). A specimen, subjected to a steady uniaxial stress σ_S with a superimposed longitudinal elastic wave with a

maximum stress amplitude of σ_A, will deform plastically when the resulting stress $\sigma_S + \sigma_A = \sigma_Y$. This proposal has been generally accepted. However, phenomena such as hardening following cessation of high-powered vibrations, more uniform micro-hardness distribution and smaller residual stresses cannot be explained by this mechanism.

Theoretical considerations, based on phenomenological theories of plastic deformation of metals [31], led Herbertz [32] to conclude that tehe decrease in stress does not exhibit proportional dependence on the amplitude of the applied vibrational stress. At a constant strain-rate, the relative reduction of stress, express as a ratio of the stress reduction $\Delta\delta$ to the amplitude of the vibrational stress δ_A., shows a distinct dependence on the amplitude of vibration δ_A (Fig.2.1.1–2); this contradicts the theory of stress superposition. Both theories predict approximately the same reduction of static stress for large vibrational stress amplitude.

Green [33] suggested that not all results, presented in literature, can be explained by the stress superposition, which is based on linear elasticity theory and assumes a constant Young's Modulus. For example, a reduction in tensile force and return of the magnitude of force to the non-oscillatory value did not occur instantaneously [6] indicating a phase difference due either to non-linear elastic or plastic effects. Green also showed that non-linear changes in the effective elastic modulus, deduced from non-linear elastic theory could, to some extent, explain a stress reduction during a tensile test.

A variety of alloys and metals were tested in tension [1, 10] and compression [9] with superimposed ultrasonic vibrations, the results of which showed an increase of stress reduction with amplitude of applied oscillations. Further, Izumi [9] reported that when the amplitude of the applied vibrations exceeded a critical value, the reduction in stress was of a magnitude that could not be explained entirely by the superposition mechanism (Fig.2.1.1-3). Moreover, in such case stress reduction was accompanied by heat generation. Temperature rise was also reported by Konovalov

[10] and Severdenko [1], both of whom observed, that the extent of heating depended on the amplitude of vibrations and that the highest temperature occurred at the stress antinodal points in the induced standing wave. Similar temperature changes were observed during wire drawing by Siegert [21]. It was concluded, that superimposed ultrasonic vibration with amplitude above a threshold value caused thermal softening of the materials due to temperature rise, which resulted in an additional stress reduction. The threshold amplitude and the magnitude of the stress reduction depend on the metallurgical and mechanical characteristics of the material. Heat generation in a vibrating body is a consequence of internal friction, which manifests itself as a stress–strain hysteresis [34]. The area within the hysteresis loop represents the energy dissipated as heat due to internal friction, the magnitude of which is a function of the metallurgical characteristics, temperature and stress.

It is generally accepted that at low amplitudes of ultrasonic vibration, the operating mechanism is stress superposition while thermal softening plays a significant role in stress reduction at higher amplitudes.

Another possible mechanism, which can account for stress reduction, is the swaging effect. It occurs when an increase in lateral stresses results in the reduction of the axial stress, consistent with either the Von Mises or Tresca Yield Criterion which states that yielding occurs when a scalar function of the principal stress differences reaches a critical constant value:

$$f(\sigma_1 - \sigma_2, \sigma_2 - \sigma_3, \sigma_3 - \sigma_1) = const \qquad (2.1.1\text{-}1)$$

Thus, any change in the magnitude of one stress has to result in changes of the remaining stresses to comply with the Yield Criterion. Therefore, for the swaging effect to occur, lateral vibrations of the tool are required. A laterally vibrating tool changes the loading scheme and consequently the stress state in the material. It has been reported that changes in a loading scheme might lead to a significant reduction in the flow strength. Korbel and Bochniak [35] observed a significant reduction in the tensile load when tensile tests were performed with simultaneous torsion, on cooper and aluminium specimens. The results are shown in Fig.2.1.1-4.

The swaging effect is rarely recognised as a mechanism that may account for stress reduction in ultrasonically assisted processes. It may play a significant role in processes such wire and strip drawing, deep drawing and in extrusion with the die oscillating radially. Few researchers [24, 1] considered this mechanism as a contributory factor in force reduction.

2.1.2. Surface effect

Many researches have observed that that application of ultrasonic vibrations in metal forming processes may reduce the frictional force at the tool-work material interface. This reduction may be the result of changes in the coefficient of friction or from a change in the magnitude of the friction vector with the coefficient of friction remaining unchanged.

Mechanisms that may contribute to the decrease in the coefficient of friction are:
(i) Softening of asperities; it has been postulated that the in shear strength of the asperities due to the generated heat is reduced.
(ii) Pumping of lubricant; it is presume that lubrication at the tool/work-material interface is improved due to a fresh lubricant being pumped in by the vibrating tool,
(iii) cleaning effect and chemical activation of the lubricant.

Changes in the magnitude of the friction vector occur as a result of a changes in the stress normal to the interface, loss of contact and the direction of the relative motion between the work material and the tool. This follows from the fact that the friction vector opposes the relative motion between the tool and work material. Changes in the direction of the friction vector can be observed in wire and tube drawing processes in which the tool vibrates parallel to the drawing direction.

These mechanisms do not occur individually: therefore, it is difficult to estimate experimentally how each of these affects the friction force. The extent to which each of these affects a particular process remains unclear.

Fundamental research on the influence of vibration on friction was initiated by Fridman and Levesque [12] who explored the effect of vibration frequency and transducer power on the coefficient of static friction between metallic surfaces by using an inclined vibrating plane and sliding body. Experiments showed (Fig.2.1.2-1) that vibrations in a range between 6kHz to 42kHz reduced the coefficient of static friction by up to 90%. It was suggested that sufficiently high frequencies and amplitudes of vibrations might reduce the coefficient of static friction to zero, thus causing the body to float. This suggestion was confirmed in 90's by levitating a polysilicon block [36] at the nodal points of a standing wave of high frequency (around 4 MHz); in another experiment a weight of 10kG [37] was levitated. It was proposed that this phenomenon might be used in the design of non-contact transportation and ultrasonic motors [38].

The influence of low frequency oscillations (20-120 Hz) on static and sliding friction was investigating by Lenkiewicz [13]. The observations were similar to those reported by Fridmen and Lavesque. Reduction of both, static and sliding friction increased with frequency and amplitude of vibration. Further, it was observed that reduction in friction was inversely proportional to the sliding velocity. In addition, the slip-stick mechanism was eliminated by the presence of surface oscillations.

The motion of a body with a sliding velocity v_S, over a surface vibrating tangential to its movement with a circular frequency ω and an amplitude A_o was analysed by Mitskevich [39]. It was shown that the velocity of the body relative to the surface $v_{rel} = (v_S - \omega \cdot A \cdot cos(\omega \cdot t))$ changed direction over the vibration period. Friction force opposes motion from which it follows that reversal of friction force would occur when $(v_S - \omega \cdot A \cdot cos(\omega \cdot t) < 0)$. As a result a body, with the initial sliding velocity v_{oS}, will come to a rest slower in the presence of vibrations. The theoretical relationships, illustrating changes in the sliding velocity with time, with vibration (curve 1), and without vibrations (curve 2), are shown in Fig.2.1.2-2.

Further, for sliding velocity $v_S << \omega \cdot A_o$, a factor υ was defined:

$$\upsilon = \frac{\pi \omega A_o}{2 v_s}, \qquad (2.1.2\text{-}1)$$

by which the friction force between the body and the vibrating surface is reduced. This was confirmed experimentally. It was suggested that this expression might be used to select the optimum parameters (ω, A_o, v_f) for ultrasonic-assisted extrusion and metal-cutting. The reduction in the friction force due to periodic changes in the direction of the friction force is commonly referred to as a friction vector effect.

Siegert and Ulmer [16] showed that the reduction of sliding friction between the longitudinally oscillating die and the work material, in sheet drawing, could be explained by the friction vector effect. Using a piezoelectric load cell and a high-speed data acquisition system, it was possible to reveal the dynamic character of the friction force. Simultaneous measurement of tool displacement showed that sinusoidal changes in the friction force are shifted by π relative to the vibrations. Generally, for small drawing velocities the reduction in friction force was in agreement with Mitskevich's [39] prediction.

Reduction in sliding friction as a result of the separation mechanism was studied by Tolstoi [14]. The sensitivity of the frictional force to the normal displacement of the sliding body was demonstrated. For a set of experimental conditions - unlubricated steel and a mean asperity height of 1.25μm- the friction force was halved when the body was raised by about 0.2μm (Fig.2.1.2-3). Further, under imposed vibrations of frequencies ranging from 100Hz to 4kHz, peak force reduction was detected at a frequency of about 2kHz. It was attributed to the existence of the normal natural micro-vibrations of the slider on the spring-like asperities. One of the factors, which played a role in friction force reduction, was the decrease of the adhesion force; this was a consequence of the decrease of the area where the distance between the opposing non-contacting asperities was less than the range over which molecular forces are active. A further factor was the decrease in the resistance to plastic

deformation, including shearing and fracture of cold-welded asperity junctions, due to reduced contact area.

Winsper et al [40], attributed the reduction in friction forces by the separation mechanism to two factors. The first was that a smaller mean friction force over the vibration period was the result of shorter contact time between the tool and the work material and, the second was that the separation results in the periodic re-establishment of the lubrication film at the contacting surfaces, thus improving lubrication conditions. The latter was confirmed experimentally by Jin et al [26]. The application of vibrations, of 14.8 kHz to ironing and 15.1 k Hz to tube drawing, enabled the replacement of high-viscosity, environmentally aggressive lubricants with low-viscosity lubricants, which, under conventional conditions, did not provide sufficient lubrication. Reduction in friction forces and an improved surface finish were also observed. The relatively low ironing (0.0383m/sec) and drawing (0.03m/sec) velocities used in these experiments may account for the results achieved; it should be expected that at higher velocities, and consequently shorter separation times, the effect would not be as pronounced.

Summarising, results of the research on the fundamental influence of ultrasonic vibrations on metal plasticity and friction conditions promised prospects of applying ultrasonic vibrations in a production environment. Consequently, new research programmes aimed at assessing the potential industrial use of such applications were developed.

2.2. Application of ultrasonic vibration to metal forming processes.

Most of the research on the application of ultrasonic vibration to metal forming processes was conducted in the 60's and 70's. Comprehensive reviews of the research was provided by Sewerdenko [1, 41], Puskar [42] and Eaves [43]. Development of the efficient ultrasonic power generators, development of new piezoelectric materials, a new generation of measuring devices and high-speed data acquisition systems as well as advances in computer-aided design enabled researches to return to their interest in this subject in the 90's.

Published literature reveals that substantial research was devoted to the influence of ultrasonic vibrations on wire and tube drawing. Research was also conducted in the application of ultrasonic vibrations in deep drawing, extrusion, cold upsetting and rolling processes.

Ultrasonic vibrations may be applied to the metal forming operation by several alternative approaches. These will be illustrated using as an example the wire drawing process. Common approaches are shown in Fig.2.2-1, these configurations use longitudinal vibrations in which the direction of drawing may be either perpendicular (Fig.2.2-1a, b) or parallel (Fig.2.2-1c, d) to that of the vibrations. The deformation zone may be located at either the antinode (Fig.2.2-1 a, c) or node (Fig.2.2-1 b, d) of the standing wave. An advantage of locating the deformation zone at the antinode is that the nodal point may be used for securing the die to the supporting structure.

2.2.1. Wire drawing

Longitudinally-vibrated dies with a deformation zone located in the antinode was the common configuration used in wire drawing processes used . During the course of drawing, die displacement changes direction; in one half of the vibrational period it assists the drawing process and in another opposing it. If the drawing speed is low relative to the maximum die vibration speed ($v = 2\pi \cdot A \cdot f$), then a gap is created periodically between the die and the wire. The critical drawing speed occurs when the drawing speed is equal to the maximum die vibration. Relative movements of the die and the wire, over one vibration cycle, is illustrated in Fig.2.2.1-1b. When the drawing speed is higher than the critical drawing speed, the prevailing conditions are such that vibration has no influence [18]. The separation mechanism accounts for the reduction in mean drawing force and improvement in lubrication. If the deformation zone is located at the node of the standing wave, a periodically changing stress is imparted to the wire by the die. Alternatively, the die may also be vibrated in a radial mode in which the die alternately expands and contracts. This swaging effect, which results from the wire being periodically compressed, is utilised in this arrangement.

The direction of the vibration is perpendicular to that of drawing. Relative movements of the die and the wire, over one vibration cycle, is illustrated in Fig.2.2-2c. In this case, the critical drawing speed depends not only on the frequency of the applied vibrations but also on the die entry angle α and is expressed by the formula $v_c = 2\pi \cdot A \cdot f \cdot tg(\frac{\alpha}{2})$. Due to the difficulty of obtaining this effect in small wire drawing dies the approach has not bee adopted [18].

Research was conducted in the 60's and 70's to assess the relationship between the reduction in force and process parameters such as amplitude of vibration, drawing speed, type of material and intensity of the delivered energy. A variety of methods of imparting vibrations to the die, different materials, process parameters and methods of measurements were employed by researchers; his made the comparison of the published results difficult. Some published papers do not provide sufficient descriptions of the experimental conditions and equipment making the comparison even more difficult. The general conclusion was that the application of ultrasonic vibrations reduces the drawing force. The higher the amplitude, the higher the reduction. This effect diminishes with the increasing drawing speed.

Some researchers claim remarkable reductions in drawing force. Severdenko [41] reported reductions of 50% and 95% in the drawing force for copper wires drawn through the dies that were vibrated axially, while the supplied power was 3kW and 7kW respectively. The drawing speed was 0.23m/s. For molybdenum wires drawn with the same vibration intensity, the drawing force was reduced by 26% and 60% respectively. In all cases the initial diameter of the wire was 1.63mm and was reduced to 1.49mm. Corresponding reduction in area was 16%. Using the arrangement shown in Fig.2.2-1c, Oelschlael and Weiss [42] reduced the cross section of the wire by 8.5% with a vibration amplitude of 0.01mm, this being achieved with a reduction in drawing force of 24 and 49% for aluminium and lead wires respectively. For an amplitude of 0.17mm, the reduction was 37 and 62% respectively. Experiments performed by Siegert at al [17] in the late the 90's did not produced comparable results; these experiments were conducted using longitudinally

vibrating dies with an amplitude of 0.01mm. The drawing direction was perpendicular to that of the vibrations. The deformation zone was located at both, the node (Fig.2.2-1a) and the antinode (Fig.2.2-1b). Stainless steel wires were used; for true strains ranging form 0.06 to 0.74 and a drawing speed in the range 0.016 – 0.16m/s, it was possible to reduce the drawing force by up to 20% and 12% for the first and second die arrangements respectively.

Pasierb [44] drew aluminium and steel wires at velocities of 0.06, 0.07 and 0.12 m/s. For a reduction of 32% the maximum reduction in drawing force was 25% and 6% for aluminium and steel wires respectively. The die was vibrated axially.

Significant force reduction for drawing steel wires at a speed ranging from 1.25 to 2.25 m/s was reported by Graff [20]. The initial diameter of wires was 5.6mm, vibration frequency was 8.5 kHz. Area reduction in the range 25-42% was obtained with 5-14% reduction in the drawing force.

Severdenko [1] and Robinson [45] observed that the mean drawing force varied with the length of the wire drawn. Further, Winsper [46] noted that the minimum force occurred when the distance between the die and gripping jaws was equal to an integral number of half wavelengths for the drawn wire. Suppressing the wave propagated in the drawn wire can eliminate fluctuation in the drawing force. Approaches for suppressing the wave have been described by Severdenko [1].

Murakawa [18], using dies oscillating radially and longitudinally, performed experiments with a view to assessing the influence of such configuration on lubrication conditions. High quality wires can only be produced by the use of high-viscosity lubricants. Experiments showed that the application of vibration to the tool enabled the production high quality wires using low-viscosity lubricants. Further, quality of the wires produced using the die vibrating in the radial mode was reported to be higher.

Some side effects were also observed; Siegert and Moeck [17] observed an excessive wear of the die surface when the wire was drawn at a speed of 0.018m/min and true strain of 0.24. At higher drawing speeds, the die surface had to be polished after a few draws.

2.2.2. Tube drawing

In a tube drawing process, ultrasonic vibrations may be introduced either through the die or the plug, or through both simultaneously. Methods of imparting vibrations to the die are the similar to those for the wire drawing dies (Fig.2.2-1c and d); the plug is vibrated axially [21, 41]. A comparison of the various methods of introducing oscillation has been reported by Pasierb [44]. The most effective was found to be the arrangement when both, the plug and the die, were vibrated axially at the same frequency. Under these conditions the reduction in the drawing force was 55%. When only the plug was vibrated, the maximum reduction of 48% and 8% was achieved for the plug positioned at the antinode and the node of the propagated standing wave respectively. A system for tube drawing with the die and the plug vibrated simultaneously was also reported by Jin [26]; experiments were performed with a view to assessing the influence on shape precision and surface finish. Results showed that tube produced with vibrating tools had superior shape precision and surface finish when compared to those produced in the conventional process.

The beneficial effects of the application of ultrasonic vibrations are:

(a) force reduction,

(b) ability to achieve greater reductions,

(c) elimination of lubricant breakdown and stick-slip phenomena,

(d) better surface finish,

(e) the ability to draw tubes with a diameter to thickness ratio of the order of 500 (for conventional drawing this ratio is limited to 50 [22].)

Reduction in the drawing force depends on drawing speed, amplitude of vibration and tube elongation. This increases with a decreases in drawing speed [47, 48], elongation factor [47] and increases in amplitude of vibrations [22,47,48]. Theoretical considerations supported by experimental work led Nosal' and Rymsha

[23] to conclude that to achieve an economically acceptable reduction in the drawing force and corresponding increase in reduction, the drawing speed should be between one-third to one-fifth of the vibration speed.

The mechanisms controlling the reduction of drawing force have not been fully explained. Experiments, conducted by Winsper and Sansome [22], using an axially vibrating plug during fixed plug drawing, showed that the reduction in drawing force could be explained only partly by the force superposition effect. A reduction of 620 lbf in the drawing force was observed while the dynamic force induced in the drawn tube had a magnitude of only 250 lbf. Reduction of friction at the plug and die surface is thought to be another factor contributing to force reduction. It was also shown that the reduction in drawing force and, consequently, the die and plug load were independent of the reduction in area.

Studies on radially vibrating dies have not been extensive. This may be due to the fact that die design is more difficult since the die must satisfy not only the criteria for radial resonance but also the geometrical constraints imposed by the [49]. Further, it is anticipated that there would be difficulty in isolating the relevant mode of vibration and maintaining the tuned condition due to the high density of vibration modes. These problems were addressed by Lucas [50]; it was proposed to adapt vibration analysis techniques to estimate modal parameter of the die and design strategy based on sensitivity analysis. Another difficulty would arise from the fact that the whole die vibrates; there are no stationary points, which can be used to secure the die. A tubular mounting system, permitting the die to vibrate freely while providing a stationary point by which the system may be fixed to the support structure, was described in by Cheers [51]. Force reductions, ranging from 10 to 30%, was achieved by Kaiyawasam at al [52] during experiments with radial ultrasonic vibration of the die with a fixed plug.

2.2.3. Tube bending and expansion

Application of ultrasonic vibrations was also successfully employed to tube bending [53]. It was shown that increasing the amplitude of vibration decreased the bending torque, the plug force and the thinning of the tube wall on the outer periphery, thus enabling the production of tighter, more accurate ends. For an amplitude of 0.016 mm, a reduction of 25% and 20% in the bending torque was achieved for a tube with a diameter to thickness ratio equal to 28 and 21 respectively. Vibrations with an amplitude of 0.009 mm resulted in 17.5% and 16% reduction in bending torque respectively.

Nakagari at al [54] applied ultrasonic vibrations to tube expansion. The plug vibrating at a frequency of 13kHz was placed at the node, antinode or midway between them. The best results - 25% reduction if forming force - was obtained when the plug was located at the nodal point. The smallest effect - 5% force reduction - was observed when the plug was located at the antinode. Further, experiments showed that when the plug was located at the node, the forming force depended on the plug position in the tube. This effect was attributed to the friction vector effect.

Tubes produced with an axially vibrating plug were shown to have an improved surface texture on the inner diameter [22] additionally. Radially vibrated dies produced tubes of improved shape precision [55]. Tubes produced with vibrations imparted to both tools resulted in precision and surface finish on both the inner and outer surfaces [26].

2.2.4. Deep drawing

In deep drawing, a criterion that describes the effectiveness of the process is the limiting draw-ratio (LDR), the value of which is a function of friction conditions. The smaller the friction at the die and punch holder and the larger the coefficient of friction at the punch, the larger is the achievable LDR. It may be anticipated that introduction of axial vibrations to the punch alone would reduce the mean drawing force due to stress superposition; this was shown not to be the case since the condition on blank/die and blank/holder contact surfaces would not be influence by

vibrations. Most of the studies reported in literature concern radially vibrating dies. The number of transducers used by different researchers to impart this mode of vibration varied from 1 [24] to 5 spaced at 60° intervals around the die [20].
Experiments with vibrating dies were reported by Pasierb [24] and Graff [20]. A draw ratio of 1.9 [24] was achieved with a reduction of force of 12% for aluminium and copper cups. Similar results [20] for steel cups with the same draw ratio were reported. Noteworthy are the means by which Graff constrained the radially vibrating die. The die simply rested on the press anvil covered with teflon sheet of low friction coefficient to minimise damping. Three, quarter-wavelength pins tuned to the frequency of the die, located around the die maintained its radial alignment. This system was shown to be efficient design configuration.

An investigation into the influence of radial blank holder vibration on the limiting draw-ratio was initiated by Smith [56]. A variant of the wedge test was used to simulate deep drawing by forming only a sector of the cup. In this test, the blank-holding wedges simulated the radial vibration by being subjected to axial vibration in a plane perpendicular to the axis of the punch. It was established that by introducing vibration to the blank holder, the limiting draw-ratio was increased by about 12% while punch load was reduced by 25%.

A deep drawing system in which both, the die and blank-holder, vibrated in a radial mode was developed by Jimma at al [24]. Both tools were vibrated at a frequency of 20kHz with an amplitude of 4.0μm. Experiments were conducted with conventional cold-rolled steel and deep-drawing, cold-rolled steel. The limiting draw-ratio for cold-rolled steel increased form 2.58 for the conventional process to 2.86 when only the blank holder was vibrated. For the arrangement when both tools were vibrated, this parameter reached a value of 2.94. For deep-drawing of cold-rolled steel, this factor increased from 2.68 to 3.01, a maximum value restricted by the tool dimensions, when only the blank-holder was vibrated. Presented results agree with earlier results [56].

2.2.5. Ironing

A radially vibrating die was used by Jin at all [26] for the ironing process. Experiments were performed with a view to assess the influence of vibrations on lubrication conditions. In the conventional ironing process, high-viscosity (harmful to the environment) lubricants are employed to provide sufficient lubrication. Experiments with four different low-viscosity lubricants showed that regardless the type of lubricant, the limiting reduction ratio of the wall thickness increased by about 3%. Experiments reported by Takemasu at al [27] were also performed with a view evaluating lubricants. Application of ultrasonic vibrations of a frequency of 24kHz to the ironing process enabled the replacement of high-viscosity lubricant (>500cSt) with the one of a low value (<1cSt). Further, the test specimen acquired improved surface texture. The target surface finish of the product set to be the same as the die surface roughness, R_Y=0.2 μm, was achieved in the 2nd stage of ironing. Additionally, it was reported that the mean punch load was reduced by about 50% and 20% in the 1st and 2nd stage respectively.

2.2.6. Extrusion, indentation and compression

Direct extrusion of metal with applied oscillatory energy was investigated by Spiers at al. [28]. An experiment was designed to establish the extent to which the reduction in extrusion pressure could be attributed to either the load superposition mechanism or to reduction of friction. The superimposed oscillatory energy was supplied to the punch in the axial direction using an electro-hydraulic excitor. It was shown that influence of oscillation is independent of frequency for frequencies of oscillation in the range 20 to 200Hz with force amplitude to a maximum of 2 T. It was found that the magnitude of the mean load was equal to the magnitude of the applied oscillatory load. It was concluded that there was no reduction in friction force.

The influence of low frequency vibrations on axisymmetric indentation and compression of elasto-viscoplastic materials was studied by Huang and Lucas [29]. Experimental and numerical techniques were employed. The authors suggest that the reduction in indentation load resulting from superimposed oscillation might be explained by a combination of stress superposition and friction reduction.

Siegert at al. [30] used an axially vibrating die at a frequency of 22kHz to effect hobbing. During vibrations, the force required to achieve a penetration of 2 mm with the tool velocity of 0.1mm/sec, was reduced by 30%. Additionally, a special work-material clamping system, which amplified the die oscillation, enabled a further reduction of 30%. Further, it was claimed that at very low strain-rates this special clamping system would reduce force by a factor of 40.

2.2.7. Patents

Research conducted in the late 50's and 60's yielded some patents. However, industrial engineers had displayed an interest in using vibrations in industrial processes much earlier. In 1933 Nell [57] patented a hollow piston hammer, which utilised the swaging effect. A few years later, Vang [58] developed oscillatory deep-drawing equipment while Green [59] proposed the vibrations of dies during the extrusion of plastics. It was claimed that, due to friction reduction between the extruding material and the die orifice, the process was more efficient. These two patents did not provide dimensions of the resonant elements; thus, the resonant frequency of these systems had to be established experimentally. Further, the method of suspending the resonant system was not described. Rosenthal [60] developed an apparatus for drawing wire, which complied with the rules for the design of resonant systems. It was suggested that the drawing force was reduced as a consequence of both the swaging effect and friction reduction between the die and wire. Another apparatus for forming wire was proposed by Gutterman [61]. Apart from claims made by previous inventors it, was also suggested that vibrations would improve the surface of the wire. The reduction in friction was attributed to the relative movement between the die and wire. This, friction vector effect, was investigated 20 years later and described mathematically by Mitskevich [39]. Jones developed equipment for vibratory squeeze forming of metal in the solid state [62] and an apparatus for ultrasonic assisted extrusion [63]. A further invention concerned the suspension of vibrating devices. Calosi [64] proposed that the vibrating element could be supported by a tube of a quarter wavelength, attached at the antinode.

Most of the patented concepts were not developed commercially. Unfortunately, most of the earlier generation of excitors was based on magnetostrictive principals and yielded low power efficiencies. This inefficiency, coupled with imperfect design, created doubts about the commercial viability of applying ultrasonic; further, inventors claims were not realised. Research, which followed from Blaha and Langenecker's discovery, resulted in a better understanding of the mechanism of oscillatory metal deformation. A wide variety of improved equipment was developed and patented. There was a considerable improvement in equipment design resulting in higher power efficiency. In 1959 Elmore [65] patented a method of mounting vibrating systems, which has been referred to as "force insensitive mounts". The proposed design was a modification of the Calosi patent in which the length of the mounting tube was an integral number of half wavelengths. Improvement of the design of the resonant support system contributed to better mechanical efficiency.

Equipment for deep drawing and extrusion was developed by Bodine [66]. About the same time Boyd at al [67, 68], on behalf of Aeroprojects Incorporated, filed two patents on fixed plug tube drawing. Equipment described in the first patent enabled the excitation of both, the plug and die. It was claimed: "results are achievable which cannot be obtained by vibratory activation of the die or of the plug alone". In the second invention ultrasonic vibrations were only imparted to the plug. This design was conditioned by economic considerations; the application of ultrasonics is generally expensive due to both, design complexity and energy consumption. A further patent was on fixed plug tube drawing, in which both the die and the plug were vibrated, was patented in the UK by Dawson and Sansome [69].

Equipment for tube drawing with floating plug was patented by Maropis [70]. This incorporated a plug whose length was an odd number of quarter wavelengths, which stabilised the floating plug in the deformation zone.

3. OBJECTIVE

The literature review suggests that the application of ultrasonic vibrations to metal forming operation would be beneficial in the industrial environment. Despite the claims made by the researchers and number of patents, widespread application did not follow. Vibration-assisted metal forming processes remain, largely, a research topic. However, while some research centres have abandoned the subject others appear to have initiated new research. In early 70's Dawson, Winsper and Sansome, stated [71, 72] that drawing of tubes with ultrasonic vibrations was the only process, which had a presence in the manufacturing environment. Aeroprojekts Incorporated in the USA carried out the development of this technique. Ultrasonically assisted tube drawing was also implemented on a small scale in Germany and USSR [41] in the late 70's. In the UK, only small (20mm diameter) cans were deep drawn with dies that resonated radially [73]. Apart from these early applications there has been little commercial success and poses a serious question: What are the reasons for the poor success rate? Biddell and Sansome [73] suggested that insufficient co-operation between the industry and research institutions was to blame for the lack of industrial applications. Researchers were focussed on describing known phenomena rather than industrially applicable equipment. Technical papers concentrate on defining only achievements while neglecting to define problems, difficulties and limitations. The absence of a coherent effort to solve common problems did little to transfer this technology from the laboratory to the shop floor. A common opinion is that the commercial success of this technology would result from a complete understanding of the mechanics of vibration-assisted material deformation. In order to make a realistic assessment of the scope of this technology it is necessary to be aware of all associated limitations and problems. New technologies will succeed existing ones only if the competitive advantageous are demonstrated.

The investigations in this research were carried out with a view to define the applicability of this technology. To achieve this goal it was necessary to:

1. Review existing knowledge of tool and equipment design.

2. Design and construct equipment on which specific technical outcomes can be realised.
3. Evaluate experimentally the influence of ultrasonic vibrations on material flow in selected processes.
4. Conduct theoretical analysis to acquire an improved understanding the mechanisms by which the applied vibration assists metal forming processes.

Two approaches were adopted; experimental and numerical. Two sets of equipment were designed and constructed. Finite element analysis was used to evolve the geometry of tools. The first tool, referred to as WT/P tool, was used to evaluate the influence of ultrasonic vibration on friction. In this tool, the direction of the vibrations was perpendicular to the direction of the forming force and parallel to that of friction. Specimens were compressed between two horizontal beams, which were excited using transducers attached to the end of each beam. The second apparatus, referred to as WT/I tool, was used to evaluate the potential for applying ultrasonic vibrations to industrial processes by referring to four selected industrial processes: indentation, heading, wire flattening and back extrusion. The tool was equipped with interchangeable components to facilitate tool development for particular processes. In the case of back extrusion, indentation and heading, the imparted vibrations were in the direction of the forming force: in the case of wire flattening, the excitation was perpendicular to the direction of wire motion. Experiments using this tool were conducted with a view to assessing the influence of vibration on the reduction of the forming force for different vibration amplitudes, deformation velocities and different work materials.

The influence of ultrasonic vibration on material flow was also investigated using numerical methods. Back extrusion and wire flattening processes were simulated using Finite Element analysis.

Theoretical consideration lead to the development of the model of ultrasonically-assisted forming processes. This model is based on the kinetics of the rigid tool and elasto-plastic model of the work material.

4. EQUIPMENT

This chapter provides descriptions of all equipment used in experiments described in the next chapter.

Section 4.1 refers to the geometrical considerations of the vibrating components and resonant conditions of the mechanical systems; information included in this section is essential to the design and development of tools. Materials used for the ultrasonic tools have to comply not only with mechanical but also acoustic conditions. This issue is discussed in Section 4.2. Section 4.3 provides detailed technical information on the generator, transducers and boosters. The concept and design details of the WT/P tool and WT/I tool are described in Section 4.4 and 4.5 respectively.

The press used in experiments, the related instrumentation and signal processing is described in Section 4.6.

4.1. Theoretical consideration of resonant conditions.

4.1.1. Length of the vibrating components.

Among the types of natural vibrations exhibited by elastic bodies, the longitudinal and radial vibrations are commonly used in the ultrasonically assisted metal forming systems. The concepts of the tools, which are described in Section 4 and 5, required the used of the longitudinal vibration. To comply with resonant conditions all components of the vibrating system must have the same natural frequency, which is equal to the selected operational frequency. The natural frequency of a components depends on its geometry, the properties of the material of which the component is made and the displacement constraints imposed to the component. Motion of the longitudinal wave is described by Eq.1.2. The general vibrational solution of this equation for a bar with free end is[74]:

$$u_i = \cos\frac{i\cdot\pi\cdot x}{l}\left(A_i\cos\frac{i\cdot\pi\cdot c\cdot t}{l}+B_i\sin\frac{i\cdot\pi\cdot c\cdot t}{l}\right) \qquad for\ i=1,2,..... \qquad (4.1.1\text{-}1)$$

where A_i and B_i are constants, which are determined by satisfying initial conditions. Frequencies of the natural modes are:

$$f_i = \frac{i}{2l}\sqrt{\frac{E}{\rho}} \qquad (4.1.1\text{-}2)$$

Shapes of first three modes of a free bar with the length l are shown in Fig.4.1.1-1. The length of the vibrating component is usually equal to an integer-number of half wavelength. Computation of component length for simple geometrical forms – prismatic or cylindrical- may be performed using Eq.4.1.1-2. Fine-tuning may be achieved be reducing the length of this component. For complex tools, Eq.4.1.1-2 provides only an approximation of the component length. Tuning to the resonant frequency would have to be achieved by decreasing the length by marginal amounts with intermediate experimental analysis to determine the extent to which a match has been achieved. However, the more economic approach would be to use Finite Element Analysis; this approach will be illustrated later in the text of this thesis.

The required practice would be to verify all modes of vibration, which are in the close proximity to the selected operating frequency. Again, this can be determined using FE. Under the operational conditions, when the dynamic characteristics of the system vary continuously, the vibrating system may switch into an alternative resonant mode if it is in the proximity of the desired resonant mode. The required mode of vibration would have to be distanced from other possible modes to prevent such switching. Often, this requires the redesign of the geometry of the component.

Regardless of the method used for computation of the length of the vibrating elements, the resonant mode would have to be verified experimentally. It is only possible to tune to the higher resonant frequency by shortening the component.

4.1.2. Resonant conditions.

The transducer used in the research was the Langevin type (Fig.1-2b), a brief description of which was provided in Chapter 1.

A suitable method of studying the behaviour of a vibrating system is to use an equivalent electrical circuits [75, 76]; the basis of this approach is the mathematical

similarity between mechanical and electrical system. A simple mechanical oscillator is shown in Fig.4.1.2-1a. Its motion may be defined by:

$$m\frac{dv}{dt} + c \cdot v + \frac{1}{\delta}\int v \cdot dt = F \qquad (4.1.2\text{-}1)$$

Since all its elements experience the same displacement, x, the oscillator may be represented by a series circuit shown in Fig.4.1.2-1b. The equivalent electrical circuit is shown in Fig.4.1.2-1c. The equation describing this circuit is:

$$L\frac{di}{dt} + R \cdot i + \frac{1}{C}\int i \cdot dt = U \qquad (4.1.2\text{-}2)$$

The analogous quantities are:

$v \Leftrightarrow i$, $F \Leftrightarrow U$, $m \Leftrightarrow L$, $c \Leftrightarrow R$, $\delta \Leftrightarrow C$.

The equivalent electrical circuit of the piezoelectric transducer (Fig.4.1.2-2a), an electro-mechanical device, contains an additional capacitor C_o representing dielectric properties of the piezoelectric disks [77, 78, 79]. This capacitance, often referred to as the "blocking capacitance", is measured when the ceramic disks are secured to prevent vibration. This is represented in the L_T-C_T-R_T branch either as a discontinuity in the circuit or as an infinite resistance. It should be stressed that the equivalent circuit of a specified parameters C_O, C_T, L_T and R_T is applicable within a narrow range of frequencies in the proximity of a well-separated, vibrational mode.

The equivalent electrical circuit is characterised by two resonant frequencies: series (f_s) and parallel (f_p). The former refers to the resonant conditions in the branch representing the mechanical part of the transducer. Resonance occurs when the reactance of this branch is equal to zero i.e. when:

$$f_s = \frac{1}{2\pi\sqrt{L_T C_T}} \qquad (4.1.2\text{-}3)$$

At this frequency the current I_T flowing in this branch is a maximum and is the phase with the voltage (Fig.4.1.2-2d). Consequently, the active power of the system, which is associated with energy that can be transferred to another system, is also a

maximum. Variation of the magnitude of the current with frequency is shown in Fig.4.1.2-3. Even marginal deviations from the resonant frequency result in a decrease in current.

By analogy, series resonance occurs in the mechanical system when the excitation system complies with the condition:

$$f_s = \frac{1}{2\pi\sqrt{m\ \delta}} \tag{4.1.2-4}$$

Under this condition, the velocity of vibrations, which is analogous to the current, is a maximum. It corresponds to the maximum amplitude of vibration in accordance with the relationship between theses two quantities:

$$v = A \cdot \omega \cdot sin(\omega \cdot t) \tag{4.1.2-5}$$

Parallel resonant frequency refers to conditions in the whole equivalent circuit and occurs when:

$$f_p = \frac{1}{2\pi\sqrt{L\ \frac{C_T C_o}{C_T + C_o}}} = f_s\sqrt{1 + \frac{C_T}{C_o}} \tag{4.1.2-6}$$

At this frequency, the resistance of the equivalent circuit is a maximum. It follows that the resultant current flowing in the circuit has a minimum value. Currents circulating in both the C_o and C-L-R branches can be several times greater than the resulting current but smaller than those that prevail during series resonance. In other words the current can be greatly magnified. By analogy, the parallel resonant frequency of the mechanical system is expressed by:

$$f_p^{mech} = f_s^{mech} \cdot \sqrt{1 + \frac{\delta}{\delta_0}} \tag{4.1.2-7}$$

At this frequency the velocity and amplitude of vibration are much smaller than during series resonant frequency. Therefore, parallel resonance conditions are disadvantageous. To achieve high efficiency, the ultrasonic excitor should work at the series resonant frequency.

An important parameter of the equivalent circuit is the distance between the series and parallel resonant frequencies. For a typical piezoelectric transducer the interval between these frequencies is in order of 1kHz and may be defined by:

$$\frac{f_p - f_s}{f_s} = \frac{1}{2} \cdot \frac{C_T}{C_o} \qquad (4.1.2\text{-}8)$$

The ultrasonic part of the UMFORM system comprises, apart from the transducer, a booster and a tool. The entire system has a relatively greater mass m, lower flexibility δ and higher mechanical resistance c than the transducer. These are reflected in the equivalent circuit by the higher inductance L_S, smaller capacitance C_S and higher resistance R_S (Fig.4.1.2-2b). Since the booster and the tool are tuned to the same frequency as the transducer, the serial resonant frequency of the whole system is the same as that of transducer. In order to satisfy Eq.4.1.2-8 for the circuit representing the whole ultrasonic part of the UMFORM ($C_S<C_T$), the parallel resonant frequency must decrease. The difference between serial and parallel resonant frequency may even decrease to a few Hz.

The natural frequency (Eq.4.1.1-2) depends on material characteristics, it is therefore implicit that the natural frequency is dependent on temperature. A portion of the energy provided to the vibrating system is used to overcome internal friction, which manifests as an increase in temperature. As a consequence of this increase, the natural frequency of the system also changes. The mechanical load imposed on the system during the forming causes additional changes. The output power of the generator, consequently the efficiency of the system, reaches a maximum when the system operates at the resonant condition. Variation of the generator output power with frequency is shown in Fig.4.1.2-4. To maintain the high efficiency, the generator supplying energy has to be equipped with a feed-back control loop, which tunes the generator to the actual resonant frequency automatically.

4.2. Materials for the ultrasonic tools.

Materials that are suitable for use in the construction of ultrasonic tools should meet technical criteria, which include it acoustic properties. Technically, the strength of the material should be sufficient to withstand operational stresses encountered during the process. Its wear resistance and toughens should be of the required order; surface treatment may be rendered to meet specific requirements. Surface coatings are particularly recommended as these produce a thin (in the range 2-10μm) hard layer incurring minimal distortion of the tool. Fatigue strength of the material is a major consideration in view of the high frequency of operation of tools.

Acoustically, materials used on ultrasonic tools should have low damping capacity – energy losses due to internal friction. Due to internal friction, the stress-strain path of an elastic body is of the form of a hysteresis loop (Fig.4.2-1). The area within the hysteresis loop represents the energy per a unit volume dissipated as heat. The quantity of this energy is a function of the metallurgical and mechanical characteristics of the material and is expressed by the formula [34]:

$$W^* = \pi \cdot \xi \cdot \sigma_{max} \cdot \varepsilon_{max} \qquad (4.2\text{-}1)$$

where ξ characterises energy loss due to internal friction. This factor is defined as a fractional decrease in vibrational energy per cycle:

$$\xi = \frac{\Delta W}{W} \qquad (4.2\text{-}2)$$

For most materials, this factor is frequency-dependent and its magnitude has to be determined experimentally either by direct measurement of the dissipated energy or by measurement of the intermediate quantity - amplitude of free vibrations. The latter method allows computation of the logarithmic decrement δ, which is defined as the logarithm of a ratio of the amplitudes of successive oscillations (Fig.4.2-2):

$$\delta = \ln \frac{a_i}{a_{i+1}} \qquad (4.2\text{-}3)$$

If the logarithmic decrement does not depend on the absolute magnitude of the amplitude or the damping is small, the following formula may be used:

$$\delta = \frac{1}{n} ln \frac{a_i}{a_{i+n}} \tag{4.2-4}$$

The relationship between the damping factor and logarithmic decrement is:

$$\xi = 2 \cdot \delta \tag{4.2-5}$$

It follows from the fact that the energy of the wave is proportional to the square of the amplitude $W \approx A^2$. In the case when the energy dissipated depends on frequency Eq.4.2-5 is true only for the resonant condition.

Energy dissipation is an important factor affecting both the vibration intensity and development of fatigue damage. If the energy dissipated into the tool material causes a substantial increase in temperature, the mechanical properties would be changed significantly. A prismatic bar of a length l, vibrating longitudinally at frequency f in the first mode (Fig.4.1.1-2a), incurs an energy loss, which is described by the following equation (refer to Appendix 4.2.1):

$$W_{lost} = \frac{\pi^3}{2 \cdot l^2} \cdot \xi \cdot E \cdot A_o^2 \cdot V \tag{4.2-6}$$

The energy, which is expended in the vibrating element, increases its temperature, which in turn decreases its Young's Modulus, decreasing natural the natural frequency (Eq.4.1.1-2). This phenomenon makes it essential that the generator is equipped with the frequency feed-back control loop. Further, to minimise this phenomenon the amplitude of vibration should be limited.

Information on damping characteristics of engineering materials is rarely available and reported data in majority cases concerns damping at low frequencies. A systematic study of damping properties of various materials at frequencies up to 1kHz, was conducted by Pisarenko [80]. This text contains information on approximately one hundred materials: damping properties of several grades of steel, non-ferrous alloys, refractory material and cast iron were specified. Many of these are Russian specifications for which there are no equivalents in the West. Damping properties of plain carbon steels, stainless steel, brasses, bronzes and aluminium

alloys at a frequency of 11625Hz are reported by Adams [81]. All presented data was obtained under the same experimental conditions, thus, enabling comparison. Information on damping of various materials is also given by Silin [34] and Kuzmenko [82]. The latter also reported a monotonic increase in fatigue strength with loading frequency when the specimen temperature remained reasonably constant. An indication of the damping characteristics of materials may be provided by the Charpy test. This test is frequently used as a measure of the material toughness, which describes ability of the material to resist fracture and to absorb energy. Low damping corresponds to low to moderate toughens.

Materials used for the ultrasonic tools should be characterised by a low damping coefficient.

4.3. Operating frequency, generator, transducers and boosters.

A frequency of 20kHz was chosen as the operating frequency. The generator, transducer and boosters used in the experiments were designed and manufactured specially for this application.

The generator supplies the transducer with a AC voltage at a frequency that should be equal or very close to the series resonant frequency of the sub-assembly comprising the transducer, booster and tool. Its frequency could be adjustable within the range 0kHz - 25kHz. The maximum output power of the generator was 1.5 kW and was equipped with a feed-back control loop which traced changes in the resonant frequency and matched the generator frequency to the current resonant frequency. In the course of the project the generator underwent several modifications. Initially, a two-channel generator (Version A, Fig.4.3-1a) was designed since it was assumed that the resonant frequencies of both beams in the WT/P would the same. For this reason both single-phase resonant converters, FBI1 and FBI2, were controlled using one control unit, either CU1 or CU2. This could be selected using the switch SW. A block diagram of the feed-back control loop and waveforms of the control signal are shown in Fig.4.3-2. However, the natural frequencies of the beams were different and had to be excited at frequencies that matched their natural frequencies. By removing

switch SW two separate generators (referred to as Version B) were created (Fig.4.3-1b). These generators were additionally equipped with the overload protection unit OCP. The feed-back control loop (Fig.4.3-2) of these generators work sufficiently well when $f_{SET} > f_S$; ie. the generator frequency had to be higher than the resonant frequency. To overcome this deficiency the feed-back control loop was redesigned. The new version of the feed-back control loop and waveforms of the control signal are shown in Fig.4.3-3. This feed-back control loop and an additional overloading switch OS were incorporated in Version C (Fig.4.3-1c). Version A and B of the generator were used in the experiments using the WT/P tool. Experiments using the WT/I tool were performed either with Version B or C.

Three, high-powered Langevin type, transducers were constructed. The design of the transducer and the materials used are shown in Fig.4.3-4. The transducer comprised four piezoelectric discs, which are retained between two metal clamps. Electrodes separate the disks. Piezoceramics are brittle; consequently the discs are liable to fracture if subjected to tensile stress, thus they are preloaded in compression by the clamp. However, a level of applied pre-stressing influence the resonant frequency of the transducer [83, 84]. More information on the design procedure of transducers is provided by Gough [85]. Performance characteristics of the transducers are shown in Table 4.3-1.

Table 4.3-1: Performance characteristics of transducers

Transducer number	f_S in Hz	f_P in Hz	R in Ω
2064	20 081	21 219	18.0
2065	20 029	21 204	17.5
2066	20 096	21 325	18.0

Efficiency of the transducers was estimated in a test in which two transducers were coupled together: one acted as an oscillator, while the another one acted as an excitor (Fig.4.3-5). By measuring the supplied and absorbed power the efficiency of each was computed using the formula:

$$\eta = \frac{P_{abs}}{P_{sup}} \qquad (4.3\text{-}1)$$

The efficiency of the transducer was found to be 0.9. The amplitude of vibrations at the face of the transducer was 0.006mm.

Two stepped-type, half wavelength boosters were used to amplify vibrations (Fig.4.3-6). These were manufactured from a high strength aluminium alloy. Magnifications of the boosters were 2:1 and 1:1. The amplifying role of elements of changing cross-sections may be explained using the wave propagation theory. It follows from Eq.1.4 that the transmitted stress form a section of larger to the section of smaller cross-section has a greater magnitude than the stress in the section of larger area. Since $\varepsilon = E/\sigma$, the strain, and consequently, the amplitude of vibration in the smaller section is larger.

4.4. WT/P tool.

4.4.1. Concept

The purpose of constructing the WT/P tool was to evaluate the influence of ultrasonic vibrations on friction. This could be accomplished by applying vibrations in the direction perpendicular to the forming force and parallel to the friction force. Under such conditions, other effects, which may contribute to the forming force reduction, are eliminated. Such conditions may be achieved during the upsetting of test specimen between two prismatic, parallel beams vibrating longitudinally. Among the vibration modes of a free bar (Fig.4.1.1-1), the second mode is the most suitable (Fig.4.1.1-1c). In this mode, the length of the beam is equal to the wavelength λ ($l = \lambda$). The concept of the tool is shown schematically in Fig.4.4.1-1. The following equations defines the motion and frequency of the second mode of the beam:

$$u(x,t) = A_o \cdot \cos\frac{2\pi x}{l} \cdot \cos(2\pi \cdot f_2 \cdot t) \qquad (4.4.1\text{-}1)$$

in which

$$f_2 = \frac{1}{l}\sqrt{E/\rho} \qquad (4.4.1\text{-}2)$$

Velocity v and stress σ at a cross section at the distance x from the end of the beam can be calculated from the following formulae:

$$v(x,t) = \frac{du(x,t)}{dt} = -2\pi \cdot f_2 \cdot A_o \cdot \cos\frac{2\pi x}{l} \cdot \sin(2\pi \cdot f_2 \cdot t) \qquad (4.4.1\text{-}3)$$

$$\sigma(x,t) = E \cdot \varepsilon(x,t) = E \cdot \frac{du(x,t)}{dx} = -\frac{2\pi}{l} \cdot E \cdot A_o \cdot \sin\frac{2\pi x}{l} \cdot \cos(2\pi \cdot f_2 \cdot t) \qquad (4.4.1\text{-}4)$$

The following condition are fulfilled:

(a) for $x = l/4$ and $x = 3l/4$ A = 0

$$v = 0$$

$$\sigma(t) = -\frac{2\pi}{l} \cdot E \cdot A_o \cdot \cos(2\pi \cdot f_2 \cdot t)$$

(b) for $x = 0,\ l/2,\ l$

$$u(t) = A_o \cdot \cos(2\pi \cdot f_2 \cdot t)$$

$$v(t) = -2\pi \cdot f_2 \cdot A_o \cdot \sin(2\pi \cdot f_2 \cdot t)$$

$$\sigma = 0$$

Points along the beam at $x = l/4$ and $x = 3l/4$, where the displacement is equal to zero at any time were selected to support the beam. Plastic deformation of the work-material was effected at the mid-section of the beams where the amplitude of vibrations is a maximum. To achieve maximum effect, the beam vibrations should be "out–of-phase" by π with respect to each other; when the beams were in phase, the test specimen would be stationary relative to the beams. To obtain π phase shift, the beams need be exited from the opposite ends using a common generator.

4.4.2. WT/P tool design.

The detailed design of the WT/P tool is shown in Fig.4.4.2-1. A die-set, comprises two plates and two columns. The lower plate (1) is fixed to the press table while the upper plate (2), equipped with ball-bearing bushes, can be displaced vertically along the columns (3) and is connected to the press ram (4) through the load cell (5).

Two beams (UB) and (LB) of a cross section 50 x 50 mm are excited longitudinally. Vibrations of the transducers (UT) and (LT) are transferred to the beams through the boosters (UH) and (LH) respectively. The lower beam (LB) rests on a supporting blocks (6) which are fixed in position on the lower plate using fixing blocks (7), (8) and (9). Springs (10) held the beam on the supporting blocks. The upper beam (UB) is attached to the underside of the upper plate in a similar manner.

4.4.3. Design of the beams and the supporting blocks.

The design of the beams is critical to the performance of the process; again these have to comply with mechanical and acoustic constraints. Steel 30HGSA of chemical composition 0.28% C, 0.8-1.1% Mn, 0.9-1.2% Si, max. 0.03% P, max. 0.025% S, max. 0.3% Ni, max. 0.3% Cu matched these requirements since it displayed high mechanical strength and low damping characteristics. The loss coefficient ξ of this steel is $3.0 \cdot 10^{-4}$ in the "as delivered conditions" and decreased to $1.4 \cdot 10^{-4}$ after heat treatment (from 860-880° C, quenching in oil, tempering 120° C for 2 hours) [34]. The beams were subjected to this heat treatment after machining; the resulting hardness was 50HRC.

The length of the beam was made to be equal to the wavelength, which can be calculated using the formula:

$$\lambda = \frac{c}{f} \qquad (4.4.3\text{-}1)$$

Sound velocity c can be calculated using Eq.1-3. Alternatively, this velocity can be measured. The latter method was used, as it was more reliable. The scheme for sound velocity measurements is shown in Fig.4.4.3-1. A specimen, made from the same material as beams, of a length L_S approximately a half wavelength was attached to the transducer, which was supplied with a voltage of variable frequency. A special measurement bridge was used to measure energy supplied by the generator; at resonant frequency f_r, the energy drawn from the generator reaches a minimum. Since the length of the test specimen is known and the resonant frequency had been established, the velocity of sound may be computed using the following formula:

$$c = 2 \cdot L_S \cdot f_r \qquad (4.4.3\text{-}2)$$

In the experimental programme, the velocity of sound was measured in two specimens - one heat-treated to beam specification and the other in the "as delivered" condition. The following table (Table. 4.4.3-1) shows the specimen lengths and results of resonance measurements.

Table 4.4.3-1: Velocity of sound

Parameters	As delivered	As heat treatment
l [m]	0.1286	0.1289
$\lambda=2 \cdot L$ [m]	0.2572	0.2578
f [Hz]	20060	19800
c [m/s]	5159.4	5104.4

The transducers, manufactured for this application, had resonant frequencies of 20081, 20029 and 20096 Hz respectively. For a sound velocity of 5104.4m/s, the corresponding resonant lengths of the beams were 0.2542, 0.2549 and 0.2540 m.
Beams of length 0.2542m and 0,2540m were produced and the final tuning was performed on assemblies comprising the transducer, booster and beam. Resonant frequencies of the assemblies are shown in the Table 4.4.3-2.

Table 4.4.3-2: Resonant frequencies of the assemblies

Assembly	f_S in Hz	f_P in Hz
Transducer 2064+ booster (2:1) + beam U	20000	20023
Transducer 2066+ booster (2:1) + beam L	19998	20022

It was observed that the specimen placed at the antinode of the vibrating beam displaced itself towards the node of the beam. To prevent this, a shallow recess to contain the specimen was machined on the lower beam. To maintain symmetry, a similar cavity was required on the opposite side of this beam. However, the incorporation of these recesses increased the resonant frequency of this beam by 50 Hz. Further, the surface hardness had to be increased to prevent the smearing of

Aluminium specimens; beams were ion-nitrided to acquire the required surface hardness of 70 HRC. This surface treatment increased the resonant frequencies of the beams. Thus, the final resonant frequencies of the assembly of the upper and lower beam were 20180 and 20230Hz respectively. This contradicted with the original tool design concept. The excitation of two beams using one generator would not be feasible because of this mismatch between the natural frequencies of the beam. The amplitude of vibration of one beam would not be sufficient to effect deformation. The alternative of exciting each beam individually would also not be feasible, as the specimen would oscillate laterally in unison with the beams. This is illustrated in Fig.4.4.3-2 using a low frequency vibration. The upper beam is excited at a frequency lower than the lower beam. Consequently the period of vibration of the lower beam is $\tau_U > \tau_L$. Graphs in Fig.4.4.3-2b show the variation of the velocity of the middle section of the both beams. Under the specified conditions, the velocities of the beams relative to the specimen changes continuously as shown schematically in Fig.4.4.3-2b. Two situations can be distinguished (refer to the vectors v_U and v_L shown above Fig.4.4.3-2b):

A - the velocities v_U and v_L have opposite directions, $\begin{matrix}\rightarrow\\ \leftarrow\end{matrix}$ or $\begin{matrix}\leftarrow\\ \rightarrow\end{matrix}$

B - the velocities v_U and v_L have the same directions, $\begin{matrix}\rightarrow\\ \rightarrow\end{matrix}$ or $\begin{matrix}\leftarrow\\ \leftarrow\end{matrix}$

It can be observed that:

(1) During one period τ_U the situations A and B occurred twice.

(2) The given values of v_U and v_L repeated every $\Delta t = \frac{\tau_L}{\varepsilon_\tau} \cdot \tau_U$ where $\varepsilon_\tau = \tau_U - \tau_L$; for the WT/P tool, the difference ε_τ was only $3 \cdot 10^{-7}$ sec.

(3) Over a period Δt, the total time in which the situation A prevails is equal to that when the situation B prevails.

(4) The longest period when either the situations A or B prevails is $\tau_L / 2$; for the WT/P tool $(\tau_L / 2) \approx 2.5 \cdot 10^{-5}$ sec,

(5) The shortest period when either the situation A or B prevails is $\varepsilon_\tau = \tau_U - \tau_L$; for the WT/P tool $\varepsilon_\tau \approx 3 \cdot 10^{-7}$ sec.

Situation A is desirable since the friction forces acting on both faces of the specimen have opposing directions. Situation B detracts from the process aims, since friction forces acting on the specimen have the same direction and may move the specimen, together with the beams, laterally. However, periods when the friction forces act in the same direction, particularly at the beginning and the end of the every Δt, appear to be too short to cause an effective movement of the specimen. It is expected that the performance of this tool would not be adversely affected by this phenomenon. Finally, the experiments were performed using two generators.

The load capacity of the beams was calculated from the maximum permissible bending stress. Assuming a comparatively low stress of 100MPa the load capacity was estimated to be 64kN. It should be noted that the maximum bending stress does not coincide with the maximum stress induced due to vibrations. The former acts at the middle of the beam, while the latter acts at the nodes.

The supporting blocks are shown in Fig.4.4.3-3a. These are made from the same material as the beams e.g. steel 30HGSA. The yield strength of which, after hardening and tempering, is equal to 1300MPa.

The supporting blocks should satisfied the following requirements:

(1) Contact area between the block and the supported beam should be as narrow as possible,
(2) Endure the upsetting stress, and
(3) Vibrations of the beams should not be transmitted through the blocks to the die set.

To fulfil the first requirement, the surface of the block, which is in contact with the beam, should have a cylindrical form. Contact pressure between a cylinder and a plate is described by the formula [86]:

$$\sigma = 0.418\sqrt{\frac{0.5 \cdot F \cdot E}{b \cdot R}} \qquad (4.4.3\text{-}3)$$

For a cylinder of radius 100mm and maximum permissible load of 64kN, the pressure at the contact is 473N/mm^2, which is much lower than the Yield Strength of the steel used for constructing the beams.

Pure longitudinal waves occur only in solids whose dimensions in all direction are greater than a wavelength. In the case of the vibrating beam, lateral contraction and elongation accompanies periodical elongation and contraction at the nodal points respectively. These periodically changing strain may be the source of the secondary wave in the supporting block. To prevent further wave propagation, the length of the blocks is specified as one-quarter wavelength. In such case the nodal points coincide with the base of the supporting block (Fig.4.4.3-3b).

4.5. WT/I tool.

4.5.1. Concept

The WT/I tool was used to evaluate the potential for applying ultrasonic excitation to commonly used industrial processes: this evaluation was conducted using processes which are characterised by different types of material flow and force variation over the process cycle. The tool was designed for use in a variety of processes. Interchangeable tooling enabled tool configurations to support experiments in heading, indentation, back extrusion and wire flattening. The excitation system, which had to comply with requirements for sustaining resonant conditions and the manner in which forces could be transmitted, was a dominant influence on the selection of these processes; a detailed description of this tool is provided in Chapter 4.5.2.

The chosen processes are defined in the following text:

Heading is an upsetting operation, performed on the end of a round rod in order to produce a larger cross section (Fig. 4.5.1-1). It is a transient forming process, that is,

the velocity field (Fig.4.5.1-2), and the other process-related quantities, especially stresses and forces, change during the process. Material flow, deformation distribution and the forming force are affected by friction conditions at the work-material/tool interface. Friction has an increasing influence with reduction of the specimen and is higher for specimens with lower aspect ratios. The forming force increases with the height reduction.

Indentation is a process in which a tool form penetrates the work-material resulting in local deformation. The process may be carried out while the test-specimen is retained in a container or while the specimen is unsupported (Fig.4.5.1-3). For the former case, the work-material is displaced in the direction opposite to tool motion; as a result, the height of the work-material increases. In the free indentation case, the work-material expands laterally while maintaining approximately, the same height. To minimise changes in the work-material dimensions, the ratio of the cross-sectional area of the tool to cross-sectional area of the work-material should not exceed 0.3. The deformation field changes with the punch penetration (Fig.4.5.1-4a). This is reflected in changes of hardness with punch penetration. The bulk of the deformation occurs in the vicinity of the tool. Both, flow stress and the indentation force increase with penetration.

Back Extrusion is adopted to produce can-like components; the component section is defined by the space between the punch and the die (Fig.4.5.1-5a). During the early stage of the process, the work-material deforms laterally to fill the container; a small amount of work-material extrudes into the space between the punch and die; further penetration of the punch results in the extrusion of material past the punch. A dead-metal-zone (dmz), adheres to the base of the punch, the scale of which is affected by the thickness of the base of the can and the reduction in area $\varepsilon = (S_o - S_1)/S_o$. Fig.4.5.1-6 shows the deformation zone during can extrusion; variation of the forming force with the punch displacement is shown in Fig.4.5-5b. The forming force increases rapidly at the beginning of the process due to both, the elastic deflection of the tool/work-material system and work-hardening of the deformed material. After

reaching a maximum, the force reduces slowly as a result of the decreasing volume of the material in the deformation zone. The force variation with punch displacement is different for different reductions, samples of which are shown in Fig.4.5.1-5b. At the end of the process, when the base thickness is small, the forming force increases again as greater upsetting forces are required to deform the remaining material due to the low aspect ratio of the material in the container.

The processes described, so far, are characterised by non-steady-state material flow. Wire or strip drawing and rolling are processes in which a steady-state deformation is sustained. Due to the steady-state of material deformation, stresses and forces remain constant during the process. Material flow in wire drawing is shown in Fig.4.5.1-7. Unfortunately, none of these processes could be subjected to experimental analysis using the proposed equipment. However, a process referred to as **Wire Flattening**, which is an alternative to the rolling to produce flat wires [87, 88] could be performed using this equipment. Wire can be drawn between two dies with a convergent space to produce flat wire. Ultrasonic vibrations can be applied to the upper die. The wire flattening process is shown schematically in Fig.4.5.1-8. The process based on these principals has been adopted for sharpening scalpel blades [89]. The blade edge thickness is reduced to 2μm in two drawings between longitudinally vibrating dies.

4.5.2. Design of WT/I Tool.

The design of the WT/I tool is shown in Fig.4.5.2-1. The die-set for the WT/I tool consists of an assembly of two plates (1) and two columns. The lower plate is fixed to the press table. The upper plate, equipped with ball-bearing bushes, may be displaced vertically along the columns (2) and was connected to the press ram through the beams (3). The forming tool sub-assembly, consisting of the punch holder, punch, booster and transducer, is suspended, by the flange (4) on the punch holder, between two nylon washers (5) and secured to the upper plate (1). Two screws (6), located diagonally on the upper plate, acted both as a stop to prevent overloading the punch and to set the gap between the tools.

The anvil, which is of one-quarter wavelength, is fixed to the lower plate of the die-set in a manner similar to the punch holder. Sets of interchangeable tooling parts enable tool modification for the four different processes: back extrusion, indentation, heading and wire flattening. The tooling used for the back extrusion and indentation processes are shown in Fig.4.5.2-2a and Fig.4.5.2-2.b respectively. The same punch, referred to as WT/I – 1.06 series (Fig.4.5.2-3), is used for both processes. Heading was performed using tools shown in Fig.4.5.2-4a and Fig.4.5.2-4.b shows the tooling used to perform wire flattening.

4.5.3. Design of punch holder.

The punch holder is an important part of the WT/I tool. This is used not only as a holder for interchangeable changeable punches but also to suspend the whole vibrating system. Being a part of a part of the vibrating system, the punch holder design has to comply with resonant conditions. The punch holder, together with the punch, should maintain the tuned vibration mode shape throughout the forming process under varying load conditions. To comply with this requirement, the punch holder geometry should be such that the chosen mode is well isolated from the other natural frequencies. The geometry of the punch should also enable its suspension without depressing the tuned vibration amplitude by transmitting vibration energy to the supporting structure. The nodal point, where the motion is minimum, is a desirable place for support. However, this is the region of the highest periodically changing stresses (Eq.A4.2.1-6, Appendix 4.2.1), which cause lateral expansion and contraction of the punch holder. A rigid support would constrain this movement. A tube with a collar, attached at the node, would create a flexible support. The tube should be strong enough to endure stresses imposed by both load and vibrations. The design of the punch holder is shown in Fig.4.5.3-1.

The relationship between the natural frequencies of longitudinal vibrations of a bar and its length is given by the theoretical formula given in Eq.4.1.1-2. This formula can be used to compute the length of an element vibrating at a given frequency f in this mode. However, this equation provides an accurate value only for elements of small cross-sectional area in which the deflection in the lateral direction may be

neglected. Frequencies of cylindrical bars of different diameters computed using Finite Element analysis showed good agreement with those obtained from Eq.4.1.1-2 only for cylinders diameters up to 4mm. The thicker cylinders were found to have higher frequencies. When the shape of the element is complex, this discrepancy would be even more significant. This is illustrated in Fig.4.5.3-2, which shows the second longitudinal mode of vibration and the corresponding frequency of three cylindrical elements (made from titanium) of varying diameter. All elements are of the same overall length of 125mm while the lengths of the section of a particular diameter are different. Further, it is apparent from the figure that the location of the nodes is also shape dependent. Thus, Eq.4.1.1-2 is used to estimate an approximate length, which requires further refinement. An important feature of the punch holder is the precise location of the tubular collar at the node. Since the punch, when attached to the punch holder, creates an additional mass it may be expected that it would affect the natural frequency and the position of the node in the punch holder; for this reason the combination of these elements should be analyse as a unit. Finite Element approach was adopted to evaluate the punch holder design. Modal analysis enabled the fine- tuning of punch holder geometry to the chosen resonant frequency without the need for iterations throughout proving trials. Further, FE analysis was used to assess the stress in the punch holder due to excitation and load. Analyses were performed using ABAQUS/Standard code; FREQUENCY procedure was used to compute natural frequencies and modes of vibrations while STEADY STATE DYNAMIC procedure was employed to estimate the response of the punch holder to harmonic excitation [90]. In the latter case the excitation input was assumed to be a time function $Q(t)$ of known amplitude A_o, of frequency *f*, which can be expressed by $Q(t) = A_o \cdot sin(2 \cdot \pi \cdot f \cdot t)$. Thus, the vibration response of the vibrating element can be expressed by $R(x,t) = u(x) \cdot sin(2 \cdot \pi \cdot f \cdot t + \varphi)$ in which $u(x)$ denotes the longitudinal displacement of the point at x and φ, the phase delay. From the forced-vibration analysis, the relation between $u(x)$ and A_o, f can be established so that the response of the tool under the applied excitation can be evaluated. This enabled the computation of strain and stress. A 2D axisymmetry model was used for simulations.

The punch holder was made from ARNE steel of the following mechanical properties shown in Table 4.5.3-1.

Table 4.5.3-1: Mechanical properties of ARNE steel

Compressive strength [Pa]	E [Pa]	ρ [kg/m^3]	μ
1800	2.05×10^{11}	7850	0.3

Finite element computations were performed for two punch designs. The one shown in Fig.4.5.3-1 has threaded hole at each end, which is referred to as the plain punch holder. The second design has a hole through the whole length of the punch holder; this is referred to as the hollow punch holder. Using Eq.4.1.1-2 the length of the punch holders at the resonant frequency 20kHz was computed to be 127.8mm. Due to the symmetry of the punch holder, the tubular collar was located half way along the punch holder length. However, the FE computation showed that the length of the plain punch holder should be 128.9mm long, while the hollow punch holder should be 130mm to comply with the resonant condition. The vibration mode of the sub-assembly with the plain punch holder at this frequency is shown in Fig.4.5.3-3a. The amplitude distribution due to forced vibration with an amplitude of A_o=10μ is shown in Fig.4.5.3-3b. Attachment of the punch to the punch holder changed the node position marginally. However, in the hollow punch holder the node shifted by a few millimetres. As a result the middle cross section of the punch holder, where the tubular collar is located, had an amplitude of about 1μm (Fig.4.5.3-3c). Consequently, the plain punch holder was used for experiments. Distribution of the equivalent σ_e and axial stress σ_{22} induced by vibration with amplitude of 10μm is shown in Fig.4.5.3-4a and Fig.4.5.3-4b. The highest stress at the nodal point had a magnitude of 55MPa. Fig.4.5.3-4c and Fig.4.5.3-4d show the axial σ_{22} and equivalent stress σ_e induced due to a compressive load of 13 kN.

4.5.4. Design of anvil.

Two approaches have been adopted for anvil design [1, 41]. In the first approach, the anvil dimensions comply with the resonant condition so the ultrasonic wave propagates in it. This arrangement is shown in Fig.4.5.4-1a. The length of the anvil may be equal to either a quarter or full length of the wave. The fixing feature on the anvil should not interfere with the vibration. The vibration system with such an anvil is referred to as a closed system. In the second approach, the anvil has arbitrary dimensions and is fixed rigidly. Therefore, the ultrasonic standing wave does not propagate beyond the tool. The vibration system with this type of anvil is referred to as an open system. The amplitude distribution along an open vibrating system is shown in Fig.4.5.4-1b. Open vibrating systems are recommended only for the deformation of soft materials or small specimens since, under high loads, the vibration of the whole system would be dampened [1,42].

Considering the above information, the decision was to use an anvil of dimensions complying with the requirements of resonating system. Because of the limiting space on the press, the anvil length was selected to be equal to one quarter of the wavelength. The anvil design is shown in Fig.4.5.4-2. The anvil has the fixing feature similar to that for the punch holder. It was assumed that the anvil would vibrate at the resonant frequency in the first mode characteristic for a bar with a fixed end. The formula defining the relationship between the natural frequencies of the longitudinal vibration, the element length and the sound velocity under such boundary conditions has the following form:

$$f_i = \frac{c}{4 \cdot l} \cdot i \quad \text{for } i = 1,\ 3,\ 5,\ \ldots \qquad (4.5.3\text{-}1)$$

For $l = 0.0665m$ and sound velocity $c = 5142 m/s$, the first longitudinal mode of vibration had a frequency of 19330Hz.

The assumption that the anvil would vibrate at this mode turned out to be incorrect. The measurement of the anvil amplitude using the inductive sensor (see Section 5.3.1) showed that the anvil was vibrating with amplitude smaller than 1 μm but at a frequency about 60kHz. These results were later confirmed by Finite Element computations which show that the natural frequency of the anvil were different from

that assumed. It was found that the first two longitudinal mode of vibration had frequencies of 38433Hz and 67955Hz. Further, at these frequencies, the anvil vibrates in a mode characteristic for a bar with free ends. This is clearly evident from Fig.4.5.4-3, which shows these modes and the amplitude distribution along the axis of the anvil.

It was estimated that the anvil behaviour had a minor influence on the experimental results. In accordance with the wave propagation theory, an anvil of natural frequency equal to the resonant frequency would vibrate with much smaller amplitude from that of the punch holder. Considering the back extrusion operation, the stress propagated in the punch before being transferred to the anvil had to travel through several interfaces (see Fig.4.5.2-2): punch-specimen, specimen-washer and washer-anvil. Since each successive cross-section increased, the magnitude of the transferred stress decreased and so did the strain and consequently, the amplitude of vibration.

The mechanical impedance of the materials used for construction of all components also influences the final magnitude the transferred stress. The lower the mechanical impedance, the smaller the magnitude of the stress. For example, in the case of back extrusion, the magnitude of the stress transferred from the punch to the steel and aluminium specimen was 0.78σ and 0.44σ respectively, where σ is the magnitude of the stress wave in the punch induced by forced vibration.

4.5.5. Design of punches.

The original design of both, punches for wire flattening and heading were experimentally shown to be correct. However, the punch WT/I – 1.06, used for back extrusion and indentation, failed during the experimental trials, requiring several developments of the design. The first solid punch was hardened throughout to 60HRC (Fig.4.5.2-3a). The succeeding versions were compounded designs, comprising a ductile tubular threaded section with a ground thread (2) and a hardened punch (1), which was fitted into the inner diameter (Fig.4.5.2-3b, c and d). The following approaches were used for fitting the punch securely in the hole:

(1) Press fitting (WT/I –1.06, WT/I – 1.06C1),

(2) Slide fitting and cementing by means of Loctite 638 (WT/I – 1.06C-L),

(3) Forging the threaded section into a circular groove on the punch (WT/I - 1.06F).

The original solid punches made from steel Arne (58-60 HRC) fractured either at the beginning (marked as I and III) or the end of the threaded section (marked as II and IV) (Fig.4.5.2-3a). The former fracture occurred during free vibration while the latter occurred when the punch was under load. The first modification of the punch was a compounded punch (Fig.4.5.2-3b) with a ductile threaded section (48-50HRC) and a hard punch (58-60HRC). Both components were manufactured from ARNE steel. This variant was not successful, either. The punch fractured in the same manner.

The threaded section was analysed under loads to establish the failure mechanism. It should be noted that the thread was subjected to both static and dynamic forces. The static load is a consequence of tightening the threaded section to the punch holder, to the load applied during the forming process and, in the case of the modified version of the punch due to press fitting. A high tightening torque is required to achieve good contact at the screw-head/punch-holder interface in order to ensure good transmission of the acoustic wave and to prevent unwinding of the screw during vibration. A torque of 39Nm was applied to tighten the screw; this level of torque is normally used to join a transducer with a booster [91]. However, in the latter case, the thread form used was M12x1; the thread on punch was M10x1. The most probably reason for fractures I and III (see Fig.4.5.2-3) were the high stresses induced by this torque, which under vibration, lead to the fatigue fracture. Increasing the size of the thread should eliminate the fracture.

The applied torque did not cause fractures IV and II since stresses due to tightening were rather small in this section of the thread. Theses fractures may be attributed to the stresses caused by the dynamic load resulting from vibrations. In a cylindrical bar the axial stress at a given cross-section is the same and depends on the distance x (Appendix 4.2.1). However, the punch holder had axial holes (Fig.4.5.3-1) that could accentuate the stress distribution, causing stress concentration in the area near to bottom of the holes. It follows that the end section of the thread would also be subjected to the higher stress. Further, an axial elongation (and contraction) of the

punch holder causes its contraction (and elongation) in the radial direction. As a result the threaded section of the punch is subjected to cyclical radial compression. The stress induced by the compression is highest in the lower part of the threaded section. These two factors are the causes of fractures II and IV; shortening the threaded section would avoid the incidence of fractures.

The above-described consideration was supported by Finite Element analysis. Stresses induced by both the tightening procedure and that by vibrations were computed. In both cases, 2-D axisymmetric FE models were used. Screw tightening was modelled by introducing interference at the punch-holder/screw-head contact surface while the surfaces of the threads were in contact. The resulting pressure at the interface and, consequently, the force depended on the interference. The relationship between tightening torque, force at the interface and geometry of the thread (refer to Fig.4.5.5-1) may be expressed by the formula [92]:

$$M = \frac{F}{2} \cdot \left[d \cdot tg(\gamma + \rho) + d_m \cdot \mu \right] \qquad (4.5.5\text{-}1)$$

The punch was tightened to the punch holder using a torque of 39Nm. The resulting average pressure at the interface was 237MPa. The interference in the FE model was chosen such that the resulting pressure at the interference screw head/punch holder had the similar magnitude.

Distribution of the axial, radial and circumferential stresses in the threaded section of the punch, after tightening, is shown in Fig.4.5.5-2. Axial stresses of to 500MPa occurred in the upper part of the thread.

Forced-vibration analysis was employed to evaluate stresses induced by vibrations. The FE procedure, which was used to compute these stresses, is described in Section 4.5.3. Distribution of the stresses in the punch is shown in Fig.4.5.5-3. The lower part of the thread, at the point where the fractures occurred during experiments, is subjected to the highest stress. The amplitude of this stress is not high; however, it should be noted that this stress changes periodically, which could result in fatigue fracture. During a forming operation, both stresses are superimposed.

In order to avoid the incidence of the fracture the following modification were introduced:

- increase of thread form from M10 to M12 to reduce stress induced by tightening
- shortening of the threaded section to incidence of high-stresses
- manufacture of the threaded section from a tougher material - P20

These changes yielded positive results; fractures did not occur in the new redesign punches WT/I-1.06C.

In the course of experiments a further problem was encountered. The punch, which was press fitted into the threaded section, had a tendency to slip out under vibrations. Cementing the punch to the screw using Loctite 638 solved the problem. Another compounded punch, (Fig.4.5.2-3d), was made by joining the threaded-component to a circular section on the mating part by forging the material. (WT/I - 1.06F). A specific forging tool was designed to perform this joint.

4.6. Instrumentation

4.6.1. WT/P Tool

Experiments using the WT/P tool were conducted on the C-framed hydraulic press. The upper plate of the die-set was connected to the press ram while the lower plate was fixed to the press anvil. A load cell, placed between the upper plate of the die-set and the press ram, was used to measure the applied load. Unfortunately, the electrical noise introduced by the generator produced a signal, of the same level as the output from the load cell (5-10 mV). At the second stage of experiments the load cell was damaged; the magnitude of the applied load was therefore evaluated from the press controls.

The measuring system, produced by Micro-Epsilon, based on eddy current principals, was used to measure longitudinal displacements of the ends of the beams, the eddy current sensors, type S05, were placed opposite to the free ends of the beams. The measuring range for which was 0–0.5 mm; the measured distance from the target was

0.05-0.55mm due to an offset 0.05 mm. The corresponding output voltage was 0–10V.

A schematic diagram of the experimental set-up is shown in Fig.4.6.1-1 while the experimental equipment is shown in Fig.4.6.1-2.

4.6.2. WT/I Tool

Experiments using WT/I tool were performed on either a 15 kN pneumatic or 250 kN hydraulic press. Tooling shown in Figs.4.5.2-2 and Fig.4.5.2-4 was used to perform indentation, back extrusion, heading and wire flattening operations. Ultrasonically assisted heading, indentation and wire flattening processes were performed only on the 15kN pneumatic press while the back extrusion process was also performed on the 250kN hydraulic press. The pneumatic press was not fitted with ram movement control: consequently, the required load was applied by adjusting the ram pressure. This limited the experimental procedure, as will be discussed later in the text. The hydraulic press enabled full control over ram speed and the load-rate.

Amplitude of vibrations was measured using either, an inductive or an eddy current sensor. The inductive transducer was used in experiments conducted on the pneumatic press while the eddy current sensor was used during the experiments on back extrusion using the hydraulic press. The eddy current sensor has to be located perpendicular to the vibrating surface. Thus, the only surface, which might be used to measure amplitude, was the free front surface of the punch holder (Fig.4.6.2-1a). However, due to the space limitations, an inductive transducer, which can be located parallel to the vibrating element, was selected. This transducer was placed on the punch holder at the end opposite to the surface (Fig.4.6.2-1a) where the punch was located. Since the punch holder is of half wavelength, amplitude of vibrations at both ends is equal. The transducer was calibrated using a capacitive sensor; a disadvantage of using this transducer was that it showed only an average magnitude of the amplitude. The inductive transducer was only used in experiments performed on the pneumatic press.

The tool was modified, subsequent to the experiments on the pneumatic press, to physically accommodate the eddy current sensor. The redesigned section of the tool, with the eddy current sensor in position, is shown in Fig.4.6.2-1b. During the experiments conducted on the hydraulic press, a load cell was used to measure the applied force. In order to relate the punch load to the punch displacement, an inductive displacement transducer was installed on the upper plate of the die-set (see Fig.4.6.2-1c) to provide punch displacement data. All extracted signals were amplified and recorded using data acquisition system described in Chapter 4.6.3. Signals from the eddy current transducer were analysed using Discrete Fourier Transform. In the case of wire flattening, the pull-through force was measured using a Force Indicator type AFG250N produced by Mecmesin.

The WT/I tool fitted on the press is shown in Fig.4.6.2-2. A detailed description of the experimental conditions for each process is provided in Section 5.2.

4.6.3. Data retrieving system and signal processing

A PC-based data acquisition system - LabView, produced by National Instruments – was configured to record output signals from the sensors and the load cell. The signals were scanned using the AT-MIO-16E1 data acquisition board. The maximum scanning rate of this card is 1.25Mscan/s. Data can be streamed to the disk at the same rate using three 16-bit DMA channels. A 12-bit Analogue-to-Digital Converter converted the analogue signals. Measurement precision depends on the actual input range and gain and is expressed:

$$\text{Precision} = \frac{\text{Input range}}{\text{Gain} \cdot 2^{\text{resolution}}} \qquad (4.6.3\text{-}1)$$

According to the Nyquist theorem, misrepresentation of a signal can be avoided if the sampling rate of a signal is greater than twice the maximum frequency of the signal. The effect of under sampling is that the signal appears to have lower frequencies. Output signals from the eddy current sensors were scanned at a rate of 200kscan/s i.e. ten times of the frequency of the measured signal.

LabView is a graphical programming language for building virtual instrumentation systems, as a substitute for laboratory equipment. It provides tools, tightly integrated with measurement hardware, to produce solutions for data acquisition, control, signal processing and presentation. Virtual instruments (VI) are built into two panels; the front panel is the user interface, giving the interactive control of the software system and the block diagram panel in which the functionality of the VI is defined.

Three virtual instruments, created in LabVIEW, were used in the experiments either to check settings and acquire the experimental data or to analyse the recorded signals. The first of the VIs was used to check and correct the distance between the sensors and the beams, which should be in the range $0.2 - 0.3mm$; this verification procedure was repeated prior to each experiment.
The second VI was used to acquire output signals from the sensors and to record these in a binary file. The high sampling rate of 200kscan/s would not allow the observation and analysis of signals in real time.

The third VI was used to perform a spectral analysis of the recorded signals. The Fourier transform, which establishes the relationship between the time domain signal and its representation in the frequency domain, was used to calculate the frequency content and the amplitude spectrum magnitude of the signals. This information cannot be derived from the time domain analysis.
The definition of the Fourier transform of a signal x(t) is :

$$X(f) = F(x(t)) = \int x(t) \cdot e^{-j2\pi ft} dt \qquad (4.6.3\text{-}2)$$

If x(t) has a discrete character e.g. is defined only by a set of n particular values x_i, the discrete representation of the Fourier transform (DFT) has a form:

$$X_k = \sum_{i=0}^{i=n-1} x_i e^{-j \cdot 2 \cdot \pi \cdot i \cdot k/n} \quad \text{for } k=0,1,2,\ldots..n\text{-}1 \qquad (4.6.3\text{-}3)$$

Both, the time domain and the frequency domain representations of the signal have the same number of samples. A frequency spacing between the components X_k in the frequency domain is:

$$\Delta f = f_s / n \qquad (4.6.3\text{-}4)$$

This is also referred to as the frequency resolution.

5. EXPERIMENTAL PROCEDURE.

5.1. WT/P tool

Specimens used in experiments are shown in Fig. 5.1-1. Experiments were performed in two stages. During the first stage, experiments were carried out to verify the performance of the WP/T tool and the generator. The frequencies and amplitudes of the beam, under various mechanical load and voltage supplied to the transducers, were examined. Configuration and values of the experimental parameters are shown in Table 5.1-1.

Table 5.1-1: Verification procedure.

Material	Voltage [V]	Load [kN]	Measured parameters
Nylon	1000	0	Amplitude and Frequency
		15	
		25.5	
		38	
	1800	0	Amplitude and Frequency
		15	
		25.5	
		38	
	2600	0	Amplitude and Frequency
		15	
		25.5	
		38	

During this stage a nylon specimen (Fig.5.1-3.1a), which did not deform plastically was used.

The influence of surface excitation, in the direction perpendicular to the forming force, on the upsetting of steel and aluminium specimens was examined during the

second stage of the experimental work. Two-upsetting procedures were used. The first consisted on compressing the same specimen twice. The specimen was, initially, compressed without excitation and, subsequent to measurement of specimen height, was subjected to a similar load before applying excitation.

Table. 5.1-2: WT/P experimental conditions

Material	Specimen shape	Load [kN]	Transducer input voltage [V]		Comments
			Lower	Upper	
Steel 010	Fig.5.1-3.1b	7	0	0	First procedure was used.
			1800	0	
		7	0	0	First procedure was used
			0	1800	
		7	0	0	First procedure was used
			1800	1800	
		7	0	0	First procedure was used
			1800	1800	
			2600	2600	
		15	0	0	First procedure was used
			1800	1800	
		15	0	0	First procedure was used
			2600	2600	
		15	2600	2600	Second procedure was used
Pure Aluminium	Fig.5.1-3.1c	15	0	0	First procedure was used
			1800	1800	
		15	1800	1800	
		15	0	0	First procedure was used
			1800	1800	
		15	0	1800	Second procedure was used

During the second procedure, specimens were subjected to the load and vibration simultaneously. In both cases, the difference between the heights of the specimens deformed without and with excitation was used as to assess the influence of surface excitation on forming force. Configurations of the experimental parameters are shown in Table 5.1-2.

In all experiments amplitudes and frequencies of beams vibrations were measured.

5.2. WT/I tool

The geometry of test specimens used in the various experiments, described in the following section, is shown in Fig.5.2-1. Subsequent to the plastic deformation of these specimens, measures of the extent of deformation were taken using the parameters shown in the last of the sketches in each of the sub-sections of the figure.

5.2.1. Indentation

The indentation process was performed on the pneumatic press. Materials, dimensions of the specimens and the punch, amplitudes and lubricants used in experiments are shown in the Table 5.2.1-1.

Specimens were subjected to the same loads with and without superimposed vibrations. In some cases, a specimen was deformed in several stages. First, the specimen was loaded without vibrations and the indentation depth DI (Fig.5.2-1a) was measured. Next, this specimen was loaded with the same static load prior to the application of ultrasonic excitation. After pre-specified excitation duration, the specimen was unloaded and the indentation depth was measured again. This cycle was repeated several times with successively greater static loads. The load dwell-time (TU), under oscillatory conditions, was either 5 or 10 seconds. Other specimens were loaded only twice, as described in the procedure defined in the proceeding text. An alternative approach for indenting the specimen was to apply the load and excitation simultaneously.

Table 5.2.1-1: Indentation – experimental conditions.

Material	Dimensions [mm]		Load [kN]	Amplitude [mm]	Lubricant
	Punch	Specimen			
Aluminium	Φ 4.0	Φ 5.0 x 7.5	5.1	0	Sodium Stearate
				0.005	
			6.5	0	
				0.0065	
			3.1	0	
				0.01	
			3.7	0	
				0.01	
Aluminium	Φ 4.0	Φ 5.0 x 7.5	4.5	0	
				0.005	
			5.3	0	
				0.005	
			5.8	0	
				0.005	
			6.5	0	
				0.005	
Steel 010	Φ 4.0	Φ 5.0 x 7.5	6.1	0	MoS_2
				0.01	
			7.4	0	
				0.01	
			10.2	0	
				0.01	
			11.47	0	
				0.01	

5.2.2. Heading

The heading process was performed only on the pneumatic press. Specimens made from pure aluminium were used in these experiments. For a specific load specimens were deformed with vibration and without vibrations. The magnitude of the load was defined by setting pressure in the press cylinder. The upper surface of the specimens was lubricated with Sodium Stearate. Conditions of the performed experiments are shown in Table 5.2.2-1.

Table 5.2.2-1: Heading – experimental conditions

Material	Specimen	Load [kN]	Amplitude [mm]
Pure Aluminium	Fig.5.2-b	3.1	0
		3.8	
		4.5	
		5.2	
		5.8	
		6.5	
		3.1	0.0065
		3.8	
		4.5	
		5.2	
		5.8	
		6.5	

5.2.3. Back extrusion

Experiments in back extrusion process were conducted on both, the pneumatic and hydraulic, presses. Different experimental procedures were adopted for each press. Experiments conducted on the pneumatic press were similar to those for heading. For a specified load, specimens were deformed with and without vibrations. Specimens'

dimensions, materials, punch's diameter, amplitudes and lubricants used in these experiments are listed in Table 5.2.3-1.

Table 5.2.3-1: Back-extrusion – experimental conditions. Stage I.

Material	Dimensions [mm]		Load [mm]	Amplitude [mm]	Lubricant
	Punch	Specimen			
Aluminium I	Φ 4.0	Φ 5.0 x 7.5	5.1	0	Sodium Stearate
			5.8		
			6.4		
			7.1		
			7.5		
			7.8		
			5.1	0.002	
			5.8		
			6.4		
			6.4	0.003	
			7.1		
			5.8	0.007	
			6.4		
	Φ 3.0	Φ 5.0 x 7.5	1.06	0	
			1.22		
			1.70		
			1.83		
			2.03		
			1.06	0.01	
			1.22		
			1.70		
			1.83		
			2.03		
			2.03	0.004	

(Continued on the next page)

Table 5.2.3-1: Back-extrusion – experimental conditions. Stage I.

Material	Dimensions [mm]		Load [mm]	Amplitude [mm]	Lubricant
	Punch	Specimen			
Aluminium I	Φ 3.0	Φ 5.0 x 7.5	2.23	0	Sodium Stearate
			2.37		
			2.71		
			3.05		
			2.23	0.004	
			2.37		
			2.71		
			3.05		
Aluminium II	Φ 4.0	Φ 5.0 x 7.5	5.8	0	Sodium Stearate
			6.4		
			7.5		
			5.8	0.007	
			6.4	0	
Armco Iron	Φ 3.0	Φ 5.0 x 7.5	8.4	0.01	MoS_2
			9.13		
			9.82		
			10.5		
			11.2		
Steel 010	Φ 3.0	Φ 5.0 x 7.5	11.8	0	MoS_2
			13.2		
			13.9		
			14.6		
			11.8	0.01	
			13.2		
			13.9		

During experiments conducted on the 250kN press, the displacement of the punch and the forming force were recorded. The punch displacement and velocity or, in some cases, the maximum applied load were the pre-set conditions for the experiments. For a selected velocity, specimens were deformed with and without superimposed vibrations. The actual amplitude under loading conditions was measured during each experiment.

Table 5.2.3-2: Back-extrusion – experimental conditions. Stage II.

Material	Dimension [mm]		Amplitude [mm]	Ram velocity [mm/s]	Lubricant
	Punch	Specimen			
Aluminium I	Φ4.0	Φ5.0 x 7.5	0.0045,	0.5	Sodium Stearate
				1	
				5	
				10	
			0.0085	0.5	
				1	
				5	
				10	
Steel 010	Φ4.0	Φ5.0 x 7.5	0.0085	0.25	MoS_2

The dimensions of the test specimens are shown in Fig.5.2-1c.

5.2.4. Wire flattening

Wires, specified in the Table 5.2.4-1, were pulled through the gap between flattening dies with an entry angle of 16° (Fig.4.5.2-4c). Experiments were performed for a several die-gaps, with and without vibrations. The pull-through force was measured. The reduction in the wire diameter is define as:

$$r = \frac{D_o - G}{D_o} \qquad (5.2.4\text{-}1)$$

where G is the distance between the forming tools.

Conditions of the performed experiments are shown in Table 5.2.4-1.

Table 5.2.4-1: Wire flattening – experimental conditions.

Material	Diameter [mm]	Amplitude [mm]		Lubricant
Aluminium	Φ 1.0	0	0.1	Sodium Stearate + mineral oil
			0.22	
			0.3	
		0.007	0.3	Sodium Stearate + mineral oil
			0.4	
			0.5	
			0.6	
		0.7	0.5	Dry conditions
			0.6	
Al-G12 alloy	Φ 1.2	0	0.1	Sodium Stearate + mineral oil 0.007
			0.12	
			0.18	
			0.21	
			0.25	
			0.37	
			0.38	
		0.007	0.42	
			0.5	
			0.58	
			0.42	
			0.5	

(Continued on the next page)

Table 5.2.4-1: Wire flattening – experimental conditions.

Material	Wire Diameter [mm]	Amplitude [mm]	$\frac{D_o - G}{D_o}$	Lubricant
Cooper	Φ 1.2	0	0.17	Sodium Stearate Soap
			0.25	
			0.42	
			0.5	
			0.58	
		0.003	0.25	
			0.42	
		0.007	0.25	Sodium Stearate Soap
			0.42	
			0.5	
			0.58	
			0.25	Dry conditionn
			0.42	
			0.5	

6. FINITE ELEMENT ANALYSIS

A complementary approach to experimentally analysis is numerical analysis. Using numerical methods, it is possible to compute the shape of the work material, velocity field, distribution of stress, strain and temperature, pressure distribution at the interface work material/tool and forces acting on the tools. Many of these quantities cannot be accurately estimated using currently available measuring techniques or analytical methods. It should be noted that the reliability of the solutions form EF depends on accuracy of the material properties and boundary conditions that influence the process. Nevertheless, the solutions give a good quantitative description of process mechanic. Therefore, numerical analysis is a useful tool in investigating the nature of ultrasonically assisted metal forming processes, in particular phenomenon occurring at the work-material/too interface. This approach has been used by researches mainly to compute frequencies and modes of natural vibrations. In the present research numerical analysis was employed to evaluate the tool design as well the mechanisms by which the applied vibration influences material flow.

Numerical simulations of the investigated processes were performed using Finite Element analysis for which FE software, ABAQUS/Explicit, was used. Several advantages may be realised by using the explicit rather than implicit method. Firstly, ABAQUS/Explicit may to be us readily analyse numerical problems involving complex contact situation. Complex contact interactions, including occurrence of the periodical loss of contact can be anticipated while simulating the influence of vibrating tools. Secondly, due to the large deformation in extrusion re-meshing was necessary. A re-meshing tool – Adaptive Meshing – is provided in ABAQUS/Explicit only. Finally, the explicit method is more efficient in solving quasi-static processes such forging and rolling which are characterised by large deformation and grid distortion.

The simulations may be divided into two groups. The first group includes simulations, which were performed with a view to assessing the characteristic features of each process under static conditions (without vibration), in particular

forming force, energy requirements and stress distribution. Results of these simulations were used to evaluate experimental results and are presented in Section8.4. In these simulations, the tools were modelled as rigid bodies defined with analytical surfaces. The dimensions of the test billets were similar to those used in the experiments. Simulations were performed for commercially pure Aluminium, which was modelled as modelled as an elastic-plastic, isotropic, Huber-Mises material with material characteristics listed in Table 6-1.

Table 6-1: Materials characteristics and other parameters

	Aluminium	Steel
Young's modulus [MPa]	69000	210000
Yield Strength [MPa]	53	200
Strain-hardening curve	$\sigma = 715 \cdot (0.001 + \varepsilon)^{0.18}$	$\sigma = 159 \cdot (0.02 + \varepsilon)^{0.28}$
Poisson's ratio	0.3	0.3
Density [kg/m^3]	2670	8750
Friction coefficient μ	0.1	0.1

The process velocity was assumed to be 0.4m/s to reduce the computation time. For all simulations, the displacement of the punch was 4mm. Three processes – heading, indentation and back extrusion – were modelled using 2D axisymmetric models. Wire flattening was analysed using a 3D model. Due to symmetry, only a half-section of the wire was modelled. The simulated process was defined in two steps. In the first step, the wire was deformed by the tools to the required thickness i.e. 0.6mm. In the second step the wire was drawn with the constant velocity. Fig.6-1 shows FE models for indentation, heading and back extrusion and Fig.6-2 for wire flattening. The mesh for billets for indentation and heading was formed using CAX4R elements while C3D8R elements were used to describe the wire. A special mesh was required for the billet for back extrusion simulations due to re-meshing. Since Adaptive Mesh option in Abaqus/Explicit operates with the same mesh topology throughout the step, the initial mesh of the billet had to be selected to make it suitable for the entire duration

of the simulation. Fig.6-3 shows the undeformed and deformed mesh of the billet for back extrusion.

Simulations included in the second group were carried out to investigate the effect of applying vibration to the forming tool on material flow. Applications of numerical analysis reported in literature refer mainly to the computation of the resonant frequency, vibration mode shapes and stress field [27, 93, 94]. Simulations of ultrasonically assisted indentation and compression were reported by Huang et al. [29, 95]. In both cases frequencies of the applied vibrations were below 100Hz and a maximum process velocity of 1.6mm/s. The modelled material was assumed to have elasto-viscoplastic properties while the tools were model as rigid bodies.

Two processes, wire flattening and back extrusion, with vibrations applied to the tool, were investigated using Finite Element analysis. The wire flattening process was defined as a 3D model while the back extrusion process was defined as a 2D axisymmetric model. Further, two approaches were adopted in tool modelling. The tools for wire flattening were assumed to be perfectly rigid and were defined as analytical surfaces. This concept of modelling the rigid tools was based on the assumption that forces acting on the tools in this process were too small to affect the amplitude of vibration. Therefore, it was assumed that the FE model with the rigid tools vibrating with constant amplitude would replicate experimental conditions. Fig.6-4 shows this model. Simulations of this process were performed in two steps. In the first step, the wire was deformed by the tools to a thickness of 0.6mm. The second step was performed at two drawing velocity $150mm/s$ and $2000mm/s$. First the wire was drawn without vibration and then with vibrations applied to the upper tool.

Two FE models were used for back extrusion simulations. In the first model, tools, the die and the punch were defined as rigid analytical surfaces. The simulated process was defined in two steps. In the first step the billet was deformed under static conditions (without vibrations) due to the die movement at a constant velocity of $v = 200mm/s$. The process was continued under this condition till the steady-state

phase of the process was established. This corresponded to a die displacement of about 1.5mm. In the second step, vibrations were introduced to the punch by imposing a boundary constraints to this tool in the form of a sinusoidal displacement $A = A_o \cdot sin(\omega \cdot t)$. The second step was performed for four different velocities of the die, *20, 100, 200* and *500mm/s,* and the amplitude of vibration $A_o = 0.0085mm$. Simulations were performed with both frictionless and friction condition. Friction was assumed to follow Coulomb's Law with a friction coefficient $\mu = 0.1$. Fig.6-5a shows this model.

In the second FE model for back extrusion, behaviour of the punch and punch holder were also analysed. However, to simplify the model, the punch holder and punch were modelled as a one deformable body. The dimensions of this tool were exactly similar to that used for experiments thus, this simplification should not have affected simulations. This model is shown in Fig.6-5b.

The second model gave a better representation of the experimental configuration. The most important feature of this model was that the amplitude of vibration at the working surface of the punch was not constrained as a boundary condition as in the first model. Since the dimensions of the model tool complied with the resonant conditions, the vibration of the tool was simulated by applying a sinusoidal displacement $A = A_o \cdot sin(\omega \cdot t)$ or pressure $p = p_o \cdot sin(\omega \cdot t)$ to the free end of the tool. The former method corresponds to the experimental conditions in which a constant amplitude was retained over the process duration. The latter method corresponds to the experimental conditions in which the amplitude of vibration was not controlled during the process and its magnitude changed due to the applied load. Such conditions occur when the generator supplying power to the exciter is not equipped with an amplitude feedback control loop. In other words, the input voltage on the transducer, which determines the magnitude of the amplitude, is constant during the entire process. Such conditions characterised the experiments. For this reason, the vibration of the punch was simulated by introducing load-boundary condition.

The resulting amplitude of vibration depended on the magnitude of the applied pressure and damping characteristics of the material. The latter can be defined in ABAQUS/Explicit using Rayleigh damping [90]. For a system with several degrees of freedom, the equation describing its movement is:

$$M\{\ddot{u}\}+C\{\dot{u}\}+K\{u\}-F=0 \qquad (6\text{-}1)$$

the Rayleigh damping matrix is a linear combination of the mass and stiffness matrixes:

$$C=\alpha\cdot M+\beta\cdot K \qquad (6\text{-}2)$$

For a system with one degree of freedom this equation takes the form:

$$c=\alpha\cdot m+\beta\cdot k \qquad (6\text{-}3)$$

The α factor defines a damping contribution proportional to the mass matrix while the β factor defines damping proportional to the elastic material stiffness. For a particular mode of vibration with a frequency ω the fraction of critical damping $\xi=\frac{c}{c_o}$ for that mode is expressed in terms of damping factors, α and β, by:

$$\xi=\frac{\alpha}{2\cdot\omega}+\frac{\beta\cdot\omega}{2} \qquad (6\text{-}4)$$

This equation form the basis for selecting α and β.

Damping characteristics of the material have a significant affect on the simulation results when the response of the system to the disturbing force is analysed. Thus, damping characteristics of the modelled material should reflect closely that of the real material. In the case of the present simulations, the main reason for introducing damping was to achieve amplitude of a finite magnitude, otherwise the amplitude of vibration would increase to infinity. Magnitude of the introduced damping only influenced the magnitude of the resulting amplitude of vibration and the time to acquire this amplitude. Only a mass proportional damping α of an assumed value *17500* was introduced. This value corresponded to the fraction of critical damping

equal to 0.07. Introducing the β factor would decrease the incremental stable time, which was already very small due to the fine mesh of the billet and the punch. A pressure of 10MPa was required to achieve an amplitude of 0.0085mm which was the amplitude used in the experiments. The build-up of the amplitude at the free surface of the punch holder is shown in Fig.6-6a. Since the punch holder was of half wavelength, the displacement of the opposite end of the punch holder was delayed by $(T/2)$. This is illustrated in Fig.6-6b, which shows the amplitude variation with time at the working surface of the punch and at the surface where the pressure was applied.

Simulations were performed in two steps similar to those in the first model. However, in these simulations the die was stationary while movement was assigned to the punch holder. This arrangement was possible only in the case when the punch holder movement was achieved by applying sinusoidally changing pressure.

Two test materials were used in simulations; commercially pure Aluminium and mild Steel. Material characteristics and other process parameters are shown in Table 6-1.

7. RESULTS

This chapter presents the results of the experiments performed and finite element simulations. The following sections contain explanations of the results derived from experiments performed using both, the WT/P and the WT/I tools. Corresponding Finite Element analyses of the plastic deformation of the work materials are also presented to enable comparison.

7.1. WT/P tool

Preliminary experiments were conducted with the WT/P tool with a view to verifying tool performance under working conditions. Both, the frequency and amplitude of vibrations of both beams, were measured under applied loads in the range 0 - 38kN. The "no load" condition was when the specimen was subjected to the dead weight of the press ram. Frequencies of vibrations for excitation voltages of 1000, 1800 and 2500 were measured; for each voltage, measurements were made under loads of 0, 15, 25 and 38kN, results from which are shown in Fig.7.1-1 and 7.1-2 for the lower and upper beam respectively. The excitation voltage did not have significant influence on beam frequency. The maximum observed variation was about 30Hz. By contrast, imposing a mechanical load increased the vibration frequency. Variation of the frequency of the beams with load for an excitation voltage 1800V is shown in Fig.7.1-3.

The amplitude of vibration for the same operating conditions as that for frequencies are shown in Fig.7.1-4 and 7.1-5, for the lower and upper beams respectively. For a given load, the amplitude of vibration increased with the supply voltage to the transducers. The load had an inverse influence on amplitude. For a given excitation voltage, the amplitude decreased with load. Variation of the amplitude of vibrations with load for an excitation voltage of 1800V is shown in Fig.7.1-6. Generally, the upper beam vibrated with a lower amplitude than the lower beam. This may be accounted for, in part, by more severe stress conditions on the upper beam than that of the lower beam. Traces of fretting corrosion discovered on the upper parts of the WT/P tool suggested that working conditions of the upper beam were more sever

than those on the lower beam. Fretting corrosion occurs due to small movements of metal surfaces under high contact pressure. The methods of fixing the beams - the lower was supported on the blocks while the upper was suspended (Fig.4.4.2-1), could also influence beam amplitudes.

Additional information about tool performance can be derived from the graphs illustrating amplitude spectrums, which were obtained by applying Discrete Fourier Transform on the recorded signals. The amplitude spectrum shows harmonic components of the periodically changing signal. Fig.7.1-7a shows signals, which illustrate the displacement of the ends of the beams with time. The results of the Fourier analysis are shown in Fig.7.1-7b and c for the upper and the lower beam respectively. The measurements were taken for an excitation voltage of 1000V while the tool was unloaded. Fig.7.1-8 and 7.1-9, show signals and their amplitude spectrum recorded for the same excitation voltage under loads of 5.5kN and 16.0kN respectively. The subsequent figure Fig.7.1-10 show results obtained under a load of 38.0kN and an excitation voltage of 2600V. All results were obtained with the nylon specimen.

A similar analysis was performed on the signals recorded in experiments with Steel specimens. Fig.7.1-11 and 7.1-12 show the vibrations under loads of 7.0kN and 15.0kN respectively, for an excitation voltage of 1800V. Fig.7.1-13 shows signals and their amplitude spectrums recorded for an excitation voltage of 2600V and a load of 15.0kN

Fig.7.1-7 to 10 shows that when beams were not loaded, these vibrated at the resonant frequency. The amplitude spectrum contains only one component corresponding to this frequency. Under higher loads, other harmonic components appeared in the amplitude spectrum. However, amplitudes of these components are negligibly small. These observations refer to experiments in which nylon specimens were used. Results of the experiments using Steel specimens (Fig.7.1-11 to 7.1-13) show that the presence of the other component in the amplitude spectrum of vibration

appears to be more pronounced. In some cases, the amplitude of these components is about a quarter of the main component. The additional component, with the highest amplitude in the spectrum, of one beam coincides with the resonant frequency of the other beam. Coupling between the beams was evident. This phenomenon was not observed in the experiments with the nylon specimen because of the excellent damping properties of this material.

Experimental conditions and results of experiments with Aluminium and Steel specimens are presented in Appendix 7.1. The reduction in the height of the specimen deformed with and without superimposed vibrations was used to assess the influence of ultrasonic vibrations on forming force. Experiments with Aluminium and Steel specimens showed that the application of surface excitation, in the direction perpendicular to the forming force, increased the extent of plastic deformation. The reduction in height of the specimens was greater than that obtained without excitation for the same load.

Regardless of the procedure of applying excitation, the average reduction in specimen height was greater by about 10% and 5% for Steel and Aluminium specimens respectively. However, the increase in true strain was greater for Aluminium than Steel specimens. Neglecting barrelling, it was estimated that the strain of the aluminium specimens deformed, on average, 0.035 when vibrations were applied. For Steel specimens, the strain increased by 0.015. The influence of vibrations was less when only one beam was vibrated.

7.2. WT/I tool

7.2.1. Indentation

Variation of the indentation depth with applied force with and without vibrations for aluminium specimen is shown in Fig.7.2.1-1. The indentation area ratio of the specimens was 0.07 and the amplitude of vibration was 0.005mm. Indentation was carried out as described earlier in the text; the specimen was subjected to increasing loads with and without vibrations, in four successive stages. After each loading, the

indentation depth (DI) was measured. Fig.7.2.1-1 also shows the results of the experiment when the specimen was subjected to a load with superimposed vibrations twice. Initially, vibrations were superimposed for 5sec and followed by subjecting the specimen to vibrations for an additional 15sec. The results show that punch penetration increases when vibrations are imparted to the punch. Further, the figure shows that the holding time of the load with superimposed vibrations also has an influence on the final punch penetration.

Results of experiments with Aluminium specimens performed using the second procedure are shown in Fig.7.2.1-2. The graph shows the variation of the reduced indentation depth (DI/d_p) with the punch pressure for three different amplitudes of vibrations. For amplitudes of vibration of 0.005 and 0.0065, the experiments were conducted using punch loads of 5.1kN and 6.5kN; the corresponding punch pressures were 405.8MPa and 517.2MPa respectively. Vibrations, of an amplitude of 0.01mm, were superimposed while loads of 3.1kN and 3.7kN were applied to the punch; the corresponding punch pressures were 246.7MPa and 294.4MPa respectively. The results support the earlier observation that amplitude of vibrations has a significant influence on forming force. A reduced indentation depth of 0.33 was achieved with the punch pressure of 246.7MPa with an applied vibration of amplitude 0.001mm. The same depth was obtained under a pressure of 405.8MPa with an amplitude of 0.005mm.

Steel specimens were deformed in accordance with the second procedure. For a given punch load, one specimen was deformed without vibrations while the other was deformed with superimposed ultrasonic vibrations. Variation of the reduced indentation depth with punch pressure is shown in Fig.7.2.1-3. The amplitude of vibrations was 0.01mm.

7.2.2. Heading

The relative reduction of the free height of the specimen, defined as $(H_F-h)/H_F$ was used to compare experimental results and to assess the role of ultrasonic excitation in

the heading process. For a given punch load, two specimens were deformed, one without vibrations and the second, with the vibrations applied to the punch. Variation of the relative reduction of the free height is presented in Fig.7.2.2-1. The results show that the effect decreases with the reduction of the free specimen height. Fig.7.2.2-2 shows changes in the average axial pressure in the specimen with reduction of the specimen height. It can be estimated that a reduction of 0.6 was achieved for about 20% lower axial pressure in the ultrasonically-assisted operation. For a reduction of 0.7, the average axial stress was lower by about 8%.

7.2.3. Back extrusion

Results of the experiments performed on the pneumatic press are presented in Fig.7.2.3-1 to 7.2.3-5. Fig.7.2.3-1 shows the variation of component height with the punch pressure and amplitude of vibrations for specimens made from pure Aluminium (Al1). Specimens were deformed with vibrations amplitudes of 0.002, 0.003 and 0.007 mm. Fig.7.2.3-2 shows results obtained in experiments using specimens made from aluminium (Al2); experiments were performed with an amplitude of vibration of 0.007mm. The influence of vibration amplitude on the component height is shown in Fig.7.2.3-3. These results were obtained for a punch pressure of 512.0MPa. Differences between component height, with and without vibrations, are shown as a percentage change in Table 7.2.3-1. The punch diameter was 4mm.

Table 7.2.3-1: Change in component height

Pressure 512.0 MPa			
Amplitude [mm]	0.002	0.003	0.007
Component height increment in %	8%	11%	31%

Influence of surface excitation was assessed by comparing the height of components produced under the similar loads for both, vibration assisted and static operations. For a selected punch pressure, the height of the component, which was produced with a vibrating punch, was greater than that which was produced without vibrations. For example, for a punch pressure of 512 MPa, the heights of the component produced

without and with vibrations of an amplitude of 0.007mm were 9.6mm and 12.6mm respectively. For the same punch pressure and vibration amplitudes of 0.002mm and 0.003mm, the component height was 10.4mm and 10.7mm, respectively. In some cases H reached a maximum permissible value H_{max}, which was restricted by the length of the working part of the punch. When $H = H_{max}$ the experiment was discontinued as the upper surface of the extruded can made contact with the punch-head.

Results of experiments using a punch with a diameter of 3mm and specimens made from aluminium Al2 are shown in Fig.7.2.3-4. For each pressure that was applied to the punch, specimens were deformed without and with vibrations. Experiments were carried out using vibrations of an amplitude of 0.004mm and 0.01mm. Graphs in Fig.7.2.3-4 show the increase in the component height obtained in the operation with superimposed vibrations with reference to that obtained in the operation without vibrations. The difference (ΔH_D - ΔH_S) is defined as follows:

$$\Delta H_D - \Delta H_S = (H - H_0)_{withvibrations} - (H - H_0)_{withoutvibrations} \qquad (7.2.3\text{-}1)$$

These results confirm earlier observations that the amplitude of vibrations has a significant influence on the forming force.

Results of experiments with Armco iron and steel 010 are shown in Fig.7.2.3-5. Experiments were performed using the 3mm diameter punch. Vibrations with amplitude of 0.01mm were superimposed on the punch. Steel specimens were deformed with and without vibrations. Specimens made from Armco iron were deformed only with ultrasonic vibrations. Fracture of the punch, during experiments with steel specimens, prevent continuation of experiments. The observed decrease in specimen height was due to the fact that, at the initial stage of the process, the specimen is deformed to fill the die cavity. Results in Fig.7.2.3-5 also show that the applied vibrations had a small effect on punch penetration. However, greater deformation was achieved when the experiment was performed with vibrations. Extrusion of Steel 010 and Armco iron requires much higher pressures; thus vibrations of amplitude of 0.001mm did not provide sufficient energy to improve the

deformation efficiency of the process. Clearly, the findings indicate that ultrasonic vibration employed in back extrusion affects the process by reducing the applied force. The applied force varies inversely with amplitude of vibrations.

During experiments performed on the 250kN hydraulic press, punch load and displacement were recorded. Therefore, all results might be presented in a form of graphs, which show the variation of punch pressure with punch penetration.

Fig.7.2.3-6 shows results obtained for two aluminium specimens at a punch velocity of 0.25mm/s and amplitude of vibrations 0.0035mm. One specimen was deformed with vibrations superimposed right from the beginning of the process while another was deformed while vibration was applied to the punch for three short intervals over the duration of the process.

Fig.7.2.3-7 to 7.2.15 show results obtained for different punch velocities. Results shown in each figure refer to a specific punch velocity and two nominal amplitudes of vibration of 0.0045 and 0.0085mm. Further, all figures also contain graphs showing the variation of punch pressure with penetration for the operation conducted without vibrations. Results presented in Fig.7.2.3-7 were obtained for a punch velocity of 0.5mm/s; the measured amplitudes of vibrations were 0.0045 and 0.0095. Fig.7.2.3-8 shows the variation of punch pressure with punch penetration for a velocity of 1.0mm/s. Under this load, the amplitudes of vibrations were 0.00045 and 0.0085mm. Fig.7.2.3-9 contains a set of results obtained for a velocity of 5mm/s. The measured amplitudes of vibrations were 0.003 and 0.0087mm. Results shown in Fig.7.2.3-10 refer to a punch velocity of 10mm/s; the measured amplitudes of vibrations were 0.0025 and 0.0078mm.

Additionally, the above-mentioned results are shown, for comparison, in Fig.7.2.3-11 and Fig.7.2.3-12. The former contains results for the nominal amplitude of vibration 0.0045mm while, in latter, the amplitude 0.0085mm. Results of amplitude measurements are listed in Table 7.2.3-2.

Table 7.2.3-2: Measured amplitudes of vibration

Velocity [mm/s]	Nominal Amplitude 0.0045 mm	Nominal Amplitude 0.0085 mm
	Measured amplitudes [mm]	
0.5 mm/s	0.0045	0.0095
1.0 mm/s	0.0045	0.0085
5.0 mm/s	0.003	0.0085
10.0 mm/s	0.0025	0.0075

Signals recorded from eddy current transducers, showing time history of the vibrations, which were used to estimate amplitude of vibrations, are shown in Appendix 7.2.3.1.

The presented experimental results clearly indicate that the velocity of the process and the amplitude of the applied vibration had significant influence on the punch pressure. This pressure varied inversely with velocity of the ram and directly with amplitude of vibration. The reduction in punch pressure with the ram velocity is shown in Fig.7.2.3-13.

Results of experiments, which were performed to investigate the influence of holding time of the load under superimposed ultrasonic vibrations on the final punch penetration, is shown in Fig.7.2.3-14. An Aluminium specimen was subjected to vibrations and a load increasing at the rate 50N/s to a maximum value of 2250N (corresponding to the punch pressure 180MPa). This load is about one third of that required in the operation without vibrations. When the maximum load was reached, the specimen was subjected to this load with superimposed vibrations for 160sec. The amplitude of the applied vibrations was 0.0075mm. Another specimen was subjected to the same load without vibrations. Results clearly indicate that the holding time of load under vibration conditions had influence on punch displacement. This observation agrees with earlier reported results obtained for indentation. Further, similar observation was reported by Bacharov et al [96].

Finally, results of experiments using steel specimens are summarised in Fig.7.2.3-15. The specimens were extruded with the punch velocity of 0.1mm/s. The nominal amplitude of the superimposed vibrations was 0.0085mm. Again, the applied vibrations did not have a sufficient effect on the steel extrusion.

7.2.4. Wire flattening

In all experiments, wires were drawn manually through the dies by attaching a force-measuring device to the wire. Variation of the pull-through force for Copper, for different die gaps, is shown in Fig.7.2.4-1. The wires were drawn under dry and lubricated conditions. The amplitudes of vibrations used in experiments were 0.003 and 0.007 mm. Results of the experiment, when wire were drawn without vibrations, are also shown in this figure.

Results of the experiments, with and without vibrations, using Al-G21 are in shown Fig.7.2.4-2; in these experiments the amplitude of vibrations remained constant and all experiments were performed with a lubricant.

Fig.7.2.4-3 shows the results of the experiments performed with pure Aluminium wires; again, the amplitude of vibrations remained constant for experiments were performed under dry and lubricated conditions.

The amplitude of vibration remained constant throughout the process, which was not the common experience during the course of these studies. The introduction of surface excitation to the wire flattening operation reduced the pull-through force. For Copper wires, the force was reduced by 37% for die gaps of 0.9mm and 0.7 mm. For pure Aluminium wire, the reduction was even greater. For the die-gap of 0.7 mm, the pulling force was reduced by 95%. A reduction of 53% was achieved for aluminium alloy wire. Clearly, such large force reduction cannot be attributed only to the reduction of friction. It should be noted that the wires were drawn manually at about 100mm/s, which was a relatively low velocity compared to industrial processes. The low drawing velocity may account for the large reduction in the pull-through force since the swaging effect would dominate in the deformation of the wire.

Wire flattening with smaller die-gaps was possible since the overall forces were relatively low. In wire-flattening operations without vibrations Aluminium wires fractured when the die-to-die gap was 0.7 mm and the drawing force 94N. By contrast, in operations with vibrations applied to the upper tool, wires were drawn successfully through a gap of 0.4 mm; in this case, the draw force was 45N. Experiments on this forming operation confirmed the earlier finding that the magnitude of the vibration affects the forming process. However, in contrast to back-extrusion, this effect was substantial even for small amplitudes. When Copper wire was drawn through a die-gap of 0.9 mm, the pull-through force decreased by 52 % for an amplitude of 0.003mm. Increasing the amplitude to 0.007mm resulted in an additional 25% force reduction. In the back-extrusion operation, amplitudes of 0.003 mm and 0.007mm resulted in 11% and 30% increase of the component height respectively.

Influence of the die-to-die gap on the magnitude of the pull-through force is illustrated by the experiments conducted on aluminium alloy wires (see Fig.7.2.4-2). For die-gaps of 0.7mm, 0.6mm and 0.5mm, the average force reduction was approximately 20 %.

Lubrication appears to have a minor influence on the force in vibration-assisted wire-flattening operations. Forces required to flatten copper wires, for a particular die-gap, had similar magnitudes under both, lubricated and dry conditions (see Fig.7.2.4-1). A similar observation was made in experiments on wire made from aluminium alloy (Fig.7.2.4-3).

The application of ultrasonic vibration to wire flattening shows significant benefits.

7.3. Finite Element Analysis

7.3.1. Wire Flattening

The EF model for wire flattening in which the tools were assumed to be rigid is shown in Fig.6.4. The lower tool remains stationary while the upper tool vibrates with a prescribed amplitude and frequency in the vertical direction, i.e. perpendicular to the drawing direction. The tool velocity changes with time according to $v_2 = A \cdot \omega \cdot cos(\omega \cdot t)$. The wire flattening process was simulated to determine the pattern of force change in tools with and without vibration applied to the upper tool. Results of the simulations for drawing velocities 150 and 2000mm/s and are shown in Fig.7.3.1-1 and 7.3.1-2, respectively. When vibrations were imposed on the tool, the forming force varied periodically form 0 to the maximum for both investigated drawing velocities. It follows that contact between the tools and the wire was periodically lost. The period when the forming force decreased to zero was longer when the drawing velocity was150mm/s than for 2000mm/s. In both cases the maximum forming force was as predicted by simulation without vibration imposed to the tool.

Two characteristic positions of the upper tool, with respect to the drawn wire, are shown schematically in Fig.7.3.1-3. The distance *S* between the wire and the working surface of the tool at the instant *t* depends, for given amplitude of vibration, on the drawing velocity v_w. For a stationary wire this distance occurs at velocity:

$$v_1 = \frac{v_2}{tg\alpha} = \frac{A \cdot \omega \cdot cos(\omega \cdot t)}{tg\alpha} \qquad (7.3.1\text{-}1)$$

The maximum velocity is;

$$v_{1max} = \frac{A \cdot \omega}{tg\alpha} \qquad (7.3.1\text{-}2)$$

For wire drawn at a velocity v_w, the distance S occurs when:

$$v = v_{1max} - v_W \qquad (7.3.1\text{-}3)$$

When ($v_w = v_{1max}$), the wire is in continuos contact with the tool. It follows that the drawing conditions would be similar to that which occurs for stationary tools. Therefore, the drawing velocity $v_w = v_{1max}$ is a critical drawing velocity. No benefit is derived by applying vibration to the tool above this velocity. For an amplitude of *0.01mm* and a frequency of *20kHz* the critical velocity is $8.94mm/s$. Eq.7.3.1-3 does not take into account the elastic deflection of the wire, therefore, in practice, it would be more reasonable to assume that the critical velocity is equal to the average velocity v_1, which is expressed by:

$$v_{w,cr} = v_{1av} = \frac{2 \cdot A}{T \cdot tg\alpha} \qquad (7.3.1\text{-}4)$$

For an amplitude of *0.01mm* and a frequency of *20kHz* the critical velocity would be approximately $5.7m/s$. The variation of the drawing force, for a drawing velocity of 2000mm/s and amplitude of 0.005mm, is shown in Fig.7.3.1-4. For an amplitude of 0.005mm, the critical drawing velocity is about $2.85m/s$. Consequently, the average drawing force shown in Fig.7.3.1-4 is only about 5% smaller than the force required to draw the wire under static conditions.

Reduction in the average drawing force does not account for the fact that application of ultrasonic vibration to the forming tool results in greater wire reduction. In the experiments the reduction of the copper wire $\varphi = 1.2mm$ increased from 0.37 to 0.58. For aluminium wire of $\varphi = 1.0mm$, the increase in wire reduction was greater; from 0.3 to 0.6. A possible explanation is that that compressive force induced by the vibrating tool changed the stress state in the deforming part of the wire. Under the new stress state, the required drawing force is lower. Korbel and Bochniak [35] observed a significant reduction in the tensile load when tensile tests were performed with simultaneous torsion. Similar effect was observed by Olejnik [97] who subjected a specimen to the tensile load while under rolling stresses. Stress induced by the tensile load was smaller than the Yield Strength while the stress induced by rolling would not deform the work material when applied independently.

Periodic changes in the drawing force are reflected in different stress distributions in the wire over the period of vibration. Distributions of equivalent stress in the wire drawn without and with vibration applied to the tool are shown in Fig.7.3.1-5 and 7.3.1-6, respectively. Fig.7.3.1-6 shows the stress in the wire at ten instances, equally spaced over the vibration cycle. In both cases the maximum magnitude of the stress reached the same value of 150MPa.

7.3.2. Back Extrusion

Simulations of the back extrusion process were performed using the two models described in Section 6. Before presenting the results, an explanation is provided as to why the linear velocities (*20, 100, 200* and *500mm/s*) of the movable tool (then after referred as a process velocity) were different from the experimental velocities (*05, 1, 5* and *10mm/s*). Attempts to use velocities lower than *20mm/s* were failed as the output history data of the movable tool were affected by the rounding-off errors. These were caused by the fact that the stable incremental time was small, which in turn resulted from the fine mesh of the punch and billet. The usual method of increasing the stable incremental time is to either increase the mesh size and/or to introduce the mass scaling. Neither of these approaches could be applied; the former method could not be used because of the dimensions of punch dimensions. Introducing mass scaling would change the velocity of elastic wave propagation (Eq.1-3), which would affect the resonant characteristics of the model. These constraints refer mainly to the second model. However, to enable a comparison between these two models, the same velocities were used in both models. The chosen velocities 20, 100, 200 and 500mm/s were sufficient to study the effect of applying vibration of an amplitude of 0.0085mm.

The term "forming force" which is used in the text following text is the computed reaction force on the punch in the direction parallel the direction of the anvil velocity. Variations of this force with the anvil displacement obtained in the FE simulations using the first model (both tools rigid) for process velocities of are shown in Fig.7.3.2-1 –7.3.2-4. The successive figures refer to process velocities of *20, 100, 200* and *500mm / s* . The figures show that when vibration is imposed on the punch,

the magnitude of the force oscillates at the same frequency as that of the punch. Further, the maximum value of the oscillating force is lower than that which was observed when the punch did not vibrate. Further, the difference between the magnitude of the force under static conditions (without vibration) and the maximum force during punch oscillation decreases as the velocity of the anvil increases. At a process velocity of *500mm/s,* the magnitudes of these forces are almost equal. The amplitude of oscillation decreases with the process velocity.

The curves illustrating the oscillations are shown in Fig.7.3.2-5, which displays a fragment (for anvil displacement from 1.9 to 2mm) of the graph shown in Fig.7.3.2-4. For a process velocity of 500mm/s, this displacement corresponds to process duration equal to four cycles of vibration. The length of the flat segments of the curve depends on process velocity. For example, for a velocity of 100mm/s and the same range of the anvil displacement, the graph in Fig.7.3.2-5 would contain 20 oscillations. It follows that the length of the flat segments would be shorter.

Fig.7.3.2-6 shows the variation of the average forming force with the anvil displacements for all four anvil velocities. The curves were computed using a moving average algorithm, which is based on the following formula [90]:

$$\tilde{F}_{(i+1)} = \frac{1}{N}\sum_{j=1}^{N} F_{(i-j+1)} \qquad (7.2)$$

where N is the number of data points included in the moving average while F and $\tilde{F}$ denote the actual and average value of the j-th data point. Ten successive data points were used to calculate the average. The magnitude of the average forming forces when vibration was imposed on the punch and the ratio of this force to the force under static conditions, are shown in Table7.3.2-1.

Table 7.3.2-1: Average forming force. FE simulations, rigid punch

Process velocity [mm/s]	$\widetilde{F}$	$\widetilde{F} / F$
20	2800	0.42
100	3900	0.56
200	4700	0.67
500	6200	0.87

It was mentioned that the maximum magnitude of the oscillating forming force, for all instigated anvil velocities, when vibration was imposed on the punch was smaller than the magnitude of the forming force under static conditions. For a process velocity of *20mm/s*, the difference between these two was about 1500N. One possible explanation for this phenomenon could be that the vibration imposed on the punch decreased the friction force. In order to verify this hypothesis the FE simulations were performed for frictionless conditions. The results of these simulations showing the relationship between the forming force and the anvil displacement for velocities of *20* and *200mm/s* are shown in Fig.7.3.2-7 and 7.3.2-8, respectively. In both cases, the maximum magnitude of the oscillating forming force was the same as the magnitude of the forming force under static condition. It follows that the application of vibration reduced friction forces. For the purpose of comparing results, Fig.7.3.2-7 and 7.3.2-8 also contain the results obtained with friction. It may be observed that the minimum magnitude of the oscillating forming force is smaller when friction prevailed at the work- material/tools interface.

In order to investigate the mechanism responsible for the reduction of the friction, the distributions of velocity in direction 2 in the work-material at different time-points of the vibration cycle were examined. Fig.7.3.2-9a shows the variation of the punch vibration velocity and the forming force, with time, for a process velocity of *20mm/s*. Numbers 1, ...,5 mark the instance at which velocity fields in the specimen are displayed in Fig.7.3.2-9b. Similar information is shown in Fig7.3.2-10a and b for a process velocity of 200mm/s. At the instant 1, the velocity of the punch has a maximum value; thus, the punch is at the mid-position and moving upwards. At the

instant 2, its velocity is still positive but the magnitude is close to zero; thus, the punch approaches its extreme upper position. After reaching the extreme upper position, the punch moves downwards and its velocity is now negative. At the instant 3, the punch velocity is still negative and the punch approaches the mid-position; upon reaching this position, the velocity remains negative but its absolute magnitude decreases. The punch moves downwards. The extreme lower position is reached between the instants 4 and 5. At the instant 5, the punch again has a positive velocity and moves upwards. The force acting on the material decreases when the difference between the punch and the process velocity is positive. Since the relative velocity between the punch and work-material changes direction, the friction force, which acts in a direction opposite to the relative velocity follows these changes. Comparing Fig.7.3.2-9a to Fig.7.3.2-10a, it may be observed that the period when the forming force decreases is shorter when the process velocity is *200mm/s*. The changes in the direction of the punch movement are reflected in changes in the velocity field in the work-material over the vibration cycle. This is illustrated in Fig.7.3.2-9b and Fig.7.3.2-10b for process velocities of *20* and *200mm/s*, respectively.

Fig.7.3.2-11 and 7.3.2-12 show the friction shear stress on the work-material surface, which is in contact with the punch and the die, respectively. Each of these figures shows stress distribution for a process velocity of *20* and *200mm/s* at the instant corresponding to the punch velocities marked 1,...,5 in Fig.7.3.2-9a and Fig.7.3.2-10a. Further, for comparison purposes, the figures also contain the friction shear stress that was computed for static conditions. Before proceeding further, an explanation is required for the interpretation of the results. In the two-dimensional models, a slave (work-material) node can slide along the master (punch or die) surface in the plane of the model. The tangent to the master surface in the plane of the model is the direction of the slip. ABAQUS defines the orientation of this tangent by the cross product of the vector into the plane of the model (0, 0, -1) and the master surface (the punch or the die) normal vector. The frictional shear stress has the sign opposite to the slip sign. Further, the magnitude of the frictional shear at the node

represents the total stress on the circumference; this is allocated a unit value MPa/mm.

The presented information provides evidence that the frictional stress and consequently friction force changes the direction during the vibration cycle. Further, the direction of the frictional stress and its magnitude depends on process velocity. For a process velocity of *20mm/s*, the friction shear stress has a direction opposite to that which prevailed when vibration was not imposed on the punch for longer than the one half of the cycle (Fig.7.3.2-11a). For a process velocity of *200mm/s,* the period, when the frictional shear stress has the opposite direction, was shorter. As a result, the decrease in the forming force is greater when the process velocity is 20mm/s. Graphs showing the variation of the forming force with time for process velocities of 20 and 200mm/s under friction and frictionless conditions are shown in Fig.7.3.2-13.

The observed phenomenon is known in the literature as "the friction vector effect". Additional information on this effect is given in Section 2.2.2. Many researches investigating the influence of vibration on material flow suggest that is this factor one of the contributors to forming force reduction. However, only Siegert and Ulmer [16] measured the friction force and showed its reversible character.

The second FE model of back extrusion, in which the vibrating tool was modelled as an elastic body was developed in order to investigate the phenomena occurring at the contact surfaces. Specifically, it was expected that this model would provide information on the amplitude at tip of the punch. In practice, the measurement of the amplitude at this point is impossible.

In the model under consideration, vibration was introduced to the elastic tool by forcing it to vibrate at the resonant frequency by applying a sinusoidal pressure to the surface opposite to the working surface (Fig.6-5b). The resulting amplitude of vibration at this surface and the tip of the punch under unloaded conditions are

shown in Fig.6-6b. Vibrational movement of the elastic tool under load will be characterised by the amplitude of vibration at three points on tool, which are shown in Fig.7.3.2-14. The points are identified as A, B and C in this figure. In the experiments on back extrusion, the amplitude of vibration was measured at point B.

Fig.7.3.2-15 and 7.3.2-16 a, b shows the displacement of points C, A and B, respectively for a process velocity of *20mm/s*. The work-material was Aluminium. The simulation was performed in two steps, vibration being introduced during the second step. During the first step, displacement results from the elastic deflection of the tool and the flange. The displacement of point C is greatest due to elastic deflection of the section with the smallest cross-area. The compressive stress induced by the load in this section of the tool is about 50 times greater than that in the section with the largest cross-section. In the case of point A, which is not subjected to the applied load, its displacement results from the elastic deflection of the flange. The displacement of point B results from the elastic deflection of the flange and the section of the tool with the largest cross-section. In the second step, points A and B oscillate around a mean value with the same amplitude of approximately 0.0085mm i.e. at the amplitude that was obtained when the load was not applied to the punch (Fig.6-6b). Therefore, a load of 7000N did not affect the amplitude at these points. On the contrary, the applied load affected the amplitude at point C. Its magnitude was equal to 0.0025mm.

The introduction of vibration to the tool decreased the displacement of the reference points, in particular, of the point C (Fig.7.3.2-15). Since the displacement of this point resulted from the elastic deflection of the tool, it may be concluded that the force acting on the tool decreased as a consequence of the introduced vibration.

Displacement of the points A and B when the steel specimen was used are shown in Fig.7.3.2-17a and b, respectively. The simulation was performed for a process velocity of $100mm/s$. The forming force required to extrude the steel specimen is about *24000N*; thus, the displacement of both surfaces is much larger than that for

Aluminium. The amplitude of vibration at the point A had a magnitude of *0.0085mm* while that at the point B was slightly smaller - *0.0075mm*. It is clearly visible in Fig.7.3.2-18, which displays both amplitudes. The displacement of point C calculated in this simulation is shown in Fig.7.3.2-19.

The magnitudes of the amplitude at point C for process velocities 20 and 100mm/s for Aluminium and 100mm/s for Steel are shown in Fig.7.3.2-20. For a process velocity of *100m/s,* the amplitude at this point is almost two times greater for an aluminium specimen (graph (b)) than for steel (graph (c)). Velocity of the process seems do not affect the amplitude at point C. At a process velocity of $20mm/s$ the amplitude at the point C has the same magnitude as at a process velocity of 100mm/s.

It has been already pointed out that the application of vibration to the tool caused the decrease in the tool deflection (Fig.7.3.2-15). Since elastic deflection results from the force acting on the tool it follows that this force, which may be considered as a mean forming force decreased. Therefore, the tool deflection may used to evaluate this force. In the simulations with the rigid tools the reaction force on the punch was assumed to be a forming force. The variation of this force with time had a smooth character. This was not the point when the model with the elastic tool was used in simulations. The variation of the reaction force on both the punch holder and the anvil had a noisy character as it is shown in Fig.7.3.2-21. Therefore, using the tool deflection to evaluate the forming force seems to be more accurate method than using the computed reaction forces.

Deflection at the point C for a process velocity of 20, 100 and 200mm/s is shown in Fig.7.3.2-22. Under static conditions, without vibration, the tool deflected about *0.042mm* (Fig.7.3.2-15). With vibrations the corresponding deflections were *0.0019, 0.0033, 0.0037* and *0.0041mm* for process velocities of *20, 100, 200* and $500mm/s$, respectively. For the clarity, the displacement of point C for a velocity of 500mm/s is not shown in Fig.7.3.2-22. The mean forming force $\bar{F}$ corresponding to each of these

tool deflections and the ratio of this force to those without vibrations are listed in Table 7.3.2-2.

Table 7.3.2-2: Average forming force. FE simulations, elastic punch

Process velocity [mm/s]	$\widetilde{F}$	$\widetilde{F}/F$
20	3100	0.45
100	5300	0.78
200	6000	0.88
500	6700	0.98

The comparison of the FE results obtained for both models are shown in Fig.7.3.2-23, which displays the ratio ($\widetilde{F}/F$) with relative process velocity, which is defined as the ratio of the ram velocity to the maximum vibrational punch velocity $(v/A\omega)$. The mean forming forces obtained using the model with the elastic tool are greater from those obtained using the model with rigid tools. None of the curves describing EF results matches the curve for experimental results obtained when the amplitude of vibration was 0.0085mm. However, the curve representing FE results obtained for the model with the elastic tool shows the same character as the experimental curve. Rapid increase in the forming force with increase in the relative velocity is observed for relative velocities in the range $(0 \sim 0.1)$. Further, the experimentally obtained forming force increases at a higher rate than that obtained from FE simulations. The observed discrepancy between the experimental and FE results may be consequence of two factors. Firstly, it is not certain whether the measured forming force is the mean force acting on the tool; this is the force defined in FE simulations. Secondly, the developed FE models may not adequately describe the real conditions. The introduction of the elastic vibrating tool and the method of imposing vibrations constitutes significant progress in modelling ultrasonically assisted metal forming operations, however, modelling the anvil as a rigid body may not allow the realisation of all phenomena occurring in this process. The anvil that was used in the experiments was mounted in the same manner as the punch holder. In spite of its length equal to a half wavelength, its basic natural frequency turned out to be three

times that of the punch holder. This would influence experimental results. The detail description of the anvil is provided in Section 4.5.4.

The oscillating character of the forming force, when vibration is imposed on the tool is reflected in the cyclically changing stress in the work-material. The stress distributions in the work-material computed using the model with the elastic tool for process of velocities *20* and $100mm/s$ are shown in Fig.7.3.2-24 and 7.3.2-25, respectively. The results were obtained from simulations using the model with the elastic tool. The figures show the stress corresponding to the punch position marked on the curve $A = A_o \sin(\omega t)$. In both cases the maximum stress has the same magnitude; however, the average stress, defined as the sum of the stress in all elements divided by the number of elements, is lower for a process velocity *20mm/s.*

8. DISCUSSION

8.1. The WP/T tool

The first problem encountered during experiments with the WP/T was damage to the load cell, which prevent force measurements. The magnitude of the applied load was assessed from the press setting. At a later stage of the trials, the generator was damaged due to overloading. As a result of this, only a qualitative estimate of the influence of ultrasonic vibration on the forming force was possible. Experiments showed that, by applying vibrations to the forming tools perpendicular to the forming force, it was possible to achieve greater specimen reduction in the upsetting operation. The direction of the vibration suggests that the reduction of friction force may account for this result. Decrease of the friction force resulted in the reduction of the forming force. Thus, subjecting a specimen to a particular load with vibrations will produce greater deformation than when the deformation is performed without vibrations. The results suggest that the reduction in the forming force increases with deformation. The forming force, when friction prevails, may be estimated using the Siebel formula for mean pressure. The formula expresses the relationship between the mean pressure, friction coefficient, specimen deformation and Yield Strength [98]:

$$\bar{p} \approx \left(1 + \frac{2 \cdot \mu \cdot r}{3 \cdot h}\right) \cdot Y \qquad (8.1\text{-}1)$$

The above expression is only true for small values of friction, provided there is no appreciable barrelling of the specimen; however, it provides a notion of mean pressure. Thus, forming force and consequently the friction force changes with deformation. When friction is not present the deformation is uniform and stress in the specimen is equal to the current Yield Strength. The variation of the ratio of mean pressure to the Yield Strength under friction conditions for μ=0.1 is shown in Fig.8.1-1. The friction force increases with deformation in a similar manner. Forming forces under frictionless and friction conditions for μ=0.1, estimated using Eq.8.1-1 (pure Aluminium, constitutive equation is $\sigma = 159 \cdot (0.02 + \varepsilon)^{0.28}$), are shown in

Fig.8.1-2. This figure shows that the increase in specimen strain, due to the reduction of friction force, is of the order of 0.001; this increases with deformation. The results of experiments on the compression of Aluminium and Steel specimens conform to those estimated theoretically. For example, strain in the Aluminium specimen increased by 0.026 as a result of applying vibrations while the theoretical increase was estimated to be 0.024. In the case of the steel specimen, the application of vibration increased the strain by 0.014, which shows good agreement with the theoretical prediction of 0.015. Decrease in the forming force, due to friction reduction, is small for small reductions of the specimen. The introduction of vibrations in the direction perpendicular to the forming force appears to have a minor influence on the process. However, for specimens with a small aspect ratio, this effect should be more prominent.

Concluding, the experiments using the WT/P tool showed that vibration of the forming tools in the direction perpendicular to compression reduced the friction force between the tools and the specimen. Consequently, the forming force was also reduced. A further conclusion, which follows from these experiments, is that the desired physical effect of ultrasonic vibrations on the metal forming operation is closely related to the method of introducing vibrations. These should be considered together prior to the design of tools. This requires an understanding of the mechanism by which metal flow is affected by the application of ultrasonic vibrations. The experience gained during the WT/P tool design and experiments enabled better design and construction of the WT/I tool. This multi-purpose tool supported experiments in four different forming operations to provide a better insight to the influence of ultrasonic vibrations on metal flow.

8.2. The WT/I Tool

8.2.1. Deformation mechanism

Experiments using the WT/I were performed on two presses - pneumatic (PP) and hydraulic (HP); load application characteristics were different since different systems were used for controlling these presses. Therefore, experimental procedures used on both presses were different as scribed in Section 5.2. Consequently, the mechanisms were different.

On the pneumatic press (PP), deformation of the specimens depended on the pressure in the cylinder. In order to explain the mechanism of deformation, with superimposed vibrations, assume that the pressure in the cylinder is set at P_1. This pressure corresponds to a force F_1 acting on the specimen, which induces in the work material a stress state with an equivalent stress, σ_{e1}. This will produce strain ε_1 in the specimen. When ultrasonic vibrations are applied to the punch an oscillatory axial stress σ_V will be produced in the work material. A new stress state, characterised by an equivalent stress $\sigma_{e2} > \sigma_{e1}$, is induced in the work material, which results in the strain $\varepsilon_2 > \varepsilon_1$. The increase in strain depends on the amplitude of vibrations. Under static conditions, plastic deformation of the work-material occurs when the applied force F induces, in the work material, an equivalent stress that is equal to the initial Yield Strength σ_Y. However, the application of vibration of sufficient amplitude enables yielding under smaller forces. Again, the resulting deformation depends on the amplitude of vibration. When a force F induces in the work material a stress state with an equivalent stress σ_e, which corresponds to a value higher than that experienced at Yield σ_Y, vibrations of any amplitude would increase the deformation; however, the increase depends on the amplitude and the variation of forming force with deformation. If the forming force increases with deformation the influence of vibration (of particular amplitude) on the specimen deformation decreases with increasing deformation. This was observed during experiments on heading (Fig.7.2.2-1). Under a load of 4500N and static conditions, the reduction of

the free specimen height was 0.54. When the specimen was deformed under the same load with superimposed vibration, the reduction increased to 0.6. Under a load of 7200N the application of vibration of the same amplitude increased the reduction of the specimen height from 0.68 to 0.69. There are two factors, which may account for this phenomenon. When the stress required deforming the work-material increases, the stress induced by the vibration of a constant amplitude accounts for a smaller proportion of that required; therefore, its influence diminishes. A second factor may be derived from the elastic-plastic wave theory. As the deformation progresses the cross-section of the specimen increases; thus, in accordance with Eq.1.4 magnitude of the stress transferred from the punch to the specimen decrease. The specimens used in experiments had an initial cross-section of 12.56mm^2. Under a forces of 4.45kN and 7.2kN its area increased by a factor of 2.14 and 3.12 respectively. Therefore, magnitudes of the stresses transmitted to the Aluminium specimens for the above cross-section would be 0.652σ, 0.615σ and 0.587σ respectively, where σ is the magnitude of the stress wave in the punch.

In can extrusion, the forming force stabilised after a rapid build-up at the beginning of the process. For a particular applied force F, the amplitude of vibration of sufficient magnitude may cause continuous deformation. For example, for a static pressure of 284MPa, the amplitude 0.004mm did not increase the specimen height while the height of specimen reached the maximum for the amplitude 0.01mm (see Fig.7.2.3-4). This accounts for the weak influence of ultrasonic vibrations on the extrusion of Steel and Iron Armco specimens. Despite the high static pressure applied to the punch (about 1900MPa), an amplitude 0.01mm appeared to be insufficient to make the process more effective (Fig.7.2.3-5). To achieve the same effect as that for Aluminium, the applied vibrations should have a greater amplitude. Further, it should be noted that in the case of back extrusion, the cross-section of the specimen in contact with the punch remained constant over the process duration; so does the magnitude of the transferred stress wave. Again, this follows from the Eq.1.4.

The mechanism of deformation using the HP press was different. This press was equipped with a control system, which enabled its operation in either force or stroke mode. In the force mode, the forming force increased to the required magnitude at the prescribed rate. In the stroke mode, which was used in the experiments, the punch travelled at the prescribed rate over the desire distance while the magnitude of the forming force was a consequence of the plastic deformation of the specimen. The forming force was measured using a load cell, which was placed between the press ram and the WT/I tool (Fig.4.5.2-1). During deformation without vibration, the forming force followed the force-punch displacement relationship. In the ultrasonically assisted operation, the static stress required to proceed with deformation decreased by the magnitude of the vibrational stress, changing from σ_{St} to σ_{St}-σ_D. It follows that the forming force F_V, in the ultrasonically assisted operation, acting on the specimen is the sum of the load F_M applied by the forming machine and force F_D induced by the vibrating tool:

$$F_V = F_M + F_D \qquad (8.2.1\text{-}1)$$

Since it has not been documented, that ultrasonic vibrations reduces the Yield Strength of a material or the rate at which it work-hardens, it may be assumed that energy required to deform the work-material in the operation with and without imposed vibrations are equal. Consequently, it can be assumed that forming force F_V is equal to the force F_S in the operation performed without vibration the following relationship holds:

$$F_M = F_S - F_D \qquad (8.2.1\text{-}2)$$

where F_D changes from 0 to $F_{D,max}$ during the vibration period.

It follows that the force F_M complies with the condition:

$$F_S \leq F_M \leq F_S - F_{D,max} \qquad (8.2.1\text{-}3)$$

The force F_M can be expected to vary at the same frequency as the vibrations; however, the load cell could not sense this oscillation because elements of the tooling, which transmitted this force to the load cell, were effectively, a low-pass

filter. It can will be shown that the natural frequency of the system consisting of elements transmitting the force to the load cell was much lower then the working frequency of vibrating system. The forming tool was suspended between two nylon washers and secured to the upper plate of the die-set (Fig.4.5.2-1). The plate was connected to the load cell by two 440mm long hollow beams and a horizontal bar, which created a joint between the beams and the load cell. The elements that transmitted the force to the load cell are schematically shown in Fig.8.2.1-1. The spring represents stiffness k_b of the beams while the mass m_p is the mass of upper plate of the die-set and the beams. The v symbol denotes the velocity of the horizontal bar of the WT/I tool (Fig.4.5.2-1). This velocity is equal to the ram velocity. The upper plate and the beams may be regarded as a system with one degree of freedom with a natural angular frequency that may be determined using the formula [74]:

$$\omega_{p-b} = \sqrt{\frac{k_b}{m_p}} \qquad (8.2.1\text{-}4)$$

Stiffness of the beams may be computed using the expression:

$$k_b = 2 \cdot \frac{S \cdot E}{l_b} = 2 \cdot \frac{\frac{\pi}{4} \cdot (D_o^2 - D_i^2) \cdot E}{l_b} \qquad (8.2.1\text{-}5)$$

where D_o and D_1 denote outer and inner diameter of the hollow beams, l_b the beam length, E-Young's modulus of the beam material. The mass of the upper plate and beams was m_p=20.5 kg while the stiffness of the beams was found to be $k_b = 5 \cdot 10^8\ Nm^{-1}$. Finally, the natural angular frequency of this system was found, using the Eq.8.2.1-4, to be $\omega_{p-b} = 4938\, s^{-1}$. The punch vibrated at an angular frequency $\omega = 2 \cdot \pi \cdot f = 125664\ s^{-1}$ 1/s; the force acting on the punch changed at the same frequency. This force was transmitted to the upper plate through the punch holder and forced the upper part of the tool WI/T to vibrate. The response of the system to the disturbing force is characterise by a magnification factor defined by the formula [74]:

$$\beta = \frac{1}{\sqrt{(1-(\omega^2/\omega_{p-b}^2))^2 + (2\cdot\frac{c}{c_r}\cdot\omega)^2}} \qquad (8.2.1\text{-}6)$$

where the ratio (c/c_r) denotes the damping ratio e.g. the ratio of the damping of the system to critical damping.

The variation of the magnification factor with the ratio ω/ω_{p-b} for various levels of damping is shown in Fig.8.2.1-2 In the case when the frequency of the forcing force is large in comparison to the natural frequency $(\omega >> \omega_{p-b})$, the magnification factor approaches zero regardless of the amount of damping. This suggests that forced vibrations are not produced and the system may be considered to be stationary. Neglecting the term for damping in the Eq.8.2.1-6, the magnification factor of the system, which transferred force, had a value of $3.9 \cdot 10^{-2}$. It follows that the dynamic force F_D exerted by the oscillatory punch movement did not cause the elements transmitting the force to vibrate. As a result, the load cell showed an average value of the force.

8.2.2. Kinetic model

In conventional forming operations velocity and displacement of the specimen surface in contact with the punch is the same as that of the press ram. The above is true if the elastic deflection of the tool is neglected. Contact between the punch and the specimen, once established, remains unchanged and the deformation of the work-material increases with the ram movement. This is illustrated in Fig.8.2.2-1a, which shows the displacement of the punch-specimen contact surface with time. In general, movement may be assigned to both, to the punch and anvil. In such a case, the resulting displacement of the punch-specimen contact surface is a function of both movements. Some cases are shown in Fig.8.2.2-1b, c and d. Force that is required to accomplish the operation is the same regardless the tool movement.

In the case when the forming operation is performed with vibrations superimposed on the punch, the movement of the punch-specimen contact surface is a combination of

two movements; linear movement of the anvil and the oscillating of the punch. In one half of the vibration period, the punch and anvil move toward each other (case c in Fig.8.2.2-1) while in the other half, these move in the same direction (case d in Fig.8.2.2-1). Assume that the anvil moves with a velocity v_A and the punch vibrates at a frequency $f = 20000Hz$ with amplitude $A_o = 0.005mm$. Assuming an anvil velocity of $100mm/s$, movement of the work-material, resulting from the anvil displacement, is illustrated by a straight line whose tangent is equal to the anvil velocity v_A. The equation describing the work-material movement has a form $s_A = v_A \cdot t + b$. Further, assume that the tool does not deflect elastically. Thus, this may be considered as a rigid surface, whose displacement and velocity are described by $s_P = A_o \cdot sin(\omega \cdot t)$ and $v_p = A_o \cdot \omega \cdot sin(\omega \cdot t)$ respectively. Such a model is a simplification of the real process since it does not consider dynamic effects that influence the real process. It also assumes that the amplitude of vibration remains constant regardless of the applied load. Nevertheless, this model may provide an insight to metal forming with superimposed ultrasonic vibration. In particular, it may be useful in qualitative analysis.

Assume that vibrations are applied to the punch at instant t=0 when the punch is in contact with the work material. Curves illustrating displacement and velocity of the punch and anvil are shown in Fig.8.2.2-2. To accommodate displacements and velocities on the same graph, the latter is scaled by a factor of 0.00001. At the beginning of the process v_P and v_A have the same direction, however, $v_P > v_A$ and contact between the punch and the work material is lost. The deformation starts at the moment t_o when $s_A(t) = s_P(t)$ and continues till the magnitude of the punch velocity v_P reaches a value equal to v_A. This occurs at t_1. From this moment the punch moves away from the work material at the velocity higher than the velocity of the anvil. As a result the specimen is unloaded. In some cases, contact between the tool and the work material may be lost. This occurs when the elastic deflection of the work-material is smaller then $2A_o$. The unloading is completed when the punch velocity again reaches a value equal to v_A. From this moment, which is marked as

t_2, the punch continues to move in the same direction as the anvil but at a velocity lower than that of the anvil. From this moment the reloading of the work material begins. The punch velocity decreases to zero and then the punch changes its direction of movement. The previous loading was reached at the moment t_3 when the sum of the anvil displacement (ΔD_p) and the actual position of the punch ($A_o \cdot sin(\omega \cdot t_3)$) was equal to the punch position when the unloading began (see Fig.8.2.2-2):

$$v_P(t_3 - t_2) + A_o \cdot sin(\omega \cdot t_3) = A_o \cdot sin(\omega \cdot t_1) \qquad (8.2.2\text{-}1)$$

Time t_3 may be calculated by finding the intersect to the curve ($A_o \cdot sin(\omega \cdot t)$) and the tangent to this curve at the point ($t_1, A_o\, sin(\omega \cdot t_1)$):

$$\begin{cases} s = A_o \cdot sin(\omega \cdot t) \\ s = v_A \cdot t + b \end{cases} \qquad (8.2.2\text{-}2)$$

where b may be determined from:

$$b = A_o \cdot sin(\omega \cdot t_1) - v_A \cdot t_1 \qquad (8.2.2\text{-}3)$$

At t_1, the velocity of the punch is equal to the anvil velocity; thus, the tangent at this point describes anvil displacement.

Further movement of the punch results in additional deformation of the work material. The deformation continues till the punch velocity again reaches a magnitude equal to the anvil velocity $v_P = v_A$. This occurs at $t_4 = t_1 + T$. From this moment, the cycle of the described events, unloading, reloading and deformation repeats at the same frequency as the punch.

Values of t_1 and t_2 may be easily determined since at these moments the velocity of the punch is equal to the velocity of the anvil (see Fig.8.2.2-2):

$$A_o \cdot \omega \cdot cos(\omega \cdot t\ ) = v_A \qquad (8.2.2\text{-}4)$$

The solution of this equation is:

$$t = \frac{arcos(\frac{v_A}{A_o \cdot \omega})}{\omega} + n \cdot T \qquad (8.2.2\text{-}5)$$

and

$$t = \frac{arcos\frac{v_A}{A_o \cdot \omega}}{\omega} + n \cdot T \qquad (8.2.2\text{-}6)$$

The former solution describes t_2, the time when the reloading begins. The latter describes t_1, the moment when unloading starts. Thus

$$t_2 = \frac{arcos(\frac{v_A}{A_o \cdot \omega})}{\omega} + n \cdot T \qquad (8.2.2\text{-}7)$$

$$t_1 = -\frac{arcos\frac{v_A}{A_o \cdot \omega}}{\omega} + n \cdot T \qquad (8.2.2\text{-}8)$$

Variation of the relative unloading time $[(t_2 - t_1)/T]$ with the relative anvil velocity $[v_A/(A_o \cdot \omega)]$ for the punch vibrating at a given angular frequency ω ($\omega = 2\pi \cdot f$) is shown in Fig.8.2.2-3. When the punch velocity $v_A > A\omega$ the unloading process does not occur and the work material is continuously deformed plastically.

The time t_3, when reloading is accomplished and the plastic deformation starts again, may be determined by solving the set of equations Eq.8.2.2-2. However, this set of equation does not have an analytical solution thus, the solution has to be determined using the interpolation method for each set of variables (v_A, A_o *and* ω) separately. Results of such calculations for $\omega = 125664 s^{-1}$, $A_o = 0.0085mm$ and the anvil velocity in the range (*2 - 800 mm/s*) are shown in Fig.8.2.2-4. When the anvil velocity $v_A \rightarrow A_o \cdot \omega$, the time during which the work-material is deformed

plastically is $(t_4 - t_3) \rightarrow T$. It follows that when $v_A > A_o \cdot \omega$ the work-material is continuously deformed.

During the period $(t_1 \sim t_2)$ the punch and the anvil move in the same direction; the punch moves at the velocity greater than that of the punch. However, contact between the punch and work-material is not lost since the work-material undergoes springback. As a result unloading of the work material takes place. The decrease in elastic deflection of the work-material e_{sb} at the end of the unloading is, for a given vibration frequency, a function of the velocity of the anvil and the amplitude of vibration and may be calculated using the expression:

$$e_{sb} = -A_o \cdot sin(\omega \cdot t_1) + A_o \cdot sin(\omega \cdot t_2) - v_A(t_2 - t_1) \qquad (8.2.2\text{-}9)$$

Changes in the elastic deflection of the work-material with time during the unloading and reloading period for a punch amplitude of A_o=*0.008mm* and velocities of the anvil of 20, 100, 200 and 500mm/s are shown in Fig.8.2.2-5. The shape of the curves is described by a the formula:

$$e_{sb} = A_o \cdot \sin(\omega \cdot t) - v_A(t - t_1) - A_o \cdot \sin(\omega \cdot t_1) \qquad (8.2.2\text{-}10)$$

which is valid within the limits $t \in < t_1, t_3 >$,

The spring back of the work-material decreases when the velocity of the anvil increases and/or when the amplitude of vibration decreases. Dotted lines in Fig.8.2.2-5 illustrates an averaged spring back over the vibration cycle, which is defined by:

$$e_{sbav} = \frac{1}{T}\int_{t_1}^{t_3} A_o \cdot \sin(\omega \cdot t) - v_A(t - t_1) - A_o \cdot \sin(\omega \cdot t_1) dt \qquad (8.2.2\text{-}11)$$

Fig.8.2.2-6 shows the variation of the maximum and average springback with the velocity of the anvil for the amplitudes of vibration of 0.0085, 0.0045 and 0.0025mm.

Decrease in the forming force during the unloading period will depend on the spring back of the work material. Consider a process, e.g. elastic-plastic compression of a cylindrical billet, for which the force history is as that shown in Fig.82.3.7. Assuming

tool to be rigid, the nominal position of the tool working face at the end of the forming cycle under the load F, is T. At the same position is the surface of the work-material, which is in contact with the tool. Let WF represents the elastic characteristic of the work-material. When the load is removed (the punch withdrawn) the work-material springback and the point W defines the new position of the work-material surface. WT represents the total springback e_{Total}. When the punch is withdrawn partially e.g. by a distance e the force F will decrease to the F' as shown in Fig.8.2.2-7. Its magnitude may be calculated using:

$$F' = F \cdot (1 - \frac{e}{e_{Total}}) \qquad (8.2.2\text{-}12)$$

It follows that the decrease in the force during the unloading period in the ultrasonically assisted operation depends not only on the magnitude of the work-material springback e_{sb} but also on the total work-material deflection which in turn depends on the elastic characteristics of the work-material and the forming operation itself.

Eq.8.2.2-12 may be expressed in a form:

$$\frac{F'}{F} = \left(1 - \frac{e}{e_{Total}}\right) \qquad (8.2.2\text{-}13)$$

which is more convenient since it defines a factor by which the force decreases during unloading. Variation of this factor with the velocity of the anvil and the amplitude of vibration will be illustrated using a data obtained in experiments on back extrusion.

The elastic stress-strain relationship, for an isotropic material, written using double suffix notation has a form [98]:

$$\left.\begin{aligned} \varepsilon_{ij} &= \frac{\sigma'_{ij}}{2G} + \frac{(1-2\nu)}{E}\delta ij \cdot \sigma_m \\ \sigma_m &= \frac{1}{3}\sigma_{ii} \\ \sigma'_{ij} &= \sigma_{ij} - \sigma_m \cdot \delta_{il} \end{aligned}\right\} \qquad (8.2.2\text{-}14)$$

The delta symbol, δ_{ij}, is equal to unity when $i = j$ and is equal to zero when $i \neq j$.

The above equation was used to evaluate the elastic deflection of the specimens in experiments on back extrusion. Pressure applied to the punch during the steady-state phase of the process in the experiments without superimposed vibration had a magnitude of 550MPa. In order to simplify the problem, it was assumed that there was no friction between the die and work-material and that the die was rigid. The ratio of the outer to inner diameter of the die was 16.8 thus, elastic deflection of the die could be neglected. Geometry of the die and the punch is shown in Fig.8.2.2-8. Since the ratio of the punch diameter to the inner diameter of the punch was 0.8, it was further assumed that stress state induced in the work-material may be consider as that induced in closed die compression. Plastic deformation of the work-material takes place when yielding conditions have been fulfilled. For Tresca criterion this occurs when:

$$\sigma_Y = \sigma_r - \sigma_z \qquad (8.2.2\text{-}15)$$

Then

$$\sigma_r = \sigma_z + \sigma_Y \qquad (8.2.2\text{-}16)$$

Substituting in the Eq.8.2.2-15 $\sigma_z = 550MPa$ and $\sigma_Y = 53MPa$ it was found that $\sigma_r = 497MPa \approx \sigma_z$. Thus, it may be assumed, that the stress-strain state of the work-material may be specified as follows:

$$\left.\begin{aligned} &\sigma_z, \quad \sigma_r = \sigma_z, \quad \sigma_\gamma = \sigma_z \\ &\varepsilon_z, \quad \varepsilon_r = 0, \quad \varepsilon_\gamma = 0 \end{aligned}\right\} \qquad (8.2.2\text{-}17)$$

Substituting these last expressions into Eq.8.2.2-13, it was found that:

$$\varepsilon_z = \frac{(1-2v)}{E} \cdot \sigma_z \qquad (8.2.2\text{-}18)$$

The natural strain under compression condition is defined as:

$$\varepsilon = ln\left(\frac{l_o}{l}\right) \qquad (8.2.2\text{-}19)$$

where l_o and l are the specimen height without load and under the load, respectively. For a punch displacement of *1.5mm*, l=*6mm* and $\sigma_z = 550MPa$ the total elastic deflection of the work-material in direction *(2)* was found to be equal to *0.019mm*.

The variation of the factor $(1-e_{sb}/e_{Total})$ or (F'/F) (Eq.8.2.2-13) with the velocity of the anvil for the calculated elastic deflection $e_{Total} = 0.019mm$ and three amplitudes of vibration *0.0085, 0.0045* and *0.0025mm* is shown in Fig.8.2.2-9. This graph also shows this ratio for the average springback e_{sbav}, which was computed using Eq.8.2.2-11. It is clear that the magnitude of the amplitude of vibration has much stronger influence on the force decrease during the unloading process than the velocity of the punch.

Experiments on back extrusion were conducted for the punch velocity in the range $(0.5 \sim 10.0mm/s)$ and nominal amplitudes of vibration of 0.0085 and 0.0045mm. The experimental results are presented in a form of curves that show the ratio of the forces measured in processes with (F_M) and without (F_S) vibration for given amplitudes of vibration and different punch velocities. The experimental curves together with the curves from Fig.8.2.2-9 are presented in Fig.8.2.2-10. The experimental curves match neither the curve illustrating the factor $(1-e_{sb}/e_{Total})$ nor $(1-e_{sbav}/e_{Total})$ for the amplitudes 0.0085 and 0.045mm. The ratio (F_M/F_S) and then the measured force F_M, increased rapidly with increase of the process velocity. It may be concluded that the observed decrease in the forming force cannot simply relate to the decrease of the force due to the unloading process but that other

mechanisms have an influence. The ratio of (F_M/F_S) obtained in the experiments are shown in Table.8.2.2-1.

Table 8.2.2-1: Ratio (F_M/F_S)

Punch velocity [mm/s]	Amplitude 0.0085mm	Amplitude 0.0045mm
0.5	0.26	0.58
1	0.35	0.63
5	0.54	0.71
10	0.65	0.78

It should be noted that the relative velocities of the punch, which were used in experiments, were in the range $(0.00046 \sim 0.0093)$ and $(0.00088 \sim 0.0177)$ for amplitudes 0.0085 and 0.0045mm, respectively. At the highest relative punch velocities *(0.0093 and 0.0177)* the reduction achieved in the forming force was 35% and 22%, respectively. It may be anticipated that to achieve a sufficient force reduction at the larger punch velocities would require the application of vibration with significantly higher amplitudes.

The ratio (F'/F) (Eq.8.2.2-13) for the average springback e_{sbav}, computed using Eq.8.2.2-11, and to the results obtained in EF simulations for both models are presented in Fig.8.2.2-11. The results obtained for the model with the rigid tool, which is based on the same principles as the kinematic model, show good agreement with the theoretical curve for an amplitude of 0.0085mm. The magnitudes of the ratio (F'/F) obtained in the simulations are smaller from the theoretical and the difference between these decreases with the relative process velocity. This discrepancy results from the fact that the reduction of the average forming force obtained in simulations resulted partially from the reduction in the friction force (Fig.7.3.2-7 and 7.3.2-8). This reduction decreased with the process velocity and consequently the difference between theoretical and simulated values decreased.

Friction conditions are not taken in to consideration in the kinetic model. The ratio (F'/F) obtained in the simulations in which friction was assumed to be zero (black diamonds in Fig.8.2.2-11) matches well the theoretical curve.

The curve illustrating the variation of ratio (F'/F), which was obtained from the simulation using the model with the elastic tool, does not match the theoretical curve so well. The curves intersect for a relative velocity of about 0.06. For the relative velocity smaller than this value theoretical values of the ratio are higher from simulated. It occurred in spite the fact that the amplitude at the working surface of the punch in the simulated process was only 0.0025mm while the theoretical curve was drawn for an amplitude of 0.0085mm.

The decreasing distance between the punch and the anvil is evidence that the plastic deformation of the work-material occurs. The distance s by which the anvil approaches the punch over one vibration cycle is the measure of deformation. The distance $\bar{s}$ depend on the velocity of the anvil and frequency f of vibration:

$$s = v_A \cdot T = \frac{v_A}{f} \tag{8.2.2-20}$$

It follows that for a given frequency the deformation s, which is achieved during the vibration period, is determined only by the velocity of the anvil (Fig.8.2.2-2) regardless of the amplitude of vibration. The deformation during one cycle increases with process velocity. For example, the amount of plastic deformation achieved per cycle is 0.0005 and 0.00005mm for velocities of 10mm/s and 1mm/s.

The deformation is partially the result of the linear movement of the anvil and partially due to the vibration of the punch. Contributions of these components in the total deformation depend on the amplitude of vibration and the velocity of the anvil. Let s_A and s_P denote the deformation over one period of vibration attributed to the anvil and punch movement, respectively. Hence,

$$s_P + s_A = s \tag{8.2.2-21}$$

this may be expressed as:

$$\frac{s_A}{s} + \frac{s_P}{s} = 1 \qquad (8.2.2\text{-}22)$$

The relationship between $\frac{s_A}{s}$ (and $\frac{s_P}{s}$) and the relative anvil velocity for an amplitude of vibration of 0.0085mm is shown in Fig.8.2.2-12. Since both variables in Fig.8.2.2-12 have relative values, the graph shows the general relationship between $\frac{s_A}{s}$ ($\frac{s_P}{s}$) and the relative anvil velocity. The contribution of the plastic deformation resulting from the anvil movement increases with increasing anvil velocity. Consequently, the work performed by the forming machine increases as the velocity of the anvil increases. The presented analysis confirms experimental observations that the influence of ultrasonic vibration on metal forming operations decreases with the increase of the ram velocity.

Contribution of the deformation attributed to the punch and anvil movement in the total deformation of the work-material during one cycle of vibration for different anvil velocities and an amplitude of vibration of 0.0085mm is shown in Fig.8.2.2-13. The deformation (s_A) attributed to the anvil movement increases, first at the increasing rate and then at the constant rate. The contribution of the deformation (s_P) attributed to the punch movement in the total deformation changes in a different manner. This deformation increases at the decreasing rate to the maximum magnitude, which is $s_P = 2A$. This occurs for a relative process velocity of about 0.78 for which, the deformation of the work material starts when punch is in its upper position. When the amplitude of vibration decreases the deformation attributed to the punch movement also decreases. This is illustrated in Fig.8.2.2-14, which show the total deformation s and attributed to the punch s_P for amplitudes of vibration of 0.0085, 0.0045 and 0.0025mm.

For the purpose of comparing the power supplied during the deformation period $(t_3 \sim t_4)$ from the sources that drive the tools the back extrusion in now examined. The reason for choosing this process is that when a steady-state phase is reached, the force F acting on the tools is constant; therefore, the power depends only on the velocity. The power input P to the work-martial is the algebraic sum of the power supplied by all external forces that act on the body. Power is calculated by integrating the scalar product of the force and the velocity vectors over the external surface of the body [99]:

$$P = \int_S v(Y) \cdot f(Y) \cdot \cos\beta(Y) dS \qquad (8.2.2\text{-}23)$$

where $f(Y)dS$ is the magnitude of the differential force vector that acts at point Y, on the elementary surface S, v(Y) is the magnitude of the velocity vector at Y and $\cos\beta(Y)$ is the angle between the force and velocity vectors. It follows that power is positive when the angle β is acute. Further, the vibrating tool provides the power when it moves towards the work-material; the formula expressing its magnitude may be defined by:

$$P_P = F \cdot v_P \qquad (8.2.2\text{-}24)$$

However, the velocity of the punch, and consequently the power, changes continuously $(v_P = A_o \cdot \omega \cdot \cos(\omega t))$. In order to compare power supplied by the punch driver to the power supplied from the anvil driver (referred to also as the forming machine) it would be convenient to compare the average powers supplied from these two sources. The formula for the average power may be obtained substituting v_P in the Eq.8.2.2-24 by the average velocity v_{Pav}. The average punch velocity during the deformation period $(t_3 \sim t_4)$ is defined as:

$$v_{Pav} = \frac{1}{(t_4 - t_3)} \int_{t_3}^{t_4} [A_o \cdot \omega \cdot \cos(\omega \cdot t)] dt \qquad (8.2.2\text{-}25)$$

Since the anvil moves at constant velocity v_A, its average velocity has the same magnitude; therefore its average power is:

$$P_{Aav} = F \cdot v_A \qquad (8.2.2\text{-}26)$$

The ratio of the average power supplied from the punch driver during the deformation period $(t_3 \sim t_4)$ to the average power supplied by the forming machine during the same period is expressed by:

$$\frac{P_{Pav}}{P_{Aav}} = \frac{v_{Pav}}{v_A} \qquad (8.2.2\text{-}27)$$

The variation of this ratio with the relative anvil velocity is shown in Fig.8.2.2-15. The curve has been computed for an amplitude of vibration of 0.0085mm. The relationship between these two variables has a hyperbolic character. The magnitude of the ratio decreases from $+\infty$ to 0 as the relative velocity of the anvil changes from 0 to 1. The figure clearly shows that within the lower range of the relative velocity of the anvil $(0 \sim 0.1)$, a small increase in the anvil velocity results in a rapid decrease in the ratio (P_{Pav}/P_{Aav}). At the relative velocity of the anvil of 0.0009 $(v_A = 1mm/s)$ the punch driver supplies 56.4 times more power than the anvil driver, while at the relative velocity of 0.046 $(5mm/s)$ only 24.8 times more. At higher velocities, the ratio changes more slowly with increase in anvil velocity e.g. at the anvil relative velocities of 0.09 and 0.19 $(100mm/s$ and $200mm/s)$ the power supplied by the punch driver is only 4.4 and 2.7, times larger than that supplied by the forming machine, respectively. The following observation may be drawn:

a. The power supplied by the punch driver in relation to the power supplied from the anvil driver decreases with the relative velocity of the anvil (and with its absolute velocity) at the decreasing rate.
b. Power supplier from the punch driver is significantly larger from that supplied from the forming machine when the relative anvil velocity is in the range $(0 \sim 0.1)$.
c. Small changes in the anvil velocity within this range result in an abrupt decrease of the power supplied from the punch driver in relation to that supplied from the anvil driver.

d. For a relative velocity of the anvil greater than 0.1, the power supplied by the punch driver, in relation to the power supplied from the anvil driver, decreases at low rate.

e. The ratio of the power supplied from the punch driver to the power supplied from the anvil driver may have a significant role on the influence of vibration on the forming force in the ultrasonic assisted operations.

f. Considerable benefits from applying vibration may be anticipated but only for small relative velocities of the anvil, up to 0.2.

The experiments on back extrusion were conducted for the ram velocity in the range $(0.5 \sim 10mm/s)$, which corresponds to a relative velocity $(0.0004 \sim 0.009)$ and $(0.0009 \sim 0.017)$ for amplitudes of vibration of 0.0085 and 0.0045mm, respectively. Therefore, findings (a) to (d) apply to the investigated ranges of the relative velocity of the ram. The results (Fig.8.2.2-10) show that the increase of the ram velocity, even within this narrow range, resulted in a rapid increase the measured forming force. In other wards the influence of the applied vibration decreased rapidly with increases of ram velocity, in particular for the amplitude 0.0085 (see Table 8.2.3-1). It may be anticipated that if the rate at which the forming force increases with the increase of ram velocity remains unchanged, the benefit from applying vibration would diminish to zero for a ram velocities less than 80 and 50mm/s for amplitudes of 0.0085 and 0.0045mm, respectively.

In the model under consideration, the amplitude of vibration remains constant. This is a consequence of the assumption that the punch is rigid. In reality, tools are made from materials, which possess elastic properties; thus, the elastic strain and stress which is induced due to the applied load may affect the amplitude of vibration. The magnitude of the induced stress and strain will depend on the load and the tool geometry. In the experiments on back extrusion, the applied load induced a compressive pressure of *550MPa* and 10MPa in the punch and the punch holder, respectively. During the experiments, the amplitudes were measured at the front face of the punch holder (see Fig.4.6.2-1b), which is about *25mm* away from the tip of the

punch. Therefore, there is no basis to assume that the same amplitude prevailed at the punch face, particularly as the punch was subjected to higher pressure than the punch holder. The amplitude at the face of the punch remains unknown. Finite Element analysis described in Section.7.3.2 revealed that the amplitude of vibration at the face of the punch was much smaller than that at the front face of the punch holder. Therefore, it may be expected that the real amplitudes at the punch tip were different from those, which were measured at the punch holder face. The lack of the knowledge of the real magnitude of the amplitudes makes the interpretation of the results difficult.

8.2.3. Energy consideration

Experimental results presented in Sections 7.2.1 to 7.2.3 show that material flow in both, the wire flattening and can extrusion processes were influenced to a greater extent by the applied vibrations than the indentation and heading processes. In wire flattening, the application of ultrasonic vibrations enabled a higher reduction of the wire. The reduction, defined as a ratio of the difference between the wire diameter and thickness of the flattened wire to the original wire diameter, for Copper wire changed from 0.42 to 0.58. For Al-G21 wire, the reduction increased from 0.37 to 0.58 while for pure Aluminium wire change was from 0.3 to 0.6. Further, in the indentation process the influence of the applied vibrations increased with deformation, while in heading, the opposite tendency was observed. These observations suggest that the influence of the longitudinal vibration applied to the tool depends on the characteristic of the metal forming operation. In order to analyse these features, the flow of material in each process was simulated using Finite Element analysis. FE models used in this analysis are described in Section 6.

Fig.8.2.3-1 to 8.2.3-3 shows the distribution of the equivalent plastic strain in indention, heading and back extrusion for a punch displacement of 2mm. Fig.8.2.3-4 shows the strain distribution in the flattened wire. The variation of the forming forces with relative punch displacement for all processes is shown in Fig.8.2.3-5. The relative punch displacement is defined as the ratio of punch displacement to the total punch displacement (x/X). In the case of wire flattening, the relative displacement is defined as the ratio of the drawn wire length to the total drawn length of 4mm.

From the experimental results and EF simulations, it may be concluded that, the magnitude of the force is not a deciding factor in determining the influence of ultrasonic vibrations on processes. Although, the force required for back extrusion was greater from the initiation of the process, compared to that required for heading, the influence of ultrasonic vibrations was observed to be greater in the former. Further, processes characterised by a constant forming force - back extrusion and wire flattening - were influenced by vibrations to a greater extent. For heading and indentation, the forming force increases with deformation. However, in heading, the increase cumulates with deformation while it reduces for indentation. Differences in the variation of the forming force are reflected in the variation of the external work that was done on the work-material.

The work to effect deformation and its variation over the duration of the process depends on both, the character of the forming force and its magnitude. The work done by the forming force can be expressed by:

$$W = \int_0^X F \cdot dx \qquad (8.2.3\text{-}1)$$

The variation of the work done by external force with the relative punch displacement for all processes is shown in Fig.8.2.3-6. It is clear from the graphs that the energy provided per unit of punch displacement depends on the process. Energy consumed is greatest in back extrusion. However, the amount of energy that had to be provided to the work-material is constant over the process duration, apart from the beginning of the process: a similar conclusion can be drawn for wire flattening. For heading, this energy increases constantly. For indentation, the energy required also increases but at a continuously reducing rate. These observations together with the experimental results suggest that changes in energy per unit time (power) supplied to the work material is a major factor for consideration in the utilisation of the process.

A further factor that should be taken into consideration, is material flow. In can extrusion and indentation, plastic deformation of the work-material takes place

mainly in the proximity of the punch. In a heading operation, the entire billet is deformed. In wire flattening the plastic deformation is a steady-state process. Another factor to be considered is the contact area between the work-material and the tool. In can extrusion, indentation and wire flattening, this area is constant while it changes continuously in heading.

An ultrasonically assisted metal forming process may be considered as one in which the energy required to deform the work-material, is supplied from two sources, the first being the forming machine while the second, the vibrating tool. This is illustrated in Fig.8.2.3-7.

Energy accumulated in the vibrating tool, is the sum of its kinetic and potential (spring) energy:

$$E = E_K + E_P \tag{8.2.3-2}$$

These energy components varies with time as described by the following formulae (refer to Appendix 8.2.3.1):

$$E_K = \pi^2 \cdot A^2 \cdot f^2 \cdot V \cdot \rho \cdot \sin^2(2\pi \cdot f \cdot t) \tag{8.2.3-3}$$

$$E_P = \pi^2 \cdot A^2 \cdot f^2 \cdot V \cdot \rho \cdot \cos^2(2\pi \cdot f \cdot t) \tag{8.2.3-4}$$

It follows that the total energy is constant and equal to a maximum of either the kinetic or potential energy. Deformation of the work-material by the vibrating tool would occur only during half the oscillatory movement of the tool when its motion is in the direction of the work-material. The amount of energy expended in the work-material will depend on amplitude and frequency of vibration. However, the decrease in tool energy ΔE cannot be significant as this would result in a change in the amplitude. The average kinetic energy of the tool may be estimated using the following equation:

$$E_{K,AV} = \frac{1}{T} \cdot \int_0^T E_K \cdot dt = \frac{\pi^2}{2} \cdot A^2 \cdot f^2 \cdot V \cdot \rho \tag{8.2.3-5}$$

For parameters: $A=10^{-5}$m, f=20kHz, $V=1.5\cdot 10^{-4}m^3$ (d=0.038m, l=0.128m) and $\rho=7850kg/m^3$ the average kinetic energy is $E_{K.,AV}=0.22J$. However, only a fraction of this energy, may be transferred to the work-material over one period of vibration.

In a conventional metal forming operation the energy delivered by the forming machine deforms the work-material and overcomes friction forces. Assuming that there is no friction at the tools/work-material interface, all work is used to deform the work-material. The average work done by the forming machine over the duration of the vibration period is:

$$\overline{W}_{Sav} = F_S \cdot v \cdot T = F_S \cdot s \qquad (8.2.3\text{-}6)$$

When vibrations are applied the forming tool, deformation of the material occurs over a small fraction of the vibration cycle, particularly at low process velocity (Fig.8.2.2-4). Over the remaining part of the cycle, during which unloading and reloading of the work material occurs, the work done by the forming machine is redundant work. The magnitude of this work depends on the process velocity, amplitude of vibration and frequency. Work done by the forming machine is always positive while that done by the vibrating tool is positive only over one half of the period when the tool moves towards the work material. However, energy used to reload the work material is recovered during unloading. Thus, the work done by the vibrating tool may be assumed to be that which deforms the work-material plastically.

Variations of the forming force over one cycle of vibration for a process velocity of 10mm/s and amplitudes of vibration of *0.0085* and *0.0045mm* are shown in Fig.8.2.3-8. These curves were derived from the kinematic model. During the unloading and reloading period the magnitude of the force changes in accordance with Eq.8.2.2-12 in which springback (e) is defined by Eq.8.2.2-10. The average force during this period is shown by the dotted line. The amplitude of vibration has a more significant influence on its magnitude than the process velocity (Fig.8.2.2-9). During the time when deformation occurs, over the interval $(t_3 \sim t_4)$, the forming force is equal to

that in the static operation (F_S) in accordance with the earlier assumption that vibrations change neither the Yield Stress nor the work-hardening rate. The total deformation during one cycle depends only on the process velocity (Eq.8.2.2-20), regardless of the amplitude of vibration. Work done by the forming machine over one vibration cycle is:

$$\overline{W}_M = F_S \cdot s_M + F_S \cdot s_R + \int_{s(t_1)}^{s(t_3)} F v ds \qquad (8.2.3\text{-}7)$$

Symbols are defined Fig.8.2.3-9. The first component in Eq.8.2.3-7 represents work, which is done to deform the work material. The second and third components represent redundant work. The second work is done during the deformation period when the velocity of the anvil and the vibrating tool have the same direction. The third work is performed during unloading and reloading period.

The average force exerted by the forming machine over the vibration cycle is:

$$F_{Mav} = \frac{\overline{W}_M}{s} = \frac{F_S \cdot s_M + F_S \cdot s_R + \int_{s(t_1)}^{s(t_3)} F ds}{s} \qquad (8.2.3\text{-}8)$$

Consequently, with the earlier assumption that the force F_S required to deform the work material is not influenced by vibrations, the average force exerted by the forming machine depends on the remaining parameters in Eq.8.2.3-9. These, in turn, depend on process velocity and amplitude for a given frequency. The latter has a more significant influence on the magnitude of force *(F)* during unloading (Fig.8.2.2-9) while the former influences the extent of deformation (Fig.8.2.2-14). Therefore, a decrease in amplitude would manifest itself as an increase in the redundant work done by the forming machine and would have a minor effect on the work done to deform the work material.

Work done by the vibrating tool over one vibration cycle is that expended to deform work material:

$$\overline{W}_U = F_S \cdot s_U \tag{8.2.3-9}$$

The total energy used to perform the operation with vibrations is the sum of these two components:

$$\overline{W}_{Total} = \overline{W}_M + \overline{W}_U = F_S \cdot (s_M + s_U) + F_S \cdot s_R + \int_{s(t_1)}^{s(t_3)} F ds \tag{8.2.3-10}$$

Since $(s_M + s_U = s)$ Eq.8.2.3-10 may be expressed as:

$$\overline{W}_{Total} = F_S \cdot s + F_S \cdot s_R + \int_{s(t_1)}^{s(t_3)} F v dt \tag{8.2.3-11}$$

Graphical illustration of Eq.8.2.3-11 is shown in Fig.8.2.3-9a. The graph was constructed for the force variation shown schematically in Fig.8.2.3-9b.

Work done by the forming machine (Eq.8.2.3-7) with vibration applied the tool is smaller than in the conditions when vibrations are not applied. However, the total energy used to perform this operation is greater (compare Eq.8.2.3-11 and 8.2.3-6). This is the disadvantage of this approach. From the viewpoint of possible industrial application, this is an important issue since energy requirement per component increases. Additionally, capital costs are incurred on ultrasonic system (generator, transducer, booster and tool) and its maintenance. Further, the energy expended to the work material is a small fraction of that required to sustain vibrations. It can be shown, using the data obtained in experiments on back extrusion. In the operations without vibration, the average work done by the forming machine over the interval equal to the vibration period was *0.0034J* and *0.00016J* at process velocities of *10* and *0.5mm/s*, respectively. Assuming the extreme case that the total deformation is achieved due to vibration, the energy expended to work material would be equal to the quoted figures. The total energy of the tool (punch and punch holder) was about *0.22J* (Appendix 8.2.3.1). It follows that the efficiency of the ultrasonic system is low.

9. CONCLUSION AND SUGGESTIONS FOR FURTHER RESEARCH

9.1. Conclusions

From the experiments, analysis and simulation conducted the following conclusions are drawn:

1. The forming force decreases when vibrations are imposed on the forming tool. This effect was observed when the direction of the applied longitudinal vibration was either perpendicular or parallel to the direction of the forming force. The decrease in the forming force was directly proportional to the amplitude of vibration. For instance, in back extrusion at a process velocity of 0.5mm/s the forming force was reduced by 72% and 41% for amplitudes of 0.0085mm and 0.0045 mm, respectively. The decrease in the forming force was inversely proportional to process velocity. In back extrusion for an amplitude of 0.0085mm the forming decreased by 72% and 35% for the process velocity 0.5 and 10mm/s, respectively.

2. It has been claimed that reduction in the forming force, in ultrasonically assisted metal forming, was attributable to stress superposition and/or reduction in friction at the interface between the vibrating tool and the work material. These two phenomena were inseparably in reported research. In the WP/T tool, longitudinal vibrations were imposed on the forming tools in a direction perpendicular to the forming force, thus, the stress superposition effect was eliminated and the reduction in the forming force may be attributed to the reduction of friction forces.

3. In the experiments performed with WP/T tool, the decrease in the specimen height was greater when the specimen was compressed with vibration than without under the same load. The true strain in the Aluminium specimen increased by 0.026, which is in agreement with the theoretical estimate of 0.024. The longitudinal vibration imposed to the forming tools, in a direction

perpendicular to the forming force, for the compression of specimen reduced friction between the tool and the work material.

4. The proposed model of ultrasonically assisted forging operations, based on kinetics of the rigid tools and elasto-plastic model of the work material, describes qualitatively the experimental results on back extrusion. Quantitative comparison of the theoretical model with the experimental results would require the extraction of data of the actual amplitude at the working surface of the punch.

5. The proposed model enabled the analysis of the force acting on the tools and energy required over one cycle of vibration for a given configuration of process velocity and amplitude of vibration. It was found that the total work done by both, the forming machine and vibrating tool is greater than that delivered by the forming machine under static conditions. The greater proportion of the work done by the forming machine, when vibrations are imposed on the tool, is redundant work, the magnitude of which is a function of process velocity and amplitude of vibration.

6. The energy delivered by the vibrating tool to effect plastic deformation account for a small fraction (a few percent) of that required to sustain vibration. Therefore, the overall efficiency of ultrasonically-assisted metal forming systems is poor.

7. Finite Element simulations of back extrusion revealed that the decrease in forming force due to longitudinal vibrations is, partially, attributable to the change in direction of friction forces acting between the work material and tools, dies and punches. This effect diminished as the velocity of the process increased. Reduction of the forming force in back extrusion as a consequence of the friction "vector effect " was confirmed by the numerical analysis.

8. Finite Element simulations of back extrusion using the model with an elastic tool revealed that the amplitude of vibration at the working surface of the punch was smaller than that at the surface of the punch holder. It was also found that the magnitude of this amplitude was dependent on the applied load. This finding confirms the fact that vibrations had an insignificant influence on the forming force when deforming Steel specimens.

9. High-strength work materials and/or large component would require vibrations of higher amplitudes. This, in turn, would require high-power generators and special materials for the construction of tools. In some operations, power requirements would outweigh the force-related advantages.

10. The amplitude and frequency of vibration are influenced by the applied load. The amplitude of vibration is additionally affected by process velocity. For this reason the ultrasonic generator that supplied power to the transducer would have to be equipped with two feed-back control loops – for frequency and amplitude - to maintain these parameters at the required level. This requirement demands a complex design of ultrasonic generator and would necessitate the installation of the devices for real-time monitoring amplitude of vibrations. All these factors increase the cost of the ultrasonic sub-system.

11. The design of the ultrasonic tools remains difficult in view of the fact that thses have to comply, not only with mechanical but also with resonant conditions. Efficiency of the ultrasonic system depends on the precision with which the geometry of the tool is matched to the resonant frequency. Mounting of the ultrasonic tool is the another factor, which has significant influence on the system efficiency. Practical knowledge in this field is required to achieve a satisfactory design solution using traditional method of iterations through proving trials.

12. The developed Finite Element approach for evaluating tool design has proven to be successful. Modal analysis enabled the tuning of tool geometry to the resonant

frequency exactly without the need for proving trials. This decreased tool production time and cost.

13. The efficient design of the ultrasonic tools has to include following considerations:
    - minimisation of internal energy losses
    - minimisation energy losses to the supporting structure
    - maintain resonance regime under changing load conditions
    - modularity of design to enable rapid replacement of the tools
    - access to the deformation zone

14. The operation and maintenance of the ultrasonic system requires craft knowledge of ultrasonic equipment and processes.

15. In a view of complexity, cost and low efficiency of ultrasonic systems, the potential of adapting ultrasonics to industrial metal forming operations is restricted to steady-state deformation under low forces. Operations, such as wire and tube drawing, and deep drawing are acceptable candidates.

16. Significant benefit from applying vibration is observed for low process velocity and load. It implies that other possible industrial applications of the UMFORM would be in the area of metal forming of small and miniature metal components and/or components of unusual shape.

9.2. Suggestions for further research

Benefit from using ultrasonic vibration in metal forming may be significant. This will depend on the efficiency of the ultrasonic system and product requirements. Refinement of equipment and identification of specific applications in which vibration may provide substantial benefit are a scope of further research.

1. Refinement of equipment refers to both components - the generator and tool design system. Efficiency of the system depends to large extent on precise control of the amplitude of vibrations. Power of the generator would be also an important feature. Development of a new generation of generators complying with these requirements is a priority. Control of the amplitude necessitates the use of instrumentation for measuring amplitude in real time. New advanced technologies, such as laser vibrometry, enable the measurement of the amplitude remote from the operation. The amplitude may be measured at the point close to the deformation zone enabling better process control. Incorporation of such devices in tooling systems has to research.

2. Refinement of the design a wide range of elements has to be investigated to improve the performance of the ultrasonic system. Ultrasonic tools are prone to troublesome modal behaviour, in particular those of a complex geometry. Under changing operational conditions, these may switch to another mode, which is in close proximity, thus negating the effect of vibration. The identification of all modes and elimination of these close to the operational mode through the refinement of tool components is an important task. Use of several analytical techniques, such as FE analysis and experimental modal analysis (EMA) would yield good results; further development of these is proposed.

3. Another task in tool design, which needs to be attended to, is tool-mounting on the supporting structure. Leak of energy to the supporting structure through the mounting manifests itself as a decrease in amplitude. From the efficiency view

point improvement and optimisation of this feature is of great significance. Since energy in the ultrasonic system is transferred through a few components, the interface between these would be the origin of some problems, including the loss of energy. These design issues should be researched further.

4. Promising results obtained for wire flattening suggests that this may be developed further. Vibrating tools may be used in the production of narrow, flat strips with unusual cross-sectional areas or of variable cross-sections. There is already demand for thin 0.2mm strips of rhombic shape cross-section.

5. Since the approach may be applied to the forming of miniature components, the response of miniature materials to sever plastic deformation would have to be assessed accurately.

10. REFERENCES

1 Severdenko W. P., Klubowitch W. W., Stepanov A. W., Ultrasonic assisted metal forming, Nauka I Techinika, Minsk 1973.

2 Amza G., Drimer., The design and construction of solid concentrators for u;trasonic energy., Ultrasonics, September 1976, pp.223-225.

3 Achenbach J.D. Wave propagation in elastic solids, North Holland Publishing Company, 1973, ISBN 0 444 10465 8

4 Plasticity and modern metal-forming technology, edited by Blazynski, Elsevier Applied Science, Chapter 4 by T. Z., Johnson W., Yu T. X., An outline of Enginnering dynamic Elasticity and Plasticity, ISBN 1 85166 272 3, 1989

5 Blaha B., Langenecker F., Strain of zinc monocrystals under the effect of ultrasonic vibration, Naturwissenschaften, 42, 1955

6 Nevill G. E., Brotzen F. R., the effect of vibration on the static yield strength of low-carbon steel, Proc. Am. Soc. Test Materials, 57, 1957, pp 751

7 Langenecker B. Effect of ultrasound on deformation on characteristics of metals, IEEE Trans Sonics Ultrasonics, SU-13, No 1, 1966

8 Blaha F, Langenecker B, Ultrasonic investigation of the plasticity of metal crystals. Acta Metallurgica, Vol 7, 2, 1959

9 Izumi O, Oyama K, Suzuki Y, Effect of superimposing ultrasonic vibration on compressive deformation of metals, Trans. Japan Institute of Metals, 1966, Vol. 7, p. 162-167

10 Konovalov E G, Skripnichenko A l, The effect of ultrasonic vibration on tensile properties of metals. Russian Engineering Journal 195, 45(8), 31-32

11 Kuzmenko V. A., Fatigue strength of structural materials at sonic and ultrasonic loading frequencies, Ultrasonics, Vol.12, 1975, pp. 21-30

12 Fridman H D, Levesque P, Reduction of static friction by sonic vibrations, Journal of Applied Physics, Vol.30, No. 10, 1959, pp1572-1575.

13 Lenkiewicz W, The sliding friction process – effect of external vibrations. Wear, 13, 1996, 99-108

14 Tolstoi D M, Significance of the normal degree of freedom and natural normal vibrations in contact friction. Wear, 10, 1967, pp 199-213

15 Rozner A G, Effect of ultrasonic vibration on coefficient of friction during strip drawing. The Journal of the Acoustic Society of America, Vol. 49, No. 5, 1971

16 Sigert K., Ulmer J., Reduction of sliding friction by ultrasonic waves, Production Engineerring Vol.V/1, 1998, pp 9-12

17 Siegert K., Moeck A., Wire drawing with ultrasonically-oscillating dies, Journal of Materials Processing Technology 60 (1996).

18 Masao Murakawa, Masahiko Jin, The utility of radially and ultrasonically vibrated dies in the wire drawing process. Journal of materials Processing Technology113, 2001, p81-86

19 Li Lianshi, Lang Xiaoping, Wire drawing with ultrasonic vibrations, Wire Industry, January 1994.

20 Graff K. F., Results from recent studies in power ultrasonic at Ohio State University, Ultrasonics International 1975 Conference Proceedings, pp 23-27

21 Siegert K., Ulmer J., Superimposing ultrasonic waves on tube and wire drawing, Advanced Technology of Plasticity, Vol. III, Proceedings of the 6th ICTP, 1999

22 Winsper C E, Sansome D H, Application of ultrasonic vibrations to the plug drawing of tube, Metal forming, 1971, March, 71-76

23 Nosal V V, Rymsha O M, Reducing the drawing force by ultrasonic oscillations of the drawplate and determining the technological parameters of tube drawing. Stal, 1966, 2, 135-137

24 Pasierb A., Wojnar A., An experimental investigation of deep drawing and drawing processes of thin-walled products with utilisation of ultrasonic vibrations, Journal of Materials Processing Technology, 34 (1992).

25 Jimma T. et al., An application of ultrasonic vibration to the deep drawing process, Journal of Materials Processing Technology, 80-81 (1998), pp. 406-412

26 Jin M. et al. Utility of ultrasonic vibration applied to metal-forming processes. Advanced Technology of Plasticity, Vol. III, Proceedings of the 6th ICTP, Sept., 1999, pp 2193-2198.

27 Takemasu T. et al., Surface finish of aluminium pipe in multi-stage ironing with ultrasonic vibrations, Advanced Technology of Plasticity, Vol. III, Proceedings of the 6th ICTP, Sept., 1999, pp 1859-1866.

28 Spiers R M, Winsper C F, Sansome D H, Direct extrusion of metal with applied oscillatory energy. Metal Forming, October 1969, pp. 271-277.

29 Huang Z., Lucas M., Adams M.J., Effect of vibration on axisymmetric indentation of a model elasto-viscoplastic material. IMechE Conference Translations, 16th Int. Conference on Computer-Aided Production Engineering CAPE 2000.

30 Siegert K, Mock A, Malek R, OH S , Flexible micro metal forming with ultrasonically oscillating dies, Advance technology of Plasticity, Columbus, Ohio, October 1996

31 Hart E. W., A phenomenological theory for plastic deformation of polycrystalline metals, Acta Metallurgica, Vol. 18, June 1970.

32 Herbertz J., The influence of mechanical vibration on plastic deformation of metals, Proceedings of Ultrasonic International Conference 1997, Brighton ,pp323-327.

33 Green R. E., Non-linear effect of high-power ultrasonic in crystalline solids. Ultrasonics, May 1975, 117-127

34 Silin L. L. et al., Ultrasonic welding, Mashgiz, Moscow, 1962.

35 Bochniak W., Korbel A., High energy saving technology of metal forming, Proceedings of the International Conference, South Africa, 1996

36 Whymark R.R., Acoustic field positioning for containerless processes, Ultrasonics 23(5), 1975, pp. 251.

37 Hashimoto Y., Koike Y., Ueha S., Near-field acoustic levitation of planar specimen using flexural vibration, Journal of Acoustic Society of America 100 (4), 1996 2057.

38 Ueha S., Hashimoto Y., Koike Y., Non-contact transportation using near-field levitation, Ultrasonics, 38, 2000, pp. 26-32.

39 Mitskevich A. W., Motion of the body over a vibrating surface., Soviet Physics – Acoustic, 13(3), 1968, 348

40 Winsper C. E., Dawson G. R., Sansome D. H., An introduction to the mechanics of oscillatory metalworking, Metals and Materials, April, 1970, pp.158-162.

41 Severdenko W. P., Klubowitch W. W., Stepanenko A. W., Ultrasound and plasticity, Nauka i Technika, 1976.

42 Puskar A. The use of high intensity ultrasonic, Elsevier Scientific Publishing, 1982

43 Eaves A., E. at al, Review of the application of ultrasonic vibrations to deforming metals, Ultrasonics, July 1975.

44 Pasierb A. Effects of ultrasonic vibrations on force parameters and friction in the process of wire and tube drawing. Scientific Bulletins of Stanislaw Staszic University of Mining and Metallurgy, Bulletin 86, Krakow 1979

45 Robinson A.T., Wire and Wire Products, 39, No2,1964

46 Winsper C.E., Dawson G.R., Sansome D. H., Journal Institute of Metal, 97, 1969, pp 274

47 Pasierb A. Ciagnienie rur z zastosowaniem ultradzwiekowych drgan trzpienia-mozliwosc zwiekszenia granicznych wskaznikow odksztalcenia, Rudy Metale R 40, Nr 11, 1995, pp 490-492.

48 Petruzelka J., Hollow ultrasonic tube drawing, Medzinarodna Konferencia Interultrasonis, Bratyslava, 1994.

49 Young M. J. R., Winsper C. E., Sansome D. H., The design of high intensity radial vibrations for metal working applications. J. Phys. D: Applied Physics., Vol. 4, 1971, pp 212-216

50 Lucas M., Vibration sensitivity in the design of ultrasonic dies, Ultrasonics, Vol. 34, 1996, pp 35-41.

51 Cheers C. F., Design and optimisation of an ultrasonic die system for forming metal cans, PhD Thesis, Loughborough University of Technology, 1995.

52 Kariyawasam V. P., Young M. J. R., Sansome D. H., An experimental and design study in of fixed plug tube drawing with radial ultrasonic vibration of the die, Wire Industry, 1979.

53 Ibrahim I. N., Sansome D. H., An experimental study of the mechanics of ultrasonic tube-bending,

54 Nikagari A., Sansome D.H., Ultrasonic tube extension, Ultrasonic International 1975, Conference Proceedings, pp 338-345.

55 Masao Murakawa, Masahiko Jin, Manufacture of Precision Aluminium Tubes as Photosensitive Drums by the Extrusion and Drawing Method Using Ultrasonic Vibration, Conference Advanced Technology of Plasticity, Ohio, October 1996.

56 Smith A. W., Sansome D. H., An experimental investigation of the effect of blank-holder vibrations on an analogue of the deep-drawing process, Ultrasonics International 1975 Conference Proceedings, pp210-213.

57 Nell M., Hallow piston hammer, US Patent No 1927499,1933.

58 Vang A. Material forming and drawing with the aid of vibration. Us patent 2393131, January 1946.

59 Green Lee B, Apparatus for extruding. US patent 2408627, October 1946.

60 Rosenthal A., Apparatus for drawing wire. US patent 2568303, September 1951.

61 Gutterman R. P., Method and apparatus for forming wire and the like, US patent 2638207, May 1953.

62 Jones J. B., Vibratory squeeze-forming of metals in the solid state and apparatus therefor, US patent 3002614, October 1961.

63 Jones J. B., Ultrasonic extrusion apparatus, US patent 3203215, August 1965.

64 Calosi C., Support for vibratory devices., US patent 2632858, March 1953

65 Elmore W. C., Support for vibratory devices., US patent 289179, June 1959.

66 Bodine A. G., Method and apparatus for forming plastic materials, US patent 3233012, February 1966.

67 Boyd C. A et al, Apparatus utilising vibratory energy, US patent 3212312, October 1965

68 Boyd C. A et al, Tube drawing apparatus employing vibratory energy., US patent 3212313, October 1965

69 Dawson G.R., Sansome D.H., Vibratory forming. UK Patent 1379234, 1971.

70 Maropis N., Method and apparatus applying vibratory energy, US patent 3295349, January 1967.

71 Dawson G.R., Wisnsper C.E., Sansome D. H., Application of high- and low-frequency oscillation to the plastic deformation of metals, Metal Forming, April, 1970, pp 158-162.

72 Dawson G.R., Wisnsper C.E., Sansome D. H., Application of high- and low-frequency oscillation to the plastic deformation of metals, Metal Forming, September, 1970, pp 254-261.

73 Biddell D.C., Sansome D.H., The development of oscillatory metal drawing equipmnet- an engineer's view. Ultrasonics, September 1974, pp-195-205.

74 Thimoshenko S., Young D.H., Weaver W., Vibration problems in engineering, John Wiley & Sons, 1974, ISBN 0471-87315-2

75 Malicki I. "Analogie elektro-mechano-akustyczne" Wydawnictwa Politechniki Warszawskiej,1981.

76 Rossing T.D., Fletcher N.H., Principles of vibration and sound, Springer-Verlag,1995.

77 Standard definition and method of measurement for piezoelectric vibrators, IEEE No.177, May 1966.

78 Zelenka J., "Piezoelectric resonators and their application", Elsevier 1986, ISBN 0444995161

79 Sashida t., An introduction to ultrasonic motors, Clarendon Press, Oxford 1993

80 Pisarenko G.S., Jakovlev A.P., Matiejev W.W., Wlasnosci tlumienia dran materialow konstrukcyjnych, Wydawnistwo Naukowo-Techniczne, Warszawa 1976.

81 Adams R.D., The damping characteristics of certain steels, cast iron and other metals, Journal of sound and vibrations, 23(2) 1972, pp 199-216.

82 Kuzmenko V.A. Fatigue strength of structural materials at sonic and ultrasonic frequwncies, Ultrasonics, January 1975, pp 21-30.

83 Arnold F.J., Muhlen S.S. The resonance frequencies on mechanically pre-stressed ultrasonic piezotransducers, Ultrasonics 39, 2001, pp 1-5

84 Arnold F.J., Muhlen S.S. The mechanical pre-stressing in ultrasonic piezotransducers, Ultrasonics 39, 2001, pp. 7-11.

85 Gough P.T., Knigth J.S., Wide bandwidth, constant beam width acoustic projectors: a simplified design procedure, Ultrasonics, July, 1989, pp 234-238.

86 Niezgodzinski M. E., Niezgodzinski T., Wzory wykresy i tablice wytrzymalosciowe, Wydawnistwo Naukowo-Techniczne,ISBN 83-24-2025-3, 1996

87 Ball A., Wire flattening, The Wire Industry, May, 1956, pp 423-456.

88 Weber R.D., Wire flattening Theory, The Wire Industry, September, 1956, pp 811-816,837.

89 http://www.kcn.ru/tat_en.economic/profiles/m/melita_k/home.htm

90 ABAQUS Manual.

91 Comnication with Mr J. Gorczynski, Instytut Tele-Radiotechniczny

92 K. Chodnikiewicz ,"Mechanika mlotow i pras mechanicznych", Wydawnictwa Politechniki Warszawskej, Warszawa 1985, pp.64.

93 Or S.W., Chan H.L.W., Lo V.C., Yun C.W. Dynamics of an ultrasonic transducer used for wire bonding. IEEE Transaction on Ultrasonic, ferroelectrics, and Frequency Control, Vol.45, No. 6, November 1998, pp 1453-1460.

94 Dubus B., Debus J.C., Decarpigny J.N., Boucher D., Analysis of mechanical limitations of high power piezoelectric transducer using finite element modelling. Ultrasonics, Vol.29, May 1991, pp 201-207.

95 Huang Z., Lucas M., Adams M.J., A finite element study for optimising wall boundry conditions in an elsto-viscoplast material forming process. Proceedings of 15th International Conference on CAPE, Part1, 117-124,1999,

96 Bacharov Y., Kobayashi S., Thomsen E. G., "The effect of vibration on plastic flow in coining", ASME Trans (J. Eng. For Industry), Nov, 1962, pp 502-505.

97 Olejnik L. The method for uniform plastic deformation at high level of tension stress. Reports of ITB, Warsaw University of Technology, 19831, 1, pp-7-21.

98 Johnson W., Mellor P.B., Engineering plasticity, Van Nostrand Reinhold Company, 1978, ISBN 0 442 30234 7.

99 Talbert S.H, Avitzur B. Elementary mechanics of plastic flow in metal forming, John Wiley & Sons, 1996, ISBN 0 471 6003 9.

100 Sliwinski A., Ultradzwieki I ich zastosowanie, Wydawnictwa Nukowo-Techniczne, ISBN 0 07 036285 8

101 Handbook of metal forming, Edited by Lange K., McGraw-Hill Book Company, ISBN 83 04 2576 0

APPENDIX 1.1 Elastic-plastic wave propagation theory.

The equation of the motion of the longitudinal wave is:

$$\frac{\partial \sigma}{\partial x} = \rho_o \cdot \frac{\partial^2 u}{\partial^2 t} \qquad \text{(A1.1-1)}$$

Using Hooke's Law $\sigma = E \cdot \varepsilon$ and the definition for strain $\varepsilon = \partial u / \partial x$, Eq.1.3 takes the following form:

$$\frac{\partial^2 u}{\partial^2 t} = c_o^2 \frac{\partial^2 u}{\partial^2 x} \qquad \text{(A1.1-2)}$$

where:

$$c_o = (E/\rho_o)^{1/2} \qquad \text{(A1.1-3)}$$

A general solution for the one-dimensional wave (Eq.A1.1-2) has a form:

$$u = f(x - c_o t) + g(x + c_o t) \qquad \text{(A1.1-4)}$$

where f and g are independent arbitrary functions. First function represents the wave travelling in the positive x direction while the second term represents wave travelling in the negative direction.

Considering only first term in the Eq.A1.1-4

$$u = f(x - c_o \cdot t) \qquad \text{(A1.1-5)}$$

it can be shown that the constant $c_o = (E/\rho_o)^{1/2}$ is the velocity of the elastic wave propagated along the bar. Assume that $u = s$ when $t = t_1$ and $x = x_1$, and also $u = s$ when $t = t_2$ and $x = x_2$ then $s = f(x_1 - c_o \cdot t_1) = f(x_2 - c_o \cdot t_2)$. Thus

$$x_1 - c_o \cdot t_1 = x_2 - c_o \cdot t_2 \qquad \text{(A1.1-6)}$$

Hence,

$$c_o = \frac{x_2 - x_1}{t_2 - t_1} \qquad \text{(A1.1-7)}$$

and is a speed of the propagation of the elastic deformation as well as of the stress wave along the bar.

The relationship between the stress σ and the velocity v of the movement of the particles at location x is:

$$\sigma = \rho_o \cdot c_o \cdot v \tag{A1.1-8}$$

The quantity $\rho_o \cdot c_o = (E/\rho_o)^{1/2}$ is referred to as mechanical impedance.

An elastic wave of intensity, σ_1, propagating in a bar will be partly transmitted and partly reflected after reaching an interface with a region in which properties are different from those previously traversed by the wave. In practice, the interface could take the form of a boundary, a change of geometry, material or a local constraint. The intensities σ_T and σ_R of the transmitted and reflected waves respectively, in a bar with a discontinuous cross-section made from two different materials (Fig.1.5), are [4]:

$$\sigma_T = \frac{2 \cdot S_1 \cdot \rho_2 \cdot c_2}{S_1 \cdot \rho_1 \cdot c_1 + S_2 \cdot \rho_2 \cdot c_2} \cdot \sigma_1 \tag{A1.1-9}$$

$$\sigma_R = \frac{S_2 \cdot \rho_2 \cdot c_2 - S_1 \cdot \rho_1 \cdot c_1}{S_1 \cdot \rho_1 \cdot c_1 + S_2 \cdot \rho_2 \cdot c_2} \cdot \sigma_1 \tag{A1.1-10}$$

If materials of both sections of the bar are identical ($\rho_1 \cdot c_1 = \rho_2 \cdot c_2$) Eq.A1.1-9 and Eq.A1.1-10 take the form:

$$\sigma_T = \frac{2 \cdot S_1}{S_1 + S_2} \cdot \sigma_1 \tag{A1.1-11}$$

$$\sigma_R = \frac{S_2 - S_1}{S_1 + S_2} \cdot \sigma_1 \tag{A1.1-12}$$

If $S_2 > S_1$, then σ_R and σ_T have the same sign, if $S_2 < S_1$, then σ_R and σ_T have opposite signs. Further, if $S_2/S_1 \to \infty$, the end of the bar is effectively fixed and $\sigma_R \to \sigma_1$ while $\sigma_T \to 0$. Next, if the ratio $S_2/S_1 \to 0$, the end of the bar is effectively free, and $\sigma_R \to -\sigma_1$ while $\sigma_T \to 2\sigma_1$. The minus sign denotes that the wave changes from compressive to tensile or vice verse. When a series of elastic

waves is produced at the one end of the free bar, the original and reflected form would superimpose on one another. Since both waves have the same magnitude, a section of the bar where the two waves interact would have a total stress equal to zero and the particle speed is twice what it was when only the incident wave was propagating. When two compressive or tensile waves interact, the resulting stress is doubled and the particles speed is zero. In the case when the propagated wave has a sinusoidal form, with a wavelength $\lambda = i \cdot c/(2 \cdot l)$, the original and reflected waves interact to produce a standing wave. This occurs when the frequency of the imposed wave is equal to the natural frequency of the bar.

When the load acting on the body induces stress of a magnitude higher than the initial Yield Strength of the material, an elastic-plastic wave will propagate in the body. The basic equation of the motion for this longitudinal plastic wave has the form:

$$\frac{\partial^2 u}{\partial t^2} = c_p \cdot \frac{\partial^2 u}{\partial x^2} \qquad \text{(A1.1-13)}$$

where $c_p = \left(\frac{1}{\rho_o} \cdot \frac{\partial \sigma}{\partial \varepsilon} \right)^{1/2}$ is the velocity of the propagation of the plastic wave. In most cases the relationship, $\sigma = \sigma(\varepsilon)$ is described by a monotonically increasing function but of a reducing slope as the strain increases, that is $\partial\sigma/\partial\varepsilon > 0$ and

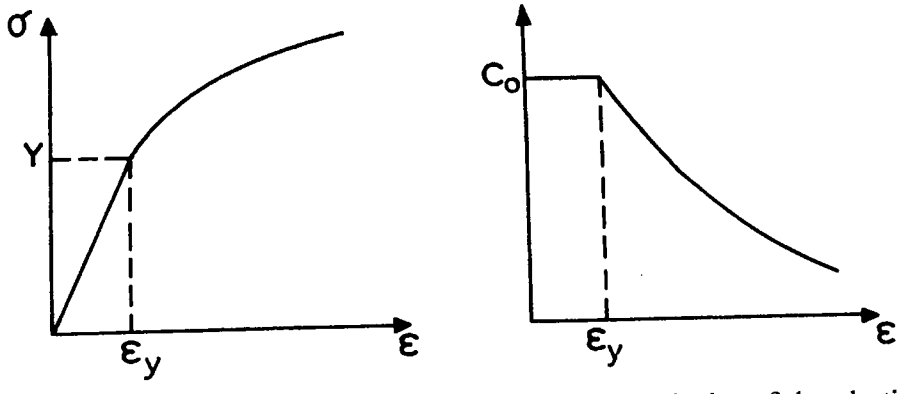

Fig.A1.1-1. (a) Hardening stress-strain curve. (b) Velocity of the elastic-plastic wave for the material characterised by (a). [92]

$\partial^2\sigma/\partial\varepsilon^2 < 0$ b; thus, the velocity of the plastic wave reduces with strain. The higher the stress intensity, the slower is the plastic wave. Fig.A1.1-1b shows the variation of the velocity of the elastic-plastic wave with strain for the material characterised by the hardening curve shown in Fig.A1.1-1ba.

By contrast, if the material strain-hardens at the increasing rate ($\partial\sigma/\partial\varepsilon > 0$ and $\partial^2\sigma/\partial\varepsilon^2 > 0$), then the velocity of the stress wave increases with stress intensity. Eq.A1.1-13 is derived from Eq.A1.1-1 by using a general relationship between stress and strain $\sigma = \sigma(\varepsilon)$, instead of applying Hooke's Law for the elastic range.

The relationship between the stress σ and the speed v of the particles is:

$$d\sigma = \rho_o \cdot c_p \cdot dv \qquad \text{(A1.1-14)}$$

where $\rho_o \cdot c_p$ is the mechanical impedance.

APPENDIX 4.2.1 Energy dissipated in the vibrating element.

Energy per a unit volume dissipated as heat due to internal friction over one cycle of vibration is defined by Eq.4.10. It follows that energy dW, which is lost in the element of the volume dV of a prismatic bar (Fig.A4.2.1-1) during the vibration period is given by:

$$dW = \pi \cdot \xi \cdot \sigma_{max} \cdot \varepsilon_{max} \cdot dV \qquad \text{(A4.2.1-1)}$$

where:

$$\varepsilon_{max} = \left(\frac{du(x,t)}{dx} \right)_{max} \qquad \text{(A4.2.1-2)}$$

$$\sigma_{max} = E \cdot \varepsilon_{max} \qquad \text{(A4.2.1-3)}$$

$$dV = \frac{\pi}{4} \cdot d^2 \cdot dx \qquad \text{(A4.2.1-4)}$$

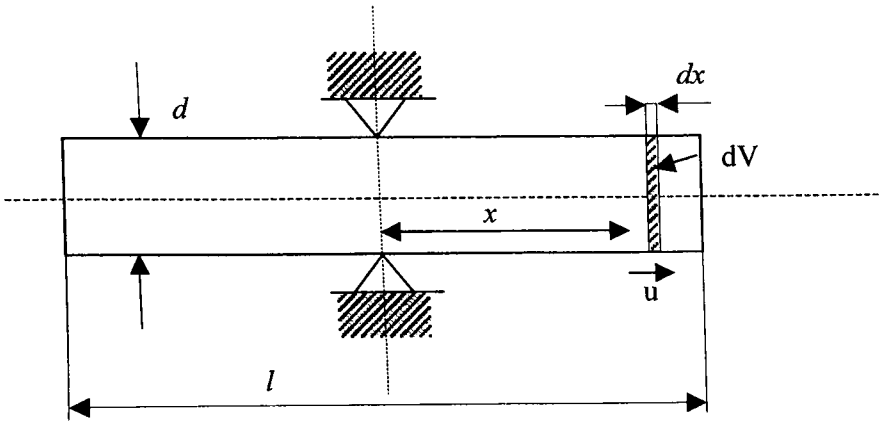

Fig. A4.2.1-1 Prismatic bar with free ends.

For the first mode of vibration of the prismatic bar with free ends the following equations apply:

$$\varepsilon_{max} = A_o \cdot \frac{\pi}{l} \cdot sin(\frac{\pi \cdot x}{l}) \qquad \text{(A4.2.1-5)}$$

$$\sigma_{max} = E \cdot A_o \cdot \frac{\pi}{l} \cdot sin(\frac{\pi \cdot x}{l}) \qquad \text{(A4.2.1-6)}$$

Substituting Eq.A4.2.1-5 and A4.2.1-6 into Eq.A4.2.1-1:

$$dW = \frac{\pi^4}{4 \cdot l^2} \cdot \xi \cdot E \cdot A_o^2 \cdot \sin^2\left(\frac{\pi \cdot x}{l}\right) \cdot dx \qquad \text{(A4.2.1-7)}$$

Therefore the energy dissipated in the whole volume of the bar is:

$$W = \int_{-l/2}^{l/2} \frac{\pi^4}{4 \cdot l^2} \cdot \xi \cdot E \cdot A_o^2 \cdot \sin^2\left(\frac{\pi \cdot x}{l}\right) \cdot dx = \frac{\pi^3}{2 \cdot l^2} \cdot \xi \cdot E \cdot A_o^2 \cdot V \qquad \text{(A4.2.1-8)}$$

APPENDIX 7.1.1 Variables and results of experiment using the WT/P tool.

The term "Static/dynamic" denotes that the specimen was compressed twice. First without vibrations and then subsequent to the measurement of its height was subjected to the same load before applying vibrations. The term "Dynamic" means that the specimen was subjected to both, load and excitation simultaneously.

Table A7.1.1 Experiment No1

Upsetting method:	"Static/dynamic"			
Lower beam: Upper beam:	Excited Not excited			
Boosters	1.5 : 1			
Specimen:	Steel; d = 4.1mm, D = 9mm; h = 13.6mm (Fig.5.1.3b)			
Mechanical load:	7 kN			
Excitor input voltage:	1800 V_{P-P}*			
Result				
Upsetting phase:	Δh*	Amplitude in μm		Frequency in Hz	
	in mm	Lower beam	Upper beam	Lower beam	Upper beam
Static	0.84	-	-	-	-
Dynamic	0	7.4	-	20284	-

Table A7.1.1 Experiment No2

Upsetting method:	"Static/dynamic"				
Lower beam: Upper beam:	Not excited Excited				
Boosters	1.5 : 1				
Specimen:	Steel; d = 4.0mm, D = 9mm; h = 13.54m (Fig.5.1.3b)				
Mechanical load:	7 kN				
Excitor input voltage:	1800 V_{P-P}				
Result					
Upsetting stage:	Δh in mm	Amplitude in μm		Frequency in Hz	
		Lower beam	Upper beam	Lower beam	Upper beam
Static	0.76	-	-	-	-
Dynamic	0.02	-	4.41	-	20199

Table A7.1.3. Experiment No.3

Upsetting method:	"Static/dynamic"				
Lower and upper beams:	Excited				
Boosters:	1.5 : 1				
Specimen:	Steel; d = 4.02mm, D = 9mm; h = 13.64m (Fig.5.1.3b)				
Mechanical load:	7 kN				
Excitor input voltage:	1800 V_{P-P} (refers to both excitors)				
Results					
Upsetting stage:	Δh in mm	Amplitude in μm		Frequency in Hz	
		Lower beam	Upper beam	Lower beam	Upper beam
Static	0.38	-	-	-	-
Dynamic	0.18	6.68	5.45	20276	20182

Table A7.1.4. Experiment No.4

Lower and lower beams:	Excited				
Boosters	1.5 : 1				
Specimen:	Steel; d = 4.1mm, D = 9mm; h = 13.6mm (Fig.5.1.3b)				
Mechanical load:	7 kN				
Excitor input voltage:	1800 V_{P-P} (refers to both excitors)				
Results					
Upsetting stage:	Δh in mm	Amplitude in μm		Frequency in Hz	
		Lower beam	Upper beam	Lower beam	Upper beam
Static	0.84				
Dynamic	0.08	7.88	7.29	20281	20187

Table A7.1.5. Experiment No.5

Lower and lower beams:	Excited				
Boosters	2 : 1				
Specimen:	That which was used in Experiments No.4				
Mechanical load:	7 kN				
Excitor input voltage:	2600 V_{P-P} (refers to both excitors)				
Results					
Upsetting stage:	Δh in mm	Amplitude in μm		Frequency in Hz	
		Lower beam	Upper beam	Lower beam	Upper beam
Dynamic	0.08	7.90	7.20	20279	20151

Table A7.1.6. Experiment No.6

Upsetting method:	"Static/dynamic"
Lower and lower beams:	Excited
Boosters	2 : 1
Specimen:	Steel; d = 6mm, h = 11.18 (Fig.5.1.3b)
Mechanical load:	15 kN
Excitor input voltage:	1800V_{P-P} (both excitors)

Results

Upsetting stage:	Δh in mm	Amplitude in μm		Frequency in Hz	
		Lower beam	Upper beam	Lower beam	Upper beam
Static	1.22	-	-	-	-
Dynamic	0.14	4.95	3.34	20307	20191

Table A7.1.7. Experiment No.7

Upsetting method:	"Static/dynamic"
Lower and lower beams:	Excited
Boosters	2 : 1
Specimen:	Steel; d = 6mm, h = 11.18 (Fig.5.1.3b)
Mechanical load:	15 kN
Excitor input voltage:	2600V_{P-P} (both excitors)

Results

Upsetting stage:	Δh in mm	Amplitude in μm		Frequency in Hz	
		Lower beam	Upper beam	Lower beam	Upper beam
Static	1.24	-	-	-	-
Dynamic	0.24	5.7	4.7	20319	20187

Table A7.1.8. Experiment No.8

Upsetting method:	"Dynamic"				
Lower and lower beams:	Excited				
Boosters	2 : 1				
Specimen:	Steel; d = 6mm, h = 11.18 (Fig.5.1.3b)				
Mechanical load:	15 kN				
Excitor input voltage:	$1800V_{P-P}$ (both excitors)				
Results					
Upsetting stage:	Δh in mm	Amplitude in μm		Frequency in Hz	
		Lower beam	Upper beam	Lower beam	Upper beam
Dynamic	1.36	4.9	4.2	20302	20184

Table A7.1.9. Experiment No.9

Upsetting method:	"Static/dynamic"				
Lower and lower beams:	Excited				
Boosters	2 : 1				
Specimen:	Aluminium; d = 11.48mm, h = 18.18 (Fig.5.1.3c)				
Mechanical load:	15 kN				
Excitor input voltage:	$1800V_{P-P}$ (both excitors)				
Results					
Upsetting stage:	Δh in mm	Amplitude in μm		Frequency in Hz	
		Lower beam	Upper beam	Lower beam	Upper beam
Static	4.72	-	-	-	-
Dynamic	0.32	5.6	3.4	20315	20192

Table A7.1.10. Experiment No.10

Upsetting method:	"Dynamic"				
Lower and lower beams:	Excited				
Boosters	2 : 1				
Specimen:	Aluminium; d = 11.50mm, h = 18.20 (Fig.5.1.3b)				
Mechanical load:	15 kN				
Excitor input voltage:	$1800V_{P-P}$ (both excitors)				
Results					
Upsetting stage:	Δh in mm	Amplitude in μm		Frequency in Hz	
		Lower beam	Upper beam	Lower beam	Upper beam
Dynamic	5.74	5.63	2.71	20330	20209

Table A7.1.11. Experiment No.11

Upsetting method:	"Static/dynamic"				
Lower and lower beams:	Excited				
Boosters	2 : 1				
Specimen:	Aluminium; d = 11.50mm, h = 18.18 (Fig.5.1.3c)				
Mechanical load:	15 kN				
Excitor input voltage:	$1800V_{P-P}$ (both excitors)				
Results					
Upsetting stage:	Δh in mm	Amplitude in μm		Frequency in Hz	
		Lower beam	Upper beam	Lower beam	Upper beam
Static + dynamic	5.14	5.85	3.5	20315	20185

Table A7.1.12. Experiment No.12

Upsetting method:	"Dynamic"				
Lower and lower beams:	Excited				
Boosters	2 : 1				
Specimen:	Aluminium; d = 11.50mm, h = 18.00 (Fig.5.1.3c)				
Mechanical load:	15 kN				
Excitor input voltage:	$1800V_{P-P}$ (both excitors)				
Results					
Upsetting stage:	Δh in mm	Amplitude in μm		Frequency in Hz	
		Lower beam	Upper beam	Lower beam	Upper beam
Dynamic	5.54	-	3.27	20332	20206

APPENDIX 7.2.3.1 Amplitude measurements.

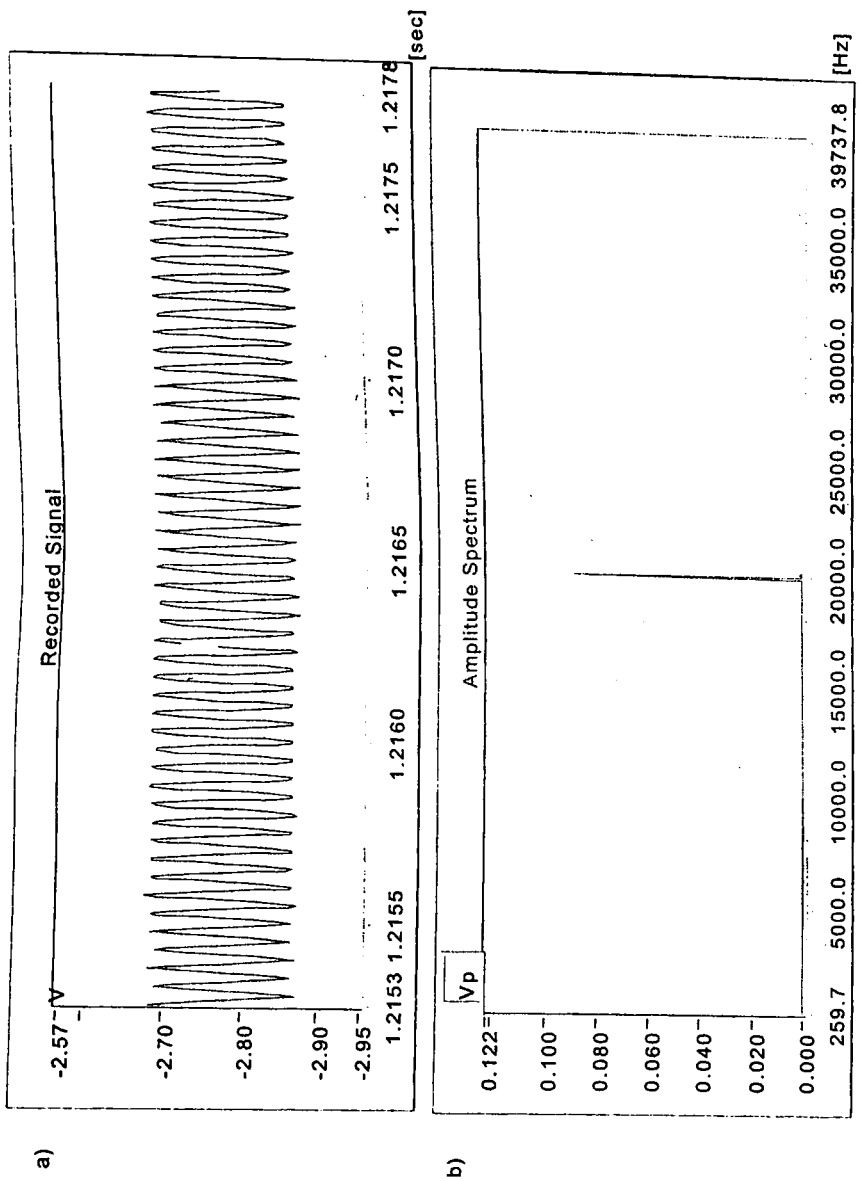

Fig.A7.2.3.1-1 Amplitude (a) recorded signal, (b) amplitude spectrum for a process velocity of 0.5mm/s and a nominal amplitude of 0.0045mm.(1μm=0.02V)

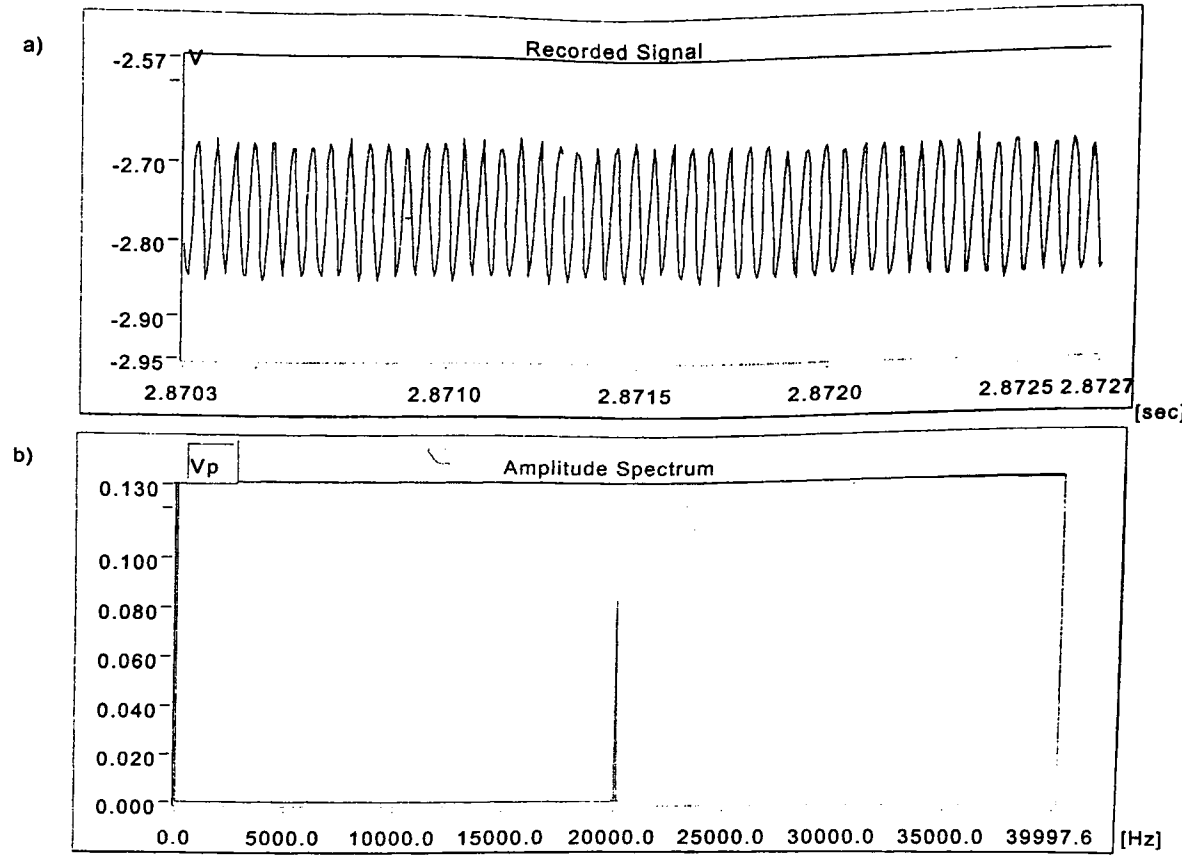

Fig.A7.2.3.1-2 Amplitude (a) recorded signal, (b) amplitude spectrum for a process velocity of 1.0mm/s and a nominal amplitude of 0.0045mm.(1μm=0.02V)

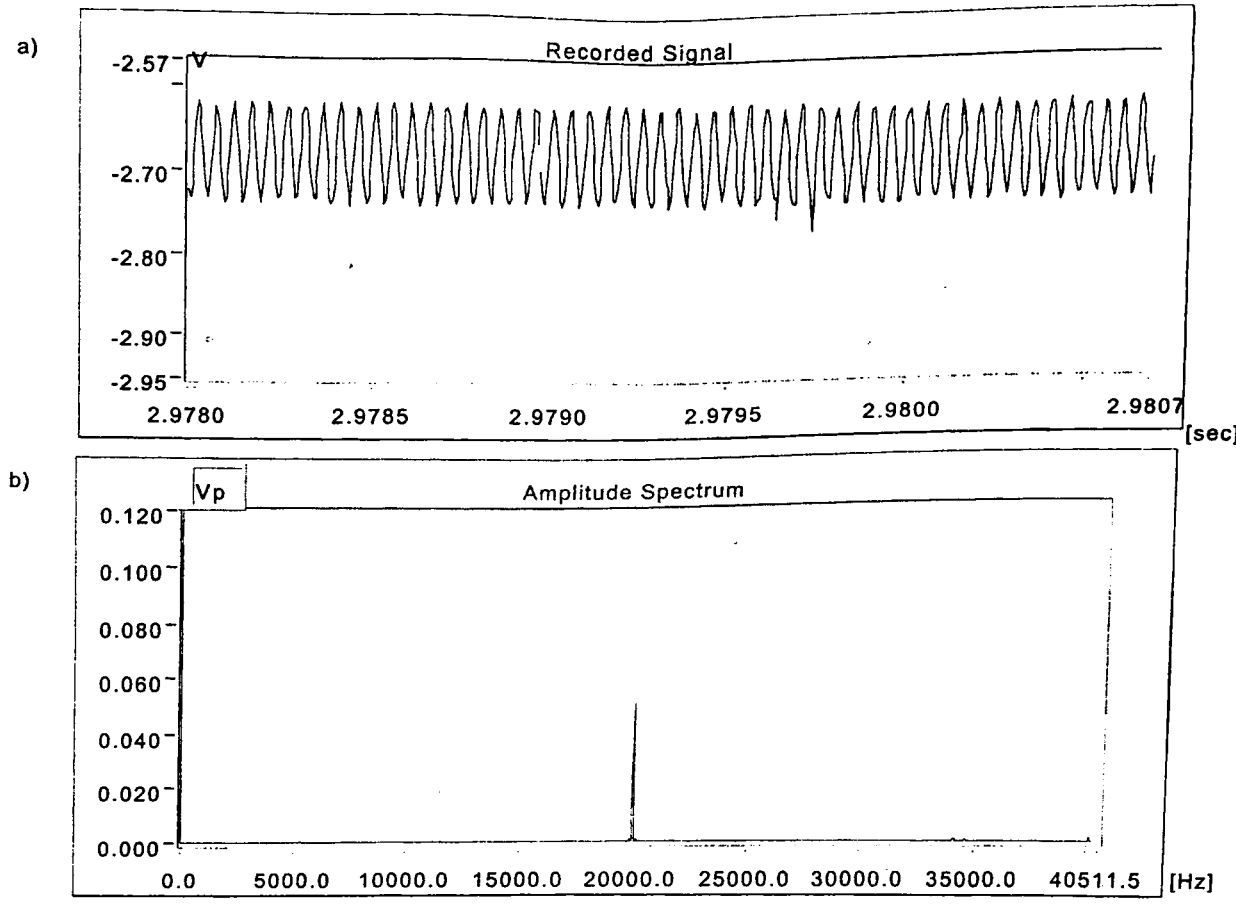

Fig.A7.2.3.1-3 Amplitude (a) recorded signal, (b) amplitude spectrum for a process velocity of 5.0mm/s and a nominal amplitude of 0.0045mm.(1μm=0.02V)

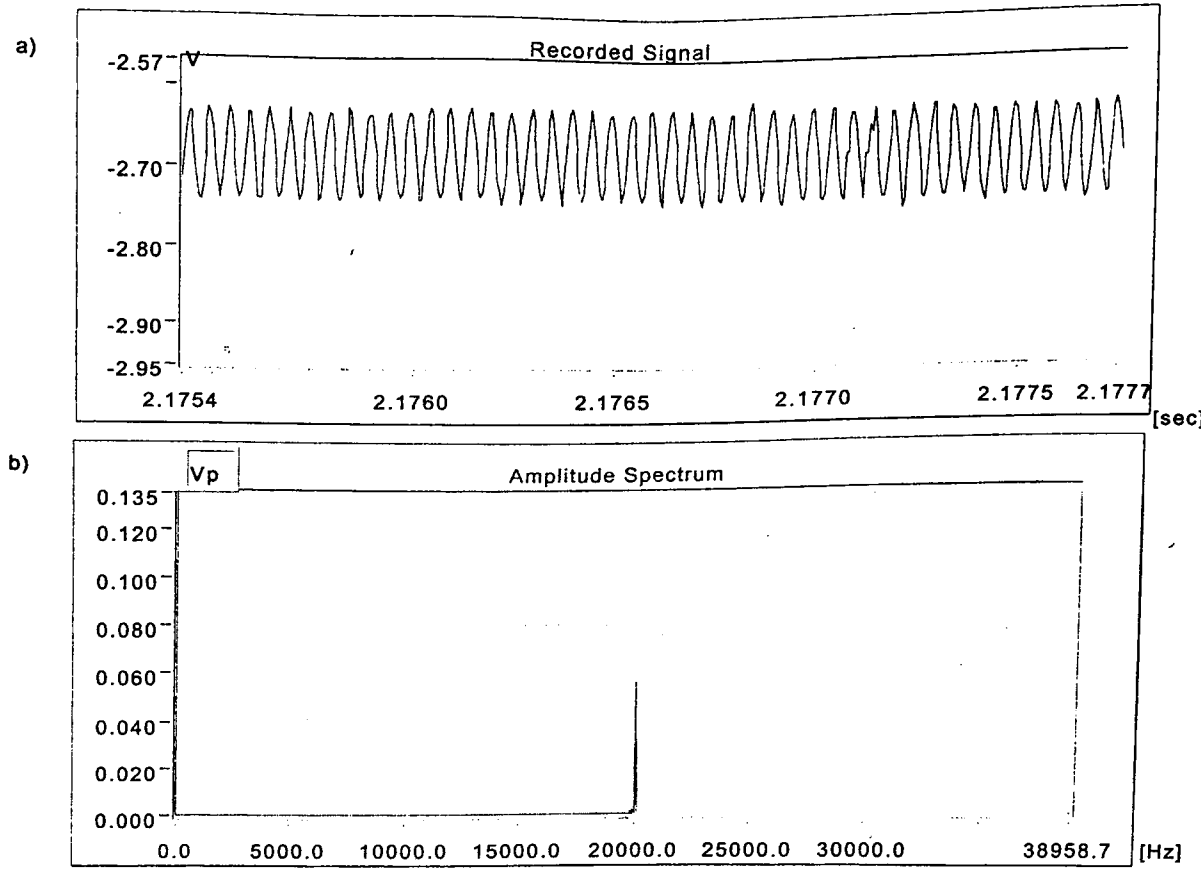

Fig.A7.2.3.1-4 Amplitude (a) recorded signal, (b) amplitude spectrum for a process velocity of 1.0mm/s and a nominal amplitude of 0.0045mm.(1μm=0.02V)

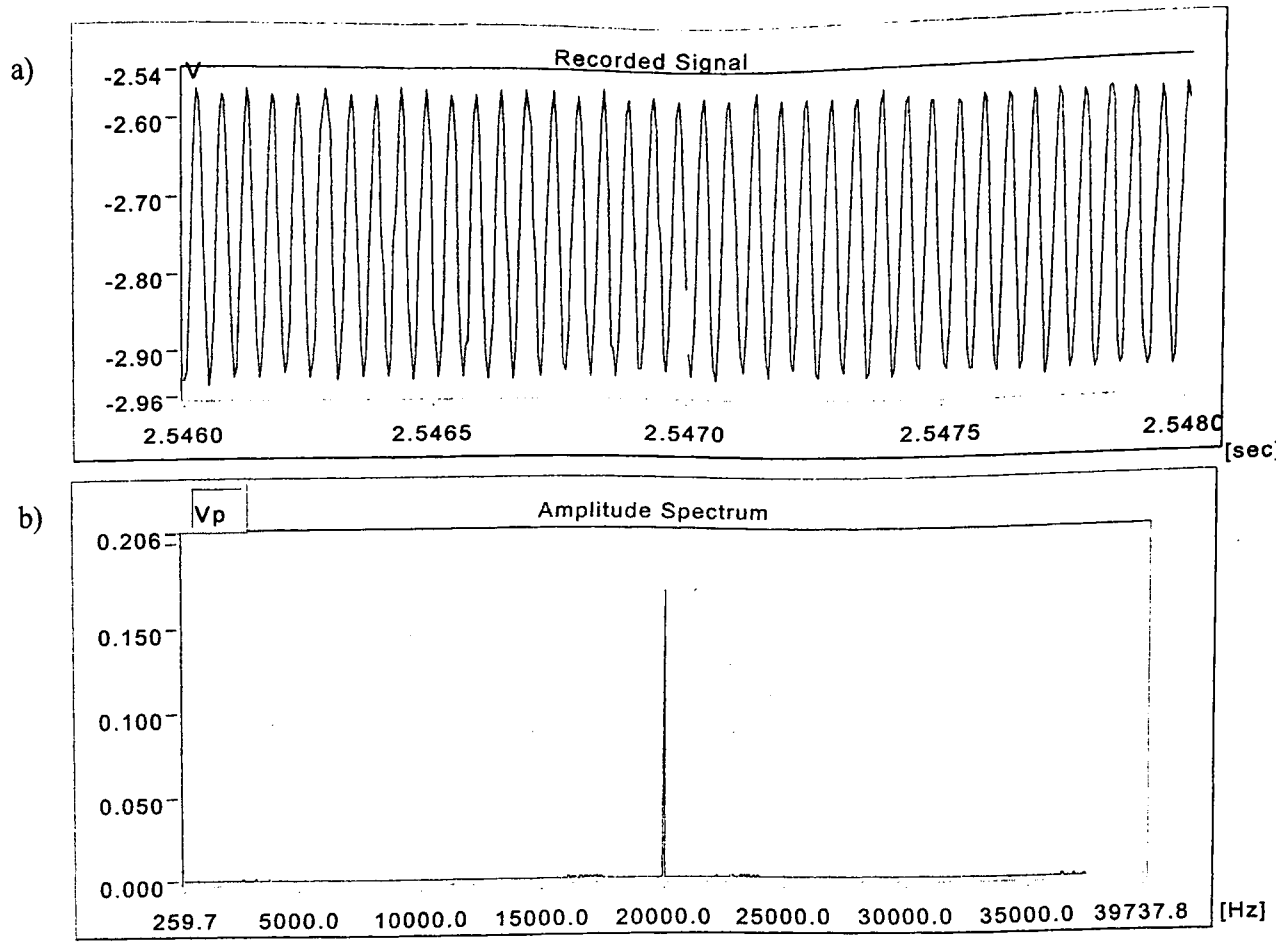

Fig.A7.2.3.1-5 Amplitude (a) recorded signal, (b) amplitude spectrum for a process velocity of 0.5mm/s and a nominal amplitude of 0.0085mm.(1μm=0.02V)

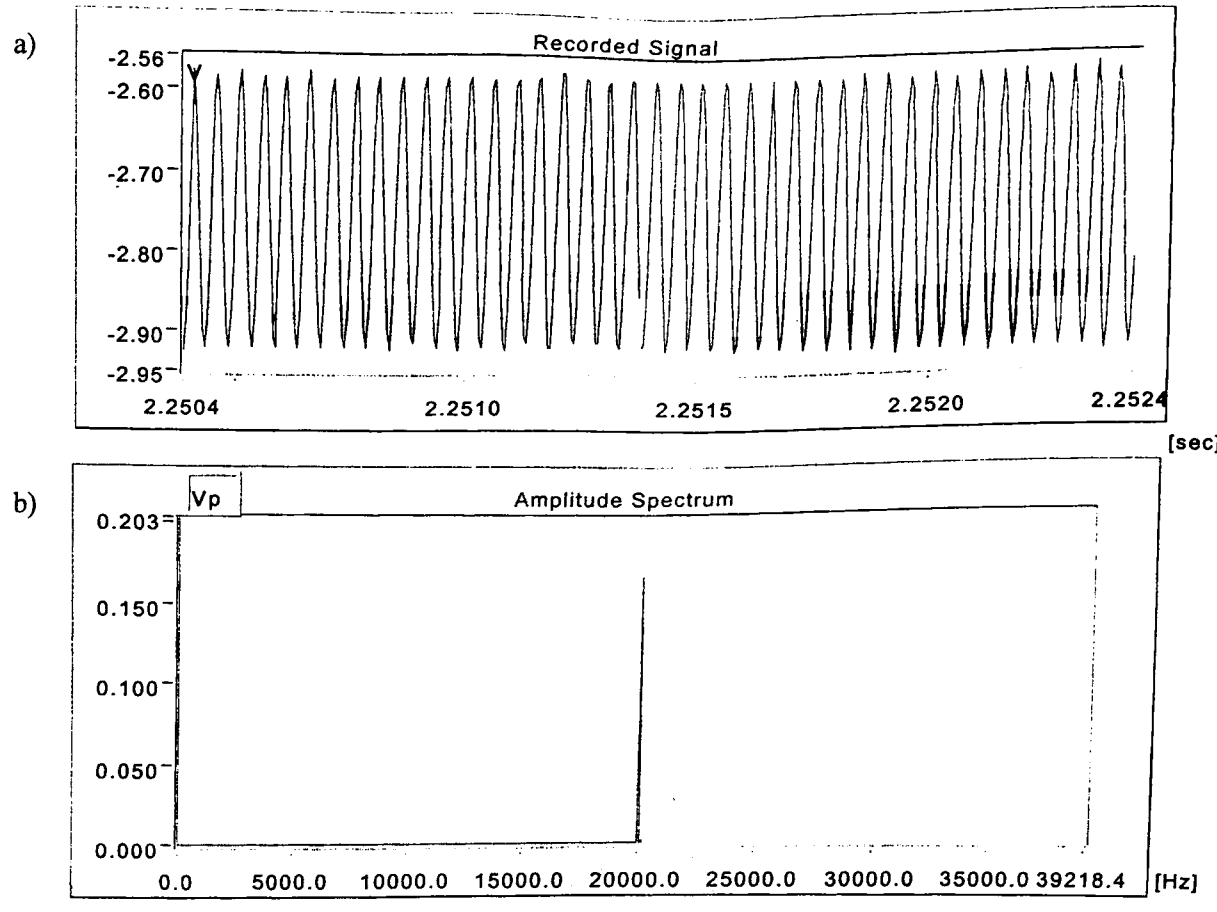

Fig.A7.2.3.1-6 Amplitude (a) recorded signal, (b) amplitude spectrum for a process velocity of 1.0mm/s and a nominal amplitude of 0.0085mm.(1μm=0.02V)

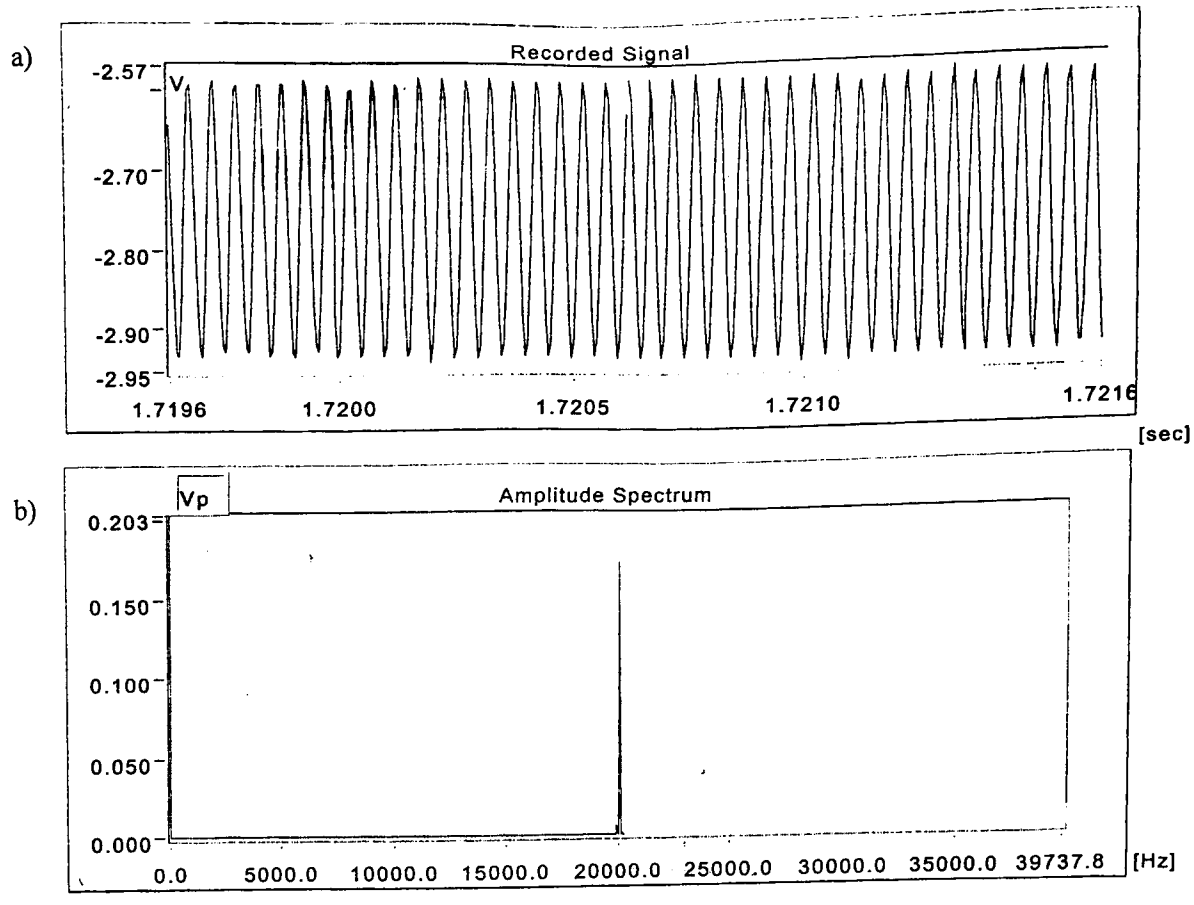

Fig.A7.2.3.1-7 Amplitude (a) recorded signal, (b) amplitude spectrum for a process velocity of 5.0mm/s and a nominal amplitude of 0.0085mm.(1μm=0.02V)

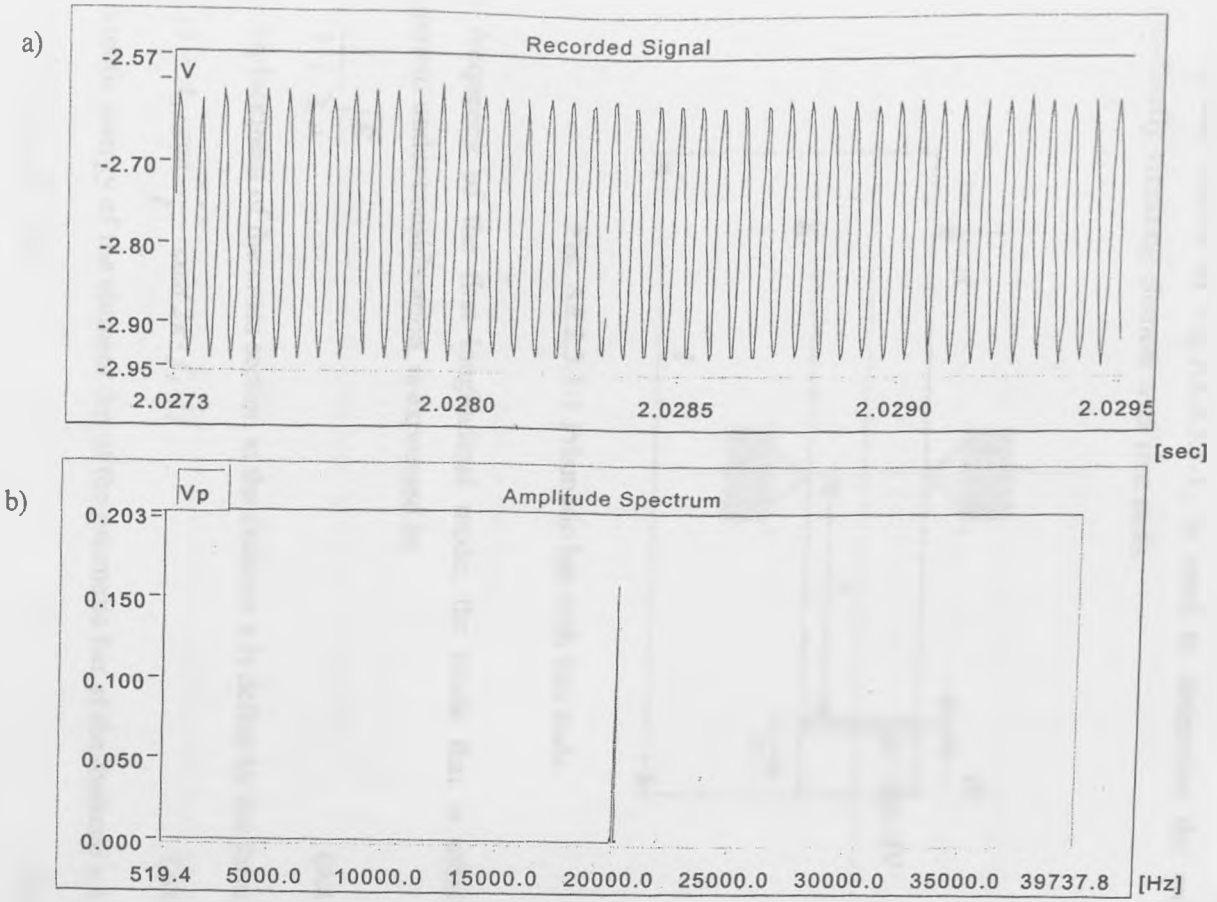

Fig.A7.2.3.1-8 Amplitude (a) recorded signal, (b) amplitude spectrum for a process velocity of 10.0mm/s and a nominal amplitude of 0.0085mm.(1μm=0.02V)

APPENDIX 8.2.3.1 Energy stored in a vibrating element.

Energy of a vibrating element is the sum of its kinetic and potential energy:

$$E_T = E_K + E_P \qquad \text{(A8.2.3.1-1)}$$

The diagram, shown in Fig.A8.2.3.1-1, is used to determine the energy of a longitudinally vibrating element with free ends.

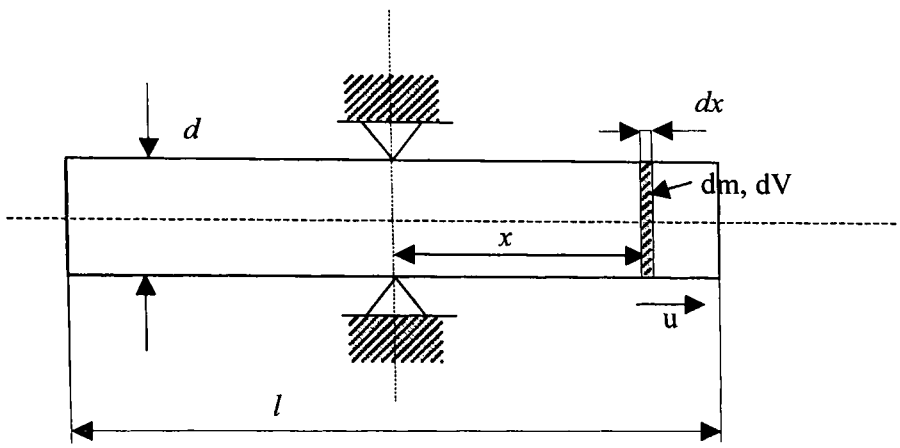

Fig. A8.2.3.1-1 Prismatic bar with free ends.

The frequency of the first longitudinal mode, the mode that is utilised in the equipment under consideration, is expressed by

$$f_l = \frac{1}{2 \cdot l} \cdot \sqrt{\frac{E}{\rho}} \qquad \text{(A8.2.3.1-2)}$$

The displacement of the cross section at the distance x is define by the formula:

$$u(x,t) = A_o \cdot cos\frac{\pi \cdot x}{l} \cdot cos(2\pi \cdot f_l \cdot t) \qquad \text{(A8.2.3.1-3)}$$

The kinetic energy of the element dm of the prismatic bar at the distance x is

$$dE_K = \frac{1}{2} \cdot [v(x,t)]^2 \cdot dm \qquad \text{(A8.2.3.1-4)}$$

where:

$$dm = \frac{\pi}{4} \cdot d^2 \cdot \rho \cdot dx \qquad \text{(A8.2.3.1-5)}$$

Velocity of the cross section of the bar at the distance x is

$$v(x,t)=\frac{du(x,t)}{dt}=-2\pi\cdot f_1\cdot A_o\cdot\cos(\frac{\pi\cdot x}{l})\cdot\sin(2\pi\cdot f_1\cdot t) \qquad \text{(A8.2.3.1-6)}$$

Substituting (A8.2.3.1-5) and (A8.2.3.1-6) into (A8.2.3.1-4):

$$dE_K=\frac{\pi^3}{2}\cdot A_o\cdot f_1^2\cdot d^2\cdot\rho\cdot\cos^2(\frac{\pi\cdot x}{l})\cdot\sin^2(2\pi\cdot f_1\cdot t)\cdot dx \qquad \text{(A8.2.3.1-7)}$$

Thus, the kinetic energy of the bar at any moment t is given by

$$E_K=\int_0^l dE_K=\pi^2\cdot A_o^2\cdot f_1\cdot V\cdot\rho\cdot\sin^2(2\pi\cdot f_1\cdot t) \qquad \text{(A8.2.3.1-8)}$$

Potential energy of the vibrating element results from its elastic deflection and is equal to the sum of the elastic work done on each unit volume. The energy accumulated in the volume dV (see Fig.A8.2.3.1-1) is described by the formula:

$$dE_P=\frac{1}{2}\cdot\sigma(x,t)\cdot\varepsilon(x,t)\cdot dV \qquad \text{(A8.2.3.1-9)}$$

Since:

$$\sigma=E\cdot\varepsilon \qquad \text{(A8.2.3.1-10)}$$

and

$$dV=\frac{\pi\cdot d^2}{4}\cdot dx \qquad \text{(A8.2.3.1-11)}$$

Eq. (A8.2.3.1-9) may be written in the form

$$dE_P=\frac{1}{2}\cdot E\cdot[\varepsilon(x,t)]^2\cdot\frac{\pi\cdot d^2}{4}\cdot dx \qquad \text{(A8.2.3.1-11)}$$

Strain in the x-cross section is computed using the expression

$$\varepsilon(x,t)=\frac{dA(x,t)}{dx}=-\frac{\pi}{l}\cdot E\cdot A_o\cdot\sin(\frac{\pi\cdot x}{l})\cdot\cos(2\pi\cdot f_1\cdot t) \qquad \text{(A8.2.3.1-11)}$$

Thus, the potential energy of the volume dV in the x-cross section at the moment t is given by the following formula:

$$dE_P=-\frac{\pi^3}{8\cdot l^2}\cdot E\cdot A_o^2\cdot d^2\cdot\sin^2(\frac{\pi\cdot x}{l})\cdot\cos^2(2\pi\cdot f_1\cdot t)\cdot dx \qquad \text{(A8.2.3.1-12)}$$

Taking into account Eq. A8.2.3.1-2 and that $\frac{\pi\cdot d^2\cdot l}{4}=V$ the formula takes a form

$$dE_P=-\frac{\pi^2}{2}\cdot E\cdot A_o^2\cdot V\cdot\rho\cdot\sin^2(\frac{\pi\cdot x}{l})\cdot\cos^2(2\pi\cdot f_1\cdot t)\cdot dx \qquad \text{(A8.2.3.1-13)}$$

Therefore, the potential energy of the bar is

$$E_P = \int_0^l dE_P = \pi^2 \cdot A_o^2 \cdot f_1 \cdot V \cdot \rho \cdot \cos^2(2\pi \cdot f_1 \cdot t) \qquad \text{(A8.2.3.1-14)}$$

Comparison of the Eq.A8.2.3.1-8 and A8.2.3.1-14 shows that the kinetic and potential energies are out of phase by π/2. The kinetic energy reaches the maximum value $E_{K.max} = \pi^2 \cdot A_o^2 \cdot f_1 \cdot V \cdot \rho$ for $t = 0 + i \cdot 0.5T$ while the potential energy reaches the maximum value $E_{P.max} = \pi^2 \cdot A_o^2 \cdot f_1 \cdot V \cdot \rho$ for $t = 0.25T + i \cdot 05T$.

Variation of the kinetic and potential energies of one half of the bar with time over the period 0.5T is shown in Fig.A8.2.3.1-2. The graphs have been drawn for the following parameters: $A_o=10^{-6}$m, f_1=20kHz, V=1.45 ·10 $^{-4}$m (d=0.038m, l=0.128m), and ρ=7850kg/m^3.

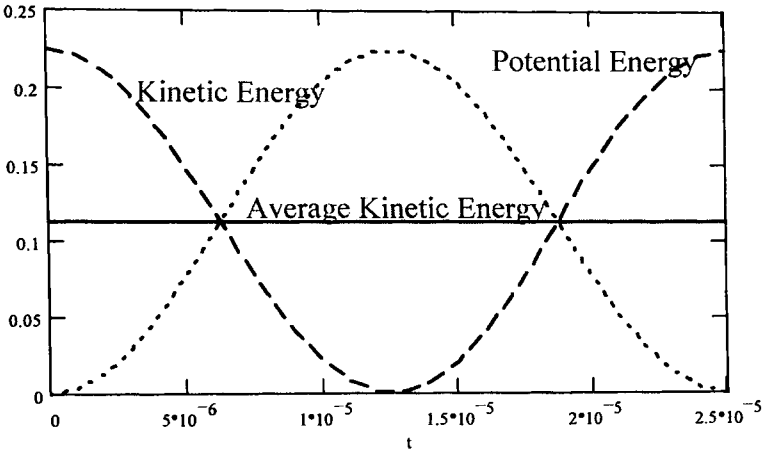

Fig.A.8.2.3.1-2. Variation of the kinetic and potential energies of one half of the bar with time, over the period 0.5T.

The total energy of the bar is

$$E_T = E_K + E_P = \pi^2 \cdot A_o^2 \cdot f_1 \cdot V \cdot \rho \cdot \left[\sin^2(2\pi \cdot f_1 \cdot t) + \cos^2(2\pi \cdot f_1 \cdot t)\right] \qquad \text{(A8.2.3.1-15)}$$

Since $\left[\sin^2(2\pi \cdot f_1 \cdot t) + \cos^2(2\pi \cdot f_1 \cdot t)\right] = 1$ the total energy is equal to

$$E_T = \pi^2 \cdot A_o^2 \cdot f_1 \cdot V \cdot \rho = E_{K,max} = E_{p,max} \qquad \text{(A8.2.3.1-16)}$$

The magnitude of this energy for the parameters listed earlier is 0.448J.

The average kinetic energy of the bar is:

$$E_{K.av} = \frac{1}{T}\int_0^T E_k dt = \frac{\pi^2}{2} \cdot A_o^2 \cdot f^2 \cdot V \cdot \rho \qquad \text{(A8.2.3.1-17)}$$